Reptation in entangled polymer networks

A simulational study of the significance of constraint release for reptation

Philipp Sebastian Lang

München 2015

Reptation in entangled polymer networks

A simulational study of the significance of constraint release for reptation

Philipp Sebastian Lang

Dissertation
an der Fakultät für Physik
der Ludwig–Maximilians–Universität
München

vorgelegt von
Philipp Sebastian Lang
aus München

München, den 3. Juni 2015

Erstgutachter: Prof. Dr. E. Frey
Zweitgutachter: Prof. Dr. K. Kroy
Tag der mündlichen Prüfung: 30. April 2015

Zusammenfassung

Ein besonderes Merkmal eukaryotischer Zellen ist, dass sie ein sogenanntes Cytoskelett enthalten, ein dichtes Netzwerk aus Polymeren. Unter anderem ist dieses Cytoskelett verantwortlich für die mechanische Stabilität der Zelle. Es gewährleistet nicht nur die äußere Form, sondern ist essentiell für passive und aktive Verformungen, sowie die dadurch mögliche Fortbewegung der Zelle. Weiterhin ist das Cytoskelett maßgeblich an intrazellulären Transportprozessen und der Positionierung der Organellen innerhalb einer Zelle beteiligt.
Das Cytoskelett als Netzwerkstruktur wird gebildet durch die Vermischung und Verschränkung vieler einzelner Stränge, bzw. Filamente, von biologischen Polymeren. Die individuellen Eigenschaften der Konstituenten und ihre Wechselwirkungen ermöglichen die Versatilität des Netzwerkes. Von besonderer Bedeutung für die Mechanik jedes einzelnen Filaments ist seine Biegesteifigkeit, die ein Charakteristikum der jeweiligen Polymerart ist. Jede Polymerkette unterliegt einer ständigen Brownschen Bewegung, die zusammen mit der Biegesteifigkeit und der Reibung des Lösungsmittels die Dynamik des Polymers bestimmt. In einem dichten Netzwerk wie dem Cytoskelett können sich die Polymere nicht frei bewegen, da sie häufig aneinander stoßen und untereinander verschränkt sind. Diese sterische Wechselwirkung verändert das Verhalten jedes einzelnen Filaments und ist einer der wesentlichen Faktoren für die Mechanik des Netzwerks.

Diese Arbeit untersucht, wie sich ein einzelnes Filament mit relevanter Biegesteifigkeit in einer konzentrierten Lösung von Polymeren verhält. Insbesondere wird geklärt, wie sich die Eigenschaften der einzelnen Filamente auf dieses Verhalten und somit auf das System auswirken. Ein Schwerpunkt dieser Arbeit ist die Erstellung einer numerischen Simulation zur Klärung dieser Frage. Zur Vereinfachung beschränken wir uns auf homogene Systeme identischer Polymere. Des Weiteren betrachten wir rein verschränkte Ketten, das heißt, es gibt keine festen Bindungen zwischen unterschiedlichen Filamenten.

Bedingt durch die sterische Wechselwirkung und die lokale Undehnbarkeit eines einzelnen Filaments ist eine exakte analytische Behandlung eines Polymernetzwerkes mit den aktuell verfügbaren Methoden nicht möglich. Das etablierte, vereinfachte Modell für unsere Fragestellung ist die Reptationstheorie. Sie beschreibt die Bewegung einer vollständig flexiblen Kette ohne Biegesteifigkeit durch ein Netzwerk aus statischen Hindernissen. Konzeptionell wird dabei angenommen, dass die umgebenden Ketten das betrachtete Filament einschränken, als ob es sich in einer kontinuierlichen Röhre befände. Diese hypothetische Röhre ist, wie auch die Hindernisse, statisch und es wird angenommen, dass das beobachtete Polymer sich nur entlang der Röhre bewegen kann.
Basierend auf den gleichen Ideen gibt es eine entsprechende Theorie, welche die Rotation von starren Stäben zwischen festen Hindernissen beschreibt. Zudem existieren einige Ansätze, um diese Modelle auf Ketten mit Biegesteifigkeit zu erweitern. Dafür wird eine weitere Längenskala definiert, die durch die Fluktuationen der Kette in der Röhre bestimmt wird. Im

Allgemeinen wird das Polymer dann auf kürzeren Längen als starrer Stab, und auf größeren Längen als vollständig flexible Kette behandelt.

Eine experimentelle Überprüfung dieser Modelle ist bisher nicht möglich gewesen. Aus diesem Grund werden numerische Simulationen verwendet, um die Vorhersagen zu überprüfen. Bisherige Simulationen betrachteten dabei entweder ausschließlich vollständig flexible Filamente, Ketten zwischen starren Hindernissen oder erzielten nicht ausreichend lange Zeiten, um die relevante Dynamik zu klären. Diese Arbeit ist die erste erfolgreiche Studie der gesamten Dynamik biegesteifer Polymere in einer rein verschränkten Lösung.

Schwerpunkte dieser Arbeit sind die Analyse der numerischen Daten, der Vergleich mit den bestehenden Modellen und die Entwicklung neuer Argumente zur Erklärung des gefundenen Verhaltens.
Zu unseren Haupterkenntnissen gehört, dass die Konformation der Filamente durch ihre Umgebung nicht fixiert wird. Die Fluktuationen der Kontur erreichen die gleiche Amplitude wie in verdünnter Lösung ohne einschränkende Umgebung. Wir interpretieren dies als Auflösung der Einschränkung einer Kette durch die umgebenden Polymere und bestimmen die Zeitskala dieses Relaxationsprozesses. Insbesondere ist diese Zeit in der Regel kürzer als die Zeit, die zum Verlassen der hypothetischen Röhre nötig ist.
Als weitere wichtige Erkenntnis finden wir ein bisher unbekanntes Skalengesetz für die terminale Relaxationszeit. Für Ketten oberhalb einer von uns eingeführten kritischen Biegesteifigkeit ist unser Ergebnis konsistent mit der existierenden Vorhersage für starre Stäbe. Für Polymere mit geringerer, aber nicht vernachlässigbarer Biegesteifigkeit finden wir hingegen eine vollkommen neue Skalierung der terminalen Relaxationszeit. Unsere Daten bestätigen ein neues Modell, nach dem in diesem Parameterbereich die Rotation durch die Konturfluktuationen dominiert wird. Somit finden wir fortlaufend, dass die bestehenden Theorien das betrachtete System nicht adäquat beschreiben.
Weiterhin diskutieren wir ein super-diffusives Regime, das vor Kurzem entdeckt wurde. Unsere Daten zeigen, dass der bisherige Erklärungsversuch nicht korrekt ist. Wir weisen nach, dass dieses Verhalten mit der Rotation des Polymers zusammenhängt.

Als weiteren Hauptpunkt führen wir extensive Simulationen durch, um die Auflösung der Einschränkung einer Kette besser zu verstehen. Wir stellen fest, dass die Annahme fester Hindernisse die Dynamik vollständig verändert. In weiteren speziell angepassten Simulationen finden wir, dass keine einzelne Bewegung die Röhrenauflösung alleine bewirken kann. Sodann lassen wir die Homogenitätsbedingung fallen und betrachten Systeme mit Ketten zweier unterschiedlicher Längen. Wir bestimmen den Einfluss der Länge der umgebenden Ketten auf die Relaxation eines Filaments. Schließlich zeigen wir durch Variation der auftretenden Zeitskalen, dass die Röhrenauflösung durch ein Zusammenspiel der Dynamik mehrerer Ketten abläuft.

Als Schlussfolgerung ergibt sich, dass unsere Daten das Bild einer statischen Röhre in einem der biologisch häufig auftretenden Parameterbereiche eindeutig widerlegen. Ebenso sind die bestehenden, darauf basierenden Theorien nicht haltbar. Somit ist die Entwicklung einer neuen Theorie notwendig, welche die Wechselwirkung der Polymere korrekt erfasst.

Contents

1 Polymer networks

Cells are a fundamental building block of life. They exhibit remarkable properties, which vary strongly depending on their specialization. Cells often have to move, deform actively or passively, or adapt their elasticity to adjust to the requirements of their usually complex environments. The functions responsible for these processes are governed by, or correspond to, the mechanical properties of the cell. In all eukaryotic cells the cytoskeleton determines almost completely the global and local mechanics [1–3]. It consists of various biopolymers with interesting characteristics. By changing the arrangement of these polymers and by directly influencing the properties of each type of polymer, the cell achieves its astounding mechanical qualities [1, 3].
Furthermore, the cytoskeleton is involved in several cellular processes like cell division or the positioning of cellular objects. Generally, it serves as a scaffold for intra-cellular transport [3]. The dynamics of individual and entangled polymers is thus of major interest due to their high relevance in biological systems.

In eukaryotic cells, the cytoskeleton is primarily composed of three biopolymers with different mechanical properties: F-actin, intermediate filaments and microtubuli [1, 3]. The mechanics of individual polymers may be quantified by their stiffness, the inverse of the flexibility. The behavior of single biopolymers with different degrees of flexibility ranging from flexible DNA [2,5] to semiflexible filaments like F-actin [6–9] and stiff microtubules [10–14] have been studied extensively.
In particular, nowadays the conformation as well as the dynamics of individual polymers are easily accessible in experiments [2]. These experiments have led, in combination with theoretical efforts, to important insights into the statistics of the conformations of single polymers in thermal equilibrium [8, 15, 16]. The effect of the bending stiffness on the relaxational dynamics in quiescent solution [6, 8, 17–19], and the linear response to weak external forces have been investigated in detail [20–22]. Even the response to strong fields and the ensuing non-equilibrium dynamics are fairly well understood [9, 23–27].

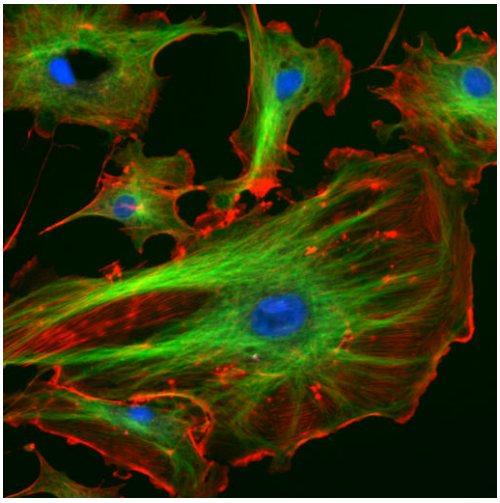

Figure 1.1: Florescence image of a whole cell showing components of the cytoskeleton. Microtubules are shown in green, actin filaments in red. The picture has been adopted from [4].

Based on this understanding of single filaments, it is desirable to derive the properties of dense polymer networks like the cytoskeleton. In spite of a lot of theoretical effort in this

direction, there still are many open questions and the discussion is ongoing [1, 28–35]. The main problem in treating networks of polymers is modeling the effects of steric interactions, which prevent the filaments from crossing each other. Several different predictions have been proposed, but a complete description is still elusive.

As a first step in analyzing the dynamics of polymer networks, the motion of a single chain through the surrounding network is considered. Clarifying this process helps in understanding stress relaxation and the rearrangement of the full network [1, 21]. The standard model for this movement is nowadays the *reptation* theory. Its fundamental concept is based on a tube picture, used for describing the entanglement. The basic idea was first introduced by de Gennes [36] for flexible polymers. Based on this concept Edwards and Doi [37–39] developed theories for both flexible chains and rigid rods. For flexible polymers these seminal models predict a diffusion proportional to $t^{1/2}$ for times smaller than the disentanglement time τ_d, where $\tau_d \propto L^3$. The parameter L is a known property of the observed chain, called the *contour length*. It is the length measured when tracing along the polymer contour. Unfortunately, the description incorporates a further, unknown phenomenological parameter a, which is referred to as the tube diameter and characterizes the network.
The analogous model for rigid rods attempts to predict the rotation of these rods, which is obviously hindered by the network. Employing again the phenomenological parameter a the relaxation time of this system is predicted to scale $\tau_r \propto L^5 a^{-2}$.

These two models only capture the limiting cases of possible polymer system. Hence, they are not valid for, e.g., semiflexible actin networks [21, 40]. As these are of high interest due to their biological relevance, several attempts have been made to combine the mechanical properties of semiflexible filaments with reptation theory [21,32,35,40–43]. In addition to the reptation process, several other mechanisms which may contribute to the movement through the network or alternative descriptions have been proposed and discussed [28, 44–47].

Due to their high relevance and in order to test contradicting theoretical predictions, many experimental measurements have been conducted. To test the theories, first the phenomenological tube diameter and its dependence on the density have been studied by comparing network properties [48, 49]. Nowadays, more refined methods allow to observe and analyze single filaments in a network [33,43,50–54]. Importantly, the existence of a tube-like confinement and a dominant motion roughly similar to reptation could be confirmed. The theoretical discussion on the stiffness dependence of the longest relaxation time has been clarified by observing the diffusion of nanotubes into a fixed network [55].

Yet, all hitherto experimental techniques have several drawbacks, which limit their comparison with theory. To achieve a good visualization, the sample thickness in experiments is usually rather thin compared to the length of the polymer filaments, typically of order 0.5–5 times the length of the polymer [33, 51]. While this may cause boundary effects, it is a necessary trade-off in order to determine single filaments in bulk. At the same time, it is difficult to track an individual chain over times comparable to the typical reptation times, and currently studies are confined to much smaller times [33, 43, 50–54]. Thus, the experiments have not yet succeeded in determining the full dynamics.
Alternative measurement approaches from bulk properties allow to determine the behavior at larger timescales [56, 57]. Yet, only indirect evidence may be gathered from these.

As it is difficult to experimentally measure the reptation of individual polymers, numerical simulations are of major importance. This technique makes the required times as well as detailed informations about each individual polymer accessible. Up to now, these simulations are the only way to test the various theoretical predictions and concepts.
E.g., the simulations of Kremer and Grest [58, 59], verifying the scaling laws predicted by de Gennes, Doi and Edwards [36, 37, 39] for flexible polymers, represent an important validation of reptation theory.

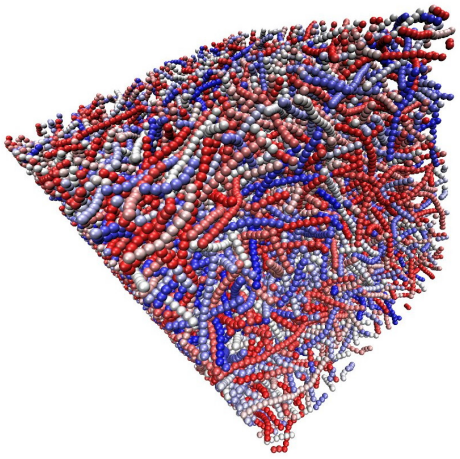

Figure 1.2: Example for a configuration occurring in our simulations. This simulation comprised 736 polymer chains of 45 beads each, and a stiffness comparable to actin.

In this thesis, we present the results of a three-dimensional Brownian dynamics simulation of an entangled polymer mesh with special focus on the regime of semiflexible polymers. Fig. 1.2 shows a typical configuration occurring in our simulations. We compare our results with theoretical predictions and previous simulational studies. We find good agreement with respect to some aspects, but severe discrepancies for other observables. Our findings show that a completely new theoretical approach is required. For the longest relaxation time we find a scaling function dependent on all characteristics of the system. Using adjusted simulations we clarify that constraint release is the dominant process for semiflexible filaments.

The thesis is organized as follows: In Chap. 2 we begin with an overview over the standard models used in the description of polymers. Starting with single molecule models, we derive the most important scaling relations for later use. We continue by introducing the standard reptation model for the movement of single, flexible chains in a dense network. Based on this model, the basic concepts and several of the major theories for the reptation of semiflexible polymers are discussed. Chap. 3 introduces our model and gives a concise characterization of the numerical algorithm used for the simulations. Also, we define the relevant observables and justify the choice of units. Then we discuss the consistency checks performed to ensure the accurateness of the simulation. In Chap. 4 we present the results of our simulations. Comparing them with existing theoretical predictions, we find good agreement for small times. At later times, however, differences arise which we attribute to constraint release. In Chap. 5 we provide a direct comparison of our results to simulations using fixed obstacles. Observing severe differences for systems with constraint release and without, we perform additional simulations and discuss their results to clarify the dominant type of constraint release. Finally, Chap. 6 summarizes our most important findings and their implications for further research. In appendix A, we discuss the viscoelasticity of polymer networks. We modify our simulation to measure the viscoelasticity and comment on the corresponding results. Appendix B contains additional figures.

2 Theoretical models for the dynamics of polymers

Based on the diverse properties of real polymers, there are several different approaches to model biological polymers. In this chapter we introduce the common models for polymers. In order to understand the behavior in a network of entangled polymers, we first discuss the dynamics of single chains. Most importantly, we derive the basic scaling laws governing the free dynamics of single polymers. Based on the concepts known from single filaments, we introduce the basic concepts of the tube picture and give a concise description of several important attempts to model the dynamics of polymers in an entangled polymer network.

2.1 Single chains

2.1.1 General introduction and definitions

Following the standard procedure of statistical physics, we employ a coarse graining approach to describe the dynamics of a given polymer filament. In other words we do not attempt an atomistic description of the polymer. This approach neglects all chemical details like differences in the binding energies of different monomers, e.g., for the different base pair combinations in DNA. We take several monomers along the polymer chain and average over them. We assume that all local discrepancies vanish in this process.
Long range relations and properties are not affected by this procedure. In particular, this applies to the contour length L. The conservation of L is crucial, as it is probably the most fundamental property for the mechanics of a polymer filament.
Furthermore, we assume that there are no chemical or physical changes taking place in the structure of the polymer, such that L is a fixed property of a given filament. While this is a simplification, the length of polymers in biological systems are dynamically kept at a certain value with high precision [3]. Therefore this assumption is well justified if we are only interested in the conformations of the contour.
As the next step, we employ the standard assumption that the diameter of the polymer chain is very small compared to any other length scale of interest, which are usually comparable to the contour length of the polymer. In this way we reduce the characteristics of the polymer in such a way that we remain with a slender, homogeneous chain, which may be described by a few parameters only. To allow for a better analytic treatment, we treat the polymers as ideal chains in the discussion of single filaments, which means that we neglect self-interactions. Thus, the chains are phantom chains, i.e., several different pieces may occupy the same point in space. While this does affect the statistics for those polymers which preferentially assumed a coiled configuration, it hardly affects the power-laws characterizing the dynamics [39]. For

the mostly straight polymers forming the focus of this work, this simplification is of minor relevance [60].

There are two approaches for modeling the simplified polymer contour: a discrete or a continuous description. While the former is more suitable for numerical purposes and is used in the simulations, in general the latter is preferential for an analytic treatment. On timescales much larger than the typical timescale of the smallest segment in the discrete model, both approaches give completely analogous results [39].
In the discrete description the contour is divided into N segments of a fixed length b. The segments are called Kuhn segments and b is referred to as the bond length. The contour length relates these two parameter by $L = Nb$.
Alternatively, we reduce the polymer filament to a continuous space curve $\mathbf{r}(s)$ in three dimensional space, parameterized by the arc length s in the interval $0 \leq s \leq L$. We use this continuous model throughout the analytical parts.

To model different types of polymers one chooses some kind of interaction between the segments of the polymer. These are realized by a suitable potential $\mathcal{U}(\mathbf{r}(s))$. In the next sections we discuss two possible choices of potentials corresponding to typical polymer models and analyze the resulting behavior of the chain.

Having simplified the polymers, the solvent surrounding all the filaments is not treated explicitly. Instead, we use effective interactions to capture the most important effects of the solvent. The solvent molecules perform fast thermal fluctuations, and hence constantly some collide with the polymer. These collisions cause a Brownian motion of the polymer and thus, we model the solvent as causing a random force $\boldsymbol{\eta}(s,t)$ on the polymer. The correlations in the motion of the solvent molecules decay on a timescale of about 10^{-10}s for nanometer sized particles in water [39], whereas we are interested in much larger times. Therefore we may idealize the collisions and the resulting force as uncorrelated in time.
The amplitude of these random forces is given by the fluctuation-dissipation theorem. Thus, with components $k, i \in \{x, y, z\}$ we write [39]:

$$\begin{aligned} \langle \boldsymbol{\eta}(s,t) \rangle &= 0 \quad \text{and} \\ \langle \eta_k(s,t) \cdot \eta_i(\tilde{s},\tilde{t}) \rangle &= 2k_B T \zeta_{k,i}(s,\tilde{s}) \delta(t-\tilde{t}) \,, \end{aligned} \tag{2.1}$$

where k_B is Boltzmann's constant, T the temperature, and $\boldsymbol{\zeta}(s,\tilde{s})$ the friction tensor. This friction tensor and the corresponding force $\boldsymbol{\zeta}\frac{\partial \mathbf{r}(s,t)}{\partial t}$ per unit length resulting from dragging the polymer through the viscous solvent are the second interaction emerging from the solvent.

Throughout this work we assume localized isotropic friction with a friction coefficient ζ, i.e., the full friction tensor is given by $\boldsymbol{\zeta}(s,s') = \zeta \mathbb{1} \delta(s-s')$, where $\mathbb{1}$ is the identity matrix. Hence, the total friction of a polymer is given by ζL and there is no hydrodynamic interaction between separated parts of a chain or different filaments. This assumption is called the free draining approximation and is well justified for single polymers with a mostly straight conformation: Evaluating the Fourier transformation of the Green's function for a hydrodynamic force field (Oseen tensor) gives only a weak (logarithmic) mode dependence of the mobility [19, 61].
In a polymer network, it is known that the anisotropy of the friction is of little relevance and has not been incorporated in most previous studies [31, 39, 59]. Thus, as the long ranged hydrodynamics would slow down the simulations significantly, we constrain our study to the free-draining approximation. As we simplify the polymer to a slender body and focus on

the low Reynolds number regime, we may describe the flow field as a Stokes flow. Then the friction per unit length is approximately [39, 62]:

$$\zeta = \frac{4\pi\mu}{\ln(L/d)}\,, \tag{2.2}$$

where d is the diameter of the filament and μ the viscosity of the solvent.

The strength of the viscous drag allows a further simplification. The typical timescale for effects of inertia is proportional to the ratio of mass and friction. As the mass per unit length of the polymer is very small, this timescale is typically on the order of 10^{-10}s [63]. This is well below the timescales of interest, hence we may treat the system as over-damped, i.e., we may neglect inertia.

Taking all these steps together the equation of motion of the polymer is governed by a Langevin equation of the form:

$$\zeta\frac{\partial \mathbf{r}(s,t)}{\partial t} = -\frac{\partial \mathcal{U}}{\partial \mathbf{r}(s,t)} + \boldsymbol{\eta}(s,t)\,. \tag{2.3}$$

In our simulations and the following theoretical studies we use the time evolution of the mean square deviation, sometimes also called autocorrelation, of the end-to-end distance $R(t) = |\mathbf{r}(L,t) - \mathbf{r}(0,t)|$ as our observable. It is defined by:

$$\delta R^2(t) = \langle (R(t) - R(0))^2 \rangle \tag{2.4}$$

Now, we introduce two standard polymer models, for later reference in the discussion of polymer networks. For each model we give the explicit potential $\mathcal{U}$ and discuss the dynamics of the system by determining $\delta R^2(t)$.

2.1.2 Flexible polymers

As a first and easy approach to model long polymers described as thin space curves, assume that there is no interaction along the polymer contour except for a local interaction causing the coherence of the chain. While obviously a simplification, this model results in good approximation of the actual behavior if the length scale of interactions along the contour is much smaller than any other length scale of interest. Polymers where this condition holds true, are called *flexible* polymers and comprise biological polymers like long strands of DNA. These chains are frequently described using the *Rouse*-model [64]. It is one of the most basic polymer models and the base for many extensions.

In the simulations presented later in this thesis we focus on semiflexible to stiff polymers, for which the worm-like chain model has been found to be more appropriate. However, as reptation theory has been developed for flexible polymers, we need several fundamental results of the Rouse model later on. Therefore we give a short introduction to this model without going into details.

The original Rouse model is a discrete description of the polymer as a set of beads, connected by springs [64] and no further interaction between the beads. It is chosen to represent the

same statistics as the freely jointed chain model, where instead of springs, rigid segments of fixed length b connect neighboring beads. However, the Rouse model has the advantage of allowing to calculate the chain dynamics more easily. Here, we discuss the continuous version of the Rouse model, which is equivalent to the original form for times much larger than the self-diffusion time of a segment $\zeta b^3/6k_BT$, which is well below the relevant timescales of this study.

Using the notation as introduced in (2.3), the Rouse model corresponds to a choice of potential $\mathcal{U} = \frac{k}{2}\int_0^L \mathrm{d}s \left(\frac{\partial \mathbf{r}(s,t)}{\partial s}\right)^2$ without further assumptions. In other words each segment of the chain acts as a local spring, with a spring constant k chosen to mimic the global properties of the chain as defined by the freely jointed chain model [39]. Therefore k corresponds to the entropic spring constant of a flexible chain $k = \frac{3k_BT}{b^2}$. Here the bond length b of a Kuhn segment of the discrete model enters even in the continuous formalism. It reflects the otherwise neglected short ranged interactions between monomers. In terms of the persistence length from the worm-like chain model, which we introduce in Sec. 2.1.3, it can be shown that $b = 2l_p$ by equating the average end-to-end distance of the two models.

Using the previously established form, the resulting equation of motion is:

$$\zeta \frac{\partial \mathbf{r}(s)}{\partial t} = k \frac{\partial^2 \mathbf{r}(s)}{\partial s^2} + \boldsymbol{\eta}(s,t)\,. \tag{2.5}$$

Together with the boundary conditions $\frac{\partial \mathbf{r}(s)}{\partial s} = 0$ this equation defines the continuous Rouse model. Using a decomposition into Cosine modes, this model may be solved exactly [39, 64].

As expected, the center of mass motion, which corresponds to the 0th mode of the decomposition, is free diffusion. In detail, the mean square displacement (MSD) of the center of mass $\mathbf{X} = \frac{1}{L}\int_0^L \mathbf{r}(s)\mathrm{d}s$ is [39, 65]:

$$\langle (\mathbf{X}(t) - \mathbf{X}(0))^2 \rangle = \frac{6k_BT}{\zeta L} t\,. \tag{2.6}$$

To characterize the internal dynamics and conformational changes of the polymer filament, we determine $\delta R^2(t)$. The MSD of the end-to-end vector is [39]:

$$\delta R^2(t) = \frac{8Lb}{\pi^2} \sum_{p:odd} \frac{1}{p^2} \left(1 - \exp\left(-tp^2/\tau_1\right)\right)\,, \tag{2.7}$$

and thus, the saturation value is $\delta R^2 \propto Lb$.
The longest internal relaxation time τ_1 is called the Rouse time τ_R and defined as:

$$\tau_R = \tau_1 = \frac{\zeta L^2 b}{3\pi^2 k_BT} = \frac{\zeta N^2 b^3}{3\pi^2 k_BT}\,, \tag{2.8}$$

where the second expression is for the analogous discrete model.

From this result, we can easily infer the dynamics of the relaxation behavior at times much smaller than τ_1 by replacing the sum in Eq. (2.7) by an integral and performing the substitution $q = p^2 t$. It follows:

$$\delta R^2(t) \propto \int \frac{1}{p^2} \left(1 - \exp\left(-tp^2/\tau_1\right)\right) \mathrm{d}p \propto \int \sqrt{\frac{t}{q^3}} \left(1 - \exp\left(-q/\tau_1\right)\right) \mathrm{d}q \propto t^{1/2}. \tag{2.9}$$

This typical scaling of the Rouse dynamics, together with the longest relaxation time $\tau_1 \propto L^2 b$ are important basics for the classical reptation theory, which we introduce later in this chapter.

2.1.3 Semiflexible to stiff chains

For a large class of biological polymers like F-actin, microtubuli or Ftsz there are strong orientational interactions between monomers. These interactions cause correlations along the contour, whose range is of the order of the length scales of interest. Polymers of this class are well described by the worm-like chain model [2, 6]. This model was introduced in its discrete form by Kratky and Porod [66] and a continuous version was established later by Saitô [67]. Since the continuous version is more suitable for calculations, here we only discuss this version.
This model incorporates the interaction between segments of the contour by an explicit potential proportional to the square of the curvature. Thus, a parallel alignment of polymer segments, which are close to each other with regard to the distance along the contour, is preferred. In general, these polymers exhibit rather straight conformations instead of coiled states. Explicitly, the continuous form of the potential is:

$$\mathcal{U}_{WLC} = \frac{1}{2} k_B T l_p \int_0^L \mathrm{d}s \left(\frac{\partial^2 \mathbf{r}}{\partial s^2} \right)^2 , \tag{2.10}$$

where l_p is called persistence length and is a material property governing the flexibility of the filament. As no further potentials occur in the worm-like chain model, from Eq. (2.3) we may write down the equation of motion for semiflexible polymers:

$$\zeta \frac{\partial \mathbf{r}(s,t)}{\partial t} = -k_B T l_p \frac{\partial^4 \mathbf{r}}{\partial s^4} + \boldsymbol{\eta}(s,t) , \tag{2.11}$$

with η as given in Eq. (2.1). The connectivity of the chain is implemented by locally inextensible contour. This constraint is:

$$\left(\left. \frac{\partial \mathbf{r}(s')}{\partial s'} \right|_s \right)^2 = 1 \quad \forall\, 0 \le s \le L . \tag{2.12}$$

Note that effects from a finite extensibility of the polymer backbone are in general weak for most biopolymers [68–71] and are neglected in this thesis.

The model is motivated by some fundamental properties of worm-like chains. Of particular interest is the tangent-tangent correlation, which decays exponentially:

$$\langle \mathbf{u}(s) \cdot \mathbf{u}(s') \rangle = \mathrm{e}^{\frac{|s-s'|}{l_p}} , \tag{2.13}$$

where we used the notation $\mathbf{u}(s) = \left. \frac{\partial \mathbf{r}(s')}{\partial s'} \right|_s$ for the tangent vector at arc length s. This relation means that the persistence length is the characteristic decay length for the orientation of the contour. Also, it allows direct measurement of the persistence length in experiments, where it is found to range from a few nm up to hundreds of μm or even several mm for microtubuli [2, 6, 11].
By comparing this length scale with the only other intrinsic length scale of our polymer model, the contour length L, we may classify all polymers into three regimes. If the stiffness l_p/L is very small, $l_p/L \ll 1$ we call the polymer flexible.[1] In this regime and for equilibrium

[1] The inverse quantity L/l_p is often used in the literature, too. It is commonly referred to as flexibility.

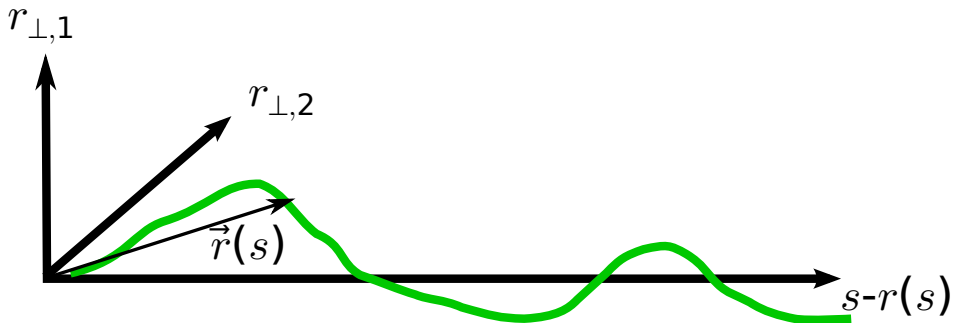

Figure 2.1: Illustration of the parameterization used in the weakly bending approximation for a polymer contour. The position vector $\mathbf{r}(s)$ of the polymer contour (green line) is split into the longitudinal ($r_\parallel$) and orthogonal ($r_\perp$) displacement relative to the orientation of the polymer idealized as a straight line.

conformations of the polymers the worm-like chains model corresponds to good approximation to the predictions of the Rouse model, which is frequently used for this case [65]. Polymers with a stiffness comparable to the contour length, $l_p/L \approx 1$ are called semiflexible. Finally we use the phrase stiff for chains with $l_p/L \gg 1$. For extremely stiff chains, the contour fluctuates hardly at all and often these polymers are described as rigid rods. While the models for both limiting regimes, rigid rods and flexible chains, allow to calculate several quantities exactly, the inextensibility constraint induces difficulties in treating semiflexible polymers analytically.

Before turning to a more involved treatment of the worm-like chain model, the given definitions of the model allow some direct conclusions. Using a scaling argument we estimate the strength of the average orthogonal fluctuations $L_\perp$ in equilibrium from the potential Eq. (2.10). The energy is of order k_BT. Then we approximate:

$$k_BT \approx \frac{1}{2} k_BT l_p \int_0^L \mathrm{d}s \left(\frac{\partial^2 \mathbf{r}}{\partial s^2}\right)^2 \propto k_BT l_p L \frac{L_\perp^2}{L^4} \tag{2.14}$$

$$\Rightarrow L_\perp^2 \propto L^3/l_p \tag{2.15}$$

From the tangent-tangent correlation Eq. (2.13) we may directly calculate several quantities [72]. For comparison, the average end-to-end distance $\langle R^2 \rangle$ is of interest. An easy calculation shows:

$$\langle R^2 \rangle = 2Ll_p \left[1 - \frac{l_p}{L}\left(1 - \mathrm{e}^{-L/l_p}\right)\right] \tag{2.16}$$

For polymers with $l_p \ll L$ this converges to $\langle R^2 \rangle \approx 2Ll_p$. Compare this expression with the corresponding value of the flexible model to identify the Kuhn length b with the persistence length by $b = 2l_p$. In the other limit $l_p \gg L$ it holds $\langle R^2 \rangle \approx L^2$ and the polymer is almost always completely stretched.

For chains or segments of chains with $l_p/L \gtrsim 1$, we employ the *weakly bending* approximation to solve the equation of motion of the worm-like chain model [9, 23, 24, 40, 73]. In this approximation we exploit the fact that for a polymer with $l_p/L \gtrsim 1$ the contour hardly deviates from a straight line. This allows to employ a convenient parametrization of the form

$\mathbf{r}(s) = (s - r_\parallel(s), \mathbf{r}_\perp(s))$, where the two-dimensional vector $\mathbf{r}_\perp$ describes the fluctuations orthogonal to the idealized straight line and $r_\parallel$ captures the parallel deviation, as depicted in Fig. 2.1. Especially $\mathbf{r}_\perp$ is a small quantity.
Note that the in-extensibility constraint connects the values of the two projections. We use the parameterization to rewrite Eq. (2.12) as:

$$(1 - r'_\parallel)^2 + \mathbf{r}'^2_\perp = 1\,, \tag{2.17}$$

where a prime denotes a derivative with respect to s. By expanding a square root and keeping only lowest orders, the chosen parametrization yields:

$$r'_\parallel(s) \approx \frac{1}{2}\mathbf{r}'^2_\perp(s)\,, \tag{2.18}$$

which shows that $r_\parallel(s)$ is of higher order and the orthogonal fluctuations dominate in the system. Consequently, we approximate the Hamiltonian by:

$$\mathcal{U}_{\mathrm{WLC}} \approx \frac{1}{2}k_B T l_p \int_0^L \mathrm{d}s \mathbf{r}''^2_\perp(s), \tag{2.19}$$

From this potential and keeping only the lowest order terms, the simplified equation of motion for $\mathbf{r}_\perp(s)$ is:

$$\zeta\frac{\partial}{\partial t}\mathbf{r}_\perp = -k_B T l_p \mathbf{r}''''_\perp + \boldsymbol{\eta}_\perp\,, \tag{2.20}$$

where $\boldsymbol{\eta}_\perp$ gives the orthogonal components of the random forces.

The equation of motion (2.20) may be solved by normal mode analysis. We decompose $\mathbf{r}_\perp$ into a set of orthonormal eigenfunctions u_n of the differential equation $u''''_n(s) = q_n^4 u_n(s)$ and write:

$$\mathbf{r}_\perp(s,t) = \sum_n \mathbf{a}_n(t)u_n(s). \tag{2.21}$$

As any curvature of the polymer filament at either end would instantly relax, the boundary condition is $u''(0) = u''(L) = 0$. Thus, the eigenfunctions are of the form $u_n(s) = a_n \sin(q_n s)$ with $q_n = \frac{n\pi}{L}$.

The orthogonal u_n yield independent linear differential equations of first order for the $\mathbf{a}_n(t)$. The solution to this equation is:

$$\mathbf{a}_n(t) = \frac{1}{\zeta}\int_{-\infty}^{\infty} \mathrm{d}\tilde{t}\boldsymbol{\eta}_\perp(\tilde{t})e^{-k_B T l_p q_n^4 (t-\tilde{t})/\zeta}\Theta(t-\tilde{t})\,, \tag{2.22}$$

where $\Theta(t)$ denotes the Heaviside function. From this solution to the equation of motion, we may now calculate the observables of interest.

Similar to flexible chains, we want to analyze the dynamics of the mean square displacement of the end-to-end vector. Since the conformation is almost straight we approximate the length of the end-to-end vector $\mathbf{R}$ by the component parallel to the orientation of the idealized line alone:

$$R \approx R_\parallel = \int_0^L [1 - r'_\parallel(s)]\mathrm{d}s \tag{2.23}$$

in the parametrization used in the weakly bending limit. As shown previously in Eq. (2.18), the dominant contribution is then given by:

$$R \approx L - \int_0^L \frac{1}{2} r_\perp'^2(s) \mathrm{d}s \,. \tag{2.24}$$

Thus, we derive the MSD of the end-to-end vector using the previous calculations determining the equation of motion of $r_\perp$:

$$\begin{aligned} \delta R^2(t) &= \left\langle \left(\frac{1}{2} \int_0^L \mathrm{d}s [\mathbf{r}_\perp'^2(s,t) - \mathbf{r}_\perp'^2(s,0)] \right)^2 \right\rangle & (2.25) \\ &= \frac{1}{2} \int_0^L \mathrm{d}s \int_0^L \mathrm{d}\tilde{s} \left[\left\langle \mathbf{r}_\perp'^2(s,0) \mathbf{r}_\perp'^2(\tilde{s},0) \right\rangle - \left\langle \mathbf{r}_\perp'^2(s,t) \mathbf{r}_\perp'^2(\tilde{s},0) \right\rangle \right] . & (2.26) \end{aligned}$$

Expanding the $\mathbf{r}_\perp(s,t)$ in the series of modes given in Eq. (2.21) and using the orthonormality of the modes we need to calculate expressions of the form:

$$\delta R^2(t) \propto \left\langle \sum_n q_n^2 a_n^2(t) \sum_m q_m^2 a_m^2(0) \right\rangle , \tag{2.27}$$

i.e., four-point correlations. In order to avoid these, we employ Wick's theorem [74], which allows to rewrite the expression in terms of two-point correlators. Thus we arrive at:

$$\delta R^2(t) = \frac{1}{2} \sum_{n,m} q_n^2 q_m^2 \left[\langle a_n^2(t) \rangle \langle a_m^2(0) \rangle + 2 \langle a_n(t) a_m(0) \rangle \right] , \tag{2.28}$$

which is easily calculated from $a_n(t)$, cf. Eq. (2.22).

In good agreement with experiments, the final result for the mean-square displacement of the end-to-end vector in the weakly-bending limit is then [6, 73]:

$$\delta R^2(t) = \frac{2}{l_p^2} \sum_n \frac{1}{q_n^4} \left[1 - \mathrm{e}^{-2 k_B T l_p q_n^4 |t|/\zeta} \right] , \tag{2.29}$$

As in the flexible case, we are primarily interested in three quantities. The longest internal relaxation time of the system $\tau_{i,l}$ is inferred directly from Eq. (2.29) as [9, 26]:

$$\tau_{i,l} = \zeta \left(\frac{L}{4.73} \right)^4 / k_B T l_p \,. \tag{2.30}$$

The saturation value of δR^2 at equilibrium is calculated explicitly as [9, 26, 40]:

$$\delta R^2(t \to \infty) = \frac{L^4}{45 l_p^2} \,. \tag{2.31}$$

Finally, the scaling behavior at times much smaller than $\tau_{i,l}$ is determined analogously to the flexible case (2.9) and we find [6, 9, 26]:

$$\delta R^2(t \ll \tau_{i,l}) \propto t^{3/4} \,. \tag{2.32}$$

This concludes the discussion of the dynamics of single polymer filaments. With those basics we now discuss the existing models for the dynamics of individual chains in a dense solution of polymers.

2.2 Polymer Networks

Recall that the results presented previously for single polymers neglect steric interactions. As flexible polymers in equilibrium acquire a coiled conformation, it is likely that interactions of segments, separated by a long distance along the contour, occur. Also, the behavior in networks is dominated by steric interactions, keeping different polymer filaments from crossing one another. Because it is virtually impossible to model these steric interactions in an analytically tractable way, some simplifying approximations are required.
The common and to our knowledge only relevant model for polymer networks is the so-called reptation or tube model. De Gennes [36] introduced the basic concept of this model. He considered the movement of a flexible polymer through an array of fixed obstacles. Due to its similarity with the movement of snakes, he termed the resulting motion *reptation*. Based on these ideas, Doi and Edwards [39] elaborated on the theory of reptation to capture the motion of single chains in a network of either flexible polymers or rigid rods. Later on, several extensions of this model tried to incorporate the semiflexible nature of many polymer filaments.
It is usually argued that these models are valid for settings with both a fixed surrounding, like a free polymer moving in a gel of strongly cross-linked filaments, and purely entangled systems where all chains move freely. For a more detailed discussion of this assumption, see Sec. 2.2.5.
Here, we first give a short introduction to the reptation theory for flexible polymers. Then we discuss several possible extensions to semiflexible polymers. For the introduction to reptation we employ the original picture of a completely flexible chain and introduce the Doi-Edwards theory of reptation, although we are later primarily interested in semiflexible polymers. We choose this approach due to its historical significance and as it helps to clarify the semiflexible to flexible transition later on.

2.2.1 The basic concepts of reptation theory and the tube picture

Consider a single, completely flexible polymer of length $L = Nb$, where b is the length of a chain segment, in a dense array of polymers. We call a system dense, if the typical distance between chains is much smaller than the end-to-end distance of the observed polymer. For a better visualization, we assume that all points of the polymer contour lie almost in a plane. Note that this assumption is not necessary and is not included in the mathematical treatment of the model. As an additional approximation for visualization, all surrounding polymers are supposed to intersect with this plane at one point only, such that the system may be depicted as in Fig. 2.2 a).

The observed chain moves freely, except for the strict condition not to cross any of the surrounding chains, i.e., these chains act as rigid obstacles for this polymer. These obstacles are assumed to be fixed without any dynamics. Thus the observed polymer is essentially confined to a small, fixed space between the nearest neighboring chains.

Due to the flexible nature of the chains under consideration here, the polymer is coiled even in this small, confined space. To simplify matters even further, most of the time we only consider what has been termed the primitive path or primitive chain by Doi and Edwards [37, 75–77],

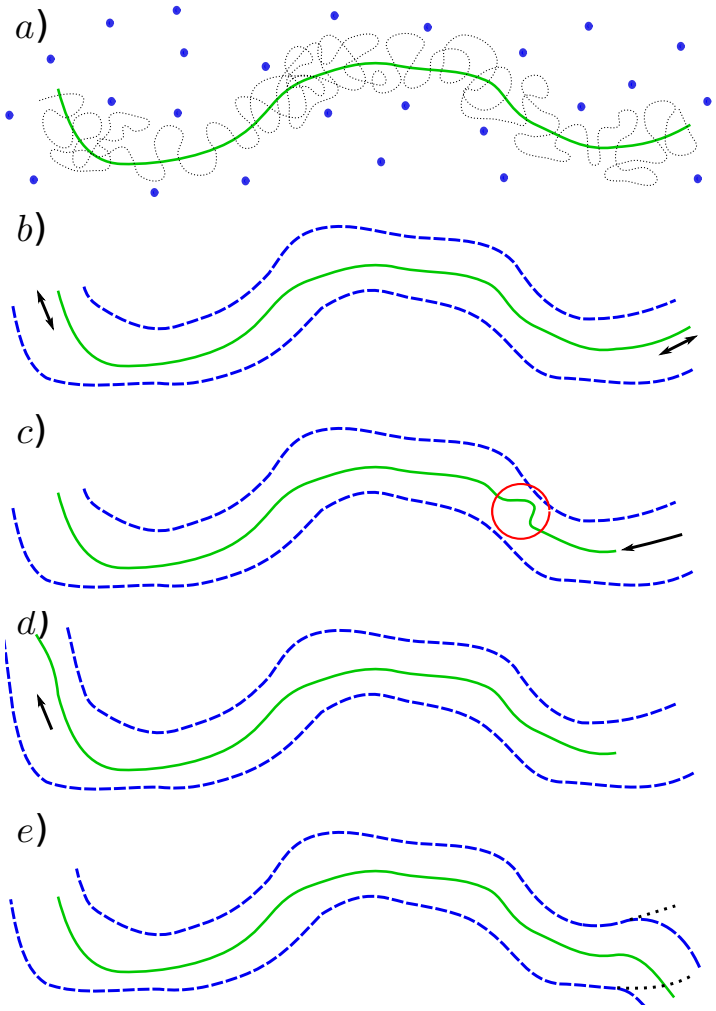

Figure 2.2: A schematic representation of the basic concepts of reptation theory. a) A polymer (black dotted curve) lies in an array of fixed obstacles (blue dots). For an easier calculation, the polymer is represented by the primitive chain drawn in green, see main text for details. b) The discrete obstacles are replaced by an effective continuous tube (blue dashed line) restricting the motion of the polymer to motion along the tube. The small arrows are supposed to indicate the possible motion. c) Fluctuations of the contour length of the primitive path are related to undulations of stored length, shown in an exemplary sketch in the red circle. These undulations may travel along the primitive path via a mechanism comparable to Rouse dynamics. d) If the primitive chain moves in one direction, e.g., to the left in this example, a part of the original tube is deserted. As the tube is only defined around the polymer this part of the tube is lost. When moving back into that region, the primitive chain may acquire a new conformation as shown in e). For better comparison the changed part of the old tube is shown by black dots.

which is shown in green in Fig. 2.2. The primitive path corresponds to the center line of the tube-like region the polymer is confined to by the surrounding obstacles. Alternatively, we may think of the primitive path as the average position of the polymer chain, if the average is taken over times much shorter than the typical timescale required for diffusion of the whole chain but much larger than the equilibration time of the individual segments.
Analogously, think of the single intersections of the neighboring chains with the plane of the observed polymer as the intersection of their respective primitive chain with this plane. It is helpful to keep in mind that the primitive chain actually represents a laterally extended object of different characteristics than the original polymer.[2] While it still is a flexible chain, both the contour length of the primitive path $\hat{L}$ and the effective segment length a are usually different.

We assume the segment length of the primitive chain a is similar to the typical distance between the surrounding obstacles, as flexible chains can choose a new direction as soon as the next obstacle is passed. This parameter a is one of the free parameters of all reptation theories and is one of the central parameters with several interpretations. While to our knowledge there is not even a scaling prediction on how a depends on the number of polymers or their length, these interpretations allow to experimentally estimate a. This data implies approximately $a \propto \nu^{-1/2}$, where ν is the polymer concentration in terms of number of chains per volume [40].
Later in the comparison with the results of our simulations, we employ the mesh size $\xi_m = \sqrt{\frac{3}{\nu L}}$ to quantify the typical distance between different polymers in accordance with previous studies [78]. While ξ_m is derived for rigid rods and is quite suitable for semiflexible to stiff polymers, which form the focus of this work, it is not clear how ξ_m relates to a for flexible chains. For simplicity we assume $a \propto \xi_m$ [31, 40].

Given the primitive path of a flexible chain, according to its definition, it may only move in an approximately tube-shaped region defined by the nearest-neighboring obstacles. Using a mean-field approximation we assume that the obstacles act on all segments of the chain, keeping them in this region. Thus, we neglect the individual obstacles and instead treat the confinement as a continuous tube around the primitive path, shown as a dashed blue line in Fig. 2.2 b). The diameter of the tube is assumed to be constant and of value a, which is frequently used in experiments to determine a [5, 39, 55]. Now obviously the polymer or rather its primitive path only diffuses and fluctuates along the tube as indicated by the black arrows in Fig. 2.2 b). In particular, it may only leave the tube at its current ends.

Additional to the diffusion of the whole chain, there is an alternative mechanism to move contour trough the tube, which is more efficient at small times. If the polymer retracts part of its contour at either end, a small undulation of stored length is formed inside the tube. As an example, an undulation is schematically drawn inside the red circle in Fig. 2.2 c) after some contour length has been contracted at the right end of the chain. These undulations may now move along the primitive path of the chain, thus transporting part of the primitive path from

[2] For the semiflexible to stiff chains discussed later in this work, the primitive path and the actual contour of the polymer hardly deviate and have only slightly different characteristics due to the preferred straight alignment and decreased lateral fluctuations of the semiflexible polymers. Thus we do not have to treat them separately.

one end to the other.[3] Once the stored length has reached the other end of the primitive chain, the polymer may elongate by a corresponding length in an arbitrary direction, cf. Fig. 2.2 d). The diffusion of the whole chain may cause an analogous offset. For the further discussion it does not matter which process dominates.
The other end of the tube remains vacated and is thus lost. In particular, this means that if the chain moves into the other direction or restores some length on this end, it does not need to occupy the same tube as before. In Fig. 2.2 e) an example shows the old tube in dotted lines and the new orientation of the tube and primitive path. This process of changing the tube is called tube renewal and is supposed to be the dominant relaxation mechanism. It is possible as the tube only exists as the confinement of the observed polymer. Thus, once the chain has been completely retracted from a part of the tube, there nothing distinguishes the direction of the old tube and the polymer may freely choose a new direction when approaching this region again.

In this process of moving along the current conformation, the polymer acquires an elongated conformation in contrast to the Gaussian coil, that a flexible polymer forms in a dilute solution. This finding justifies an elongated shape of all polymers in the system, as tacitly assumed initially.

With this model and using some results for flexible polymers in dilute solution, we now derive several predictions for the dynamics of the chain through the network. Note that the scaling behavior in dilute solution is in good approximation also valid for the slightly elongated conformations occurring in reptation theory [39].

2.2.2 Predictions for flexible chains from reptation theory

Following Doi and Edwards [39] we start by calculating the mean-square displacement of a segment of the primitive chain. Note that this quantity is closely related to the MSD of the end-to-end vector determined previously for the single chains in dilute solution. It can easily be shown that both exhibit an identical time dependence for times smaller than the longest relaxation time of the chain. Both can be used to quantify the dynamics of the chain. We elaborate on all observables used in our numerical simulation and data analysis in Sec. 3.3.
The standard calculation assumes that the contour length of the primitive path stays constant throughout the reptation process. Afterwards we discuss the additional effects caused by the length fluctuations of the actual polymer and thus the primitive chain. The basic equation of motion may be written as:

$$\mathbf{r}_p(s, t + \Delta t) = \mathbf{r}_p(s + \Delta\psi(t), t) \; , \tag{2.33}$$

where $\mathbf{r}_p(s,t)$ denotes the position of the primitive path at arc length s with $0 \leq s \leq \hat{L}$ at time t. Δt is an arbitrary time increment and $\Delta\psi(t)$ is the distance covered by the primitive chain in time Δt. In words, this formula expresses that the primitive path moves in a time Δt along itself such that if a segment has covered a distance $\Delta\psi(t)$ it reaches the position occupied by the segment at arc length $s + \Delta\psi(t)$ at time t. As the length is fixed, the origin of the motion

[3] This movement of undulations, referred to as defects, along the tube is part of the problem originally studied by de Gennes.

along the tube is diffusion of the whole polymer chain. Then a Gaussian distribution holds for $\Delta\psi$ equivalent to this one-dimensional diffusion. Explicitly we write:

$$\langle \Delta\psi(t) \rangle = 0 \; ; \qquad \langle (\Delta\psi(t))^2 \rangle = 2\frac{k_B T}{Nb\zeta}\Delta t \; . \tag{2.34}$$

Recall that the orientation of the newly generated chain outside the tube is uncorrelated to the parts of the chain remaining in the tube. Therefore, Eq. (2.33) suffices to describe the dynamics in spite of holding only for the segments staying within the tube existing a time t, i.e., for arc length $0 \leq s + \Delta\psi(t) \leq \hat{L}$.

With these basic equations, we may determine $\langle (\mathbf{r}_p(s,t) - \mathbf{r}_p(s,0))^2 \rangle$ the mean-square displacement for a primitive chain segment at arc length s. For shorter notation, we define [39]:

$$\Phi(s, s', t) = \langle (\mathbf{r}_p(s,t) - \mathbf{r}_p(s',0))^2 \rangle \; . \tag{2.35}$$

From Eq. (2.33) it follows:

$$\Phi(s, s', t + \Delta t) = \langle \Phi(s + \Delta\psi(t), s', t) \rangle, \tag{2.36}$$

where the brackets denote the average over $\Delta\psi$. As the first moment of $\Delta\psi$ is zero, a Taylor expansion of $\langle \Phi(s + \Delta\psi, s', t) \rangle$ in $\Delta\psi$ to second order results in $\langle \Phi(s + \Delta\psi(t), s', t) \rangle \approx \left(1 + \frac{k_B T}{Nb\zeta}\Delta t \frac{\partial^2}{\partial s^2}\right) \Phi(s, s', t)$. Thus from Eq. (2.36) it follows:

$$\frac{\partial}{\partial t}\Phi(s, s', t) = \frac{k_B T}{Nb\zeta}\frac{\partial^2}{\partial s^2}\Phi(s, s', t) \; . \tag{2.37}$$

The initial condition used for solving this equation follows from the properties of a Gaussian chain. The mean square distance between two segments separated by a length L on any Gaussian chain of bond length a may be approximated by [39]:

$$\langle (\mathbf{r}(s,t) - \mathbf{r}(s',t))^2 \rangle = aL \; , \tag{2.38}$$

for $L \gg a$. Applied here with $L = |s - s'|$, the initial condition is $\Phi(s, s', t = 0) = a|s - s'|$. Finally a suitable set of boundary conditions is found to be [39]:

$$\left.\frac{\partial}{\partial s}\Phi(s, s', t)\right|_{s=\hat{L}} = a \; ; \qquad \left.\frac{\partial}{\partial s}\Phi(s, s', t)\right|_{s=0} = -a \; . \tag{2.39}$$

With these boundary conditions the solution for the mean-square displacement for a primitive chain segment is [39]:

$$\langle (\mathbf{r}_p(s,t) - \mathbf{r}_p(s,0))^2 \rangle = \frac{2k_B T a^2}{N^2 b^3 \zeta} t + \sum_{k=1}^{\infty} \frac{4\hat{L}a}{k^2\pi^2} \cos\left(\frac{k\pi s}{\hat{L}}\right)^2 [1 - \exp(-tk^2/\tau_d)] \; , \tag{2.40}$$

where τ_d is called the reptation or disentanglement time and is given by [36, 39]:

$$\tau_d = \frac{\zeta N^3 b^5}{\pi^2 k_B T a^2} = \frac{\zeta L^3 b^2}{\pi^2 k_B T a^2} \; . \tag{2.41}$$

Increasing with the third power of the polymer contour length, for long polymers with $N \gg 1$ the reptation time is much longer than the rouse time, compare Eq. (2.8), which scales as N^2.

Note that due to the flexible nature of the polymer, this time measures both the rotation of the primitive path as well as the fluctuations of the end-to-end distance. For semiflexible to stiff polymers, see the next sections, we have to distinguish between these processes. Here, we define τ_d as the time required to leave the initial tube around the polymer, i.e., to diffuse a distance L.

Like for the chains in dilute solution, compare Eq. (2.9), we may derive simple scaling laws in two limits relative to τ_d. For $t \ll \tau_d$ it follows:

$$\langle (\mathbf{r}_p(s,t) - \mathbf{r}_p(s,0))^2 \rangle \approx a \left(\frac{k_B T}{N b \zeta} t \right)^{1/2} . \tag{2.42}$$

For later times, $t \gg \tau_d$ we approximate:

$$\langle (\mathbf{r}_p(s,t) - \mathbf{r}_p(s,0))^2 \rangle \approx \frac{k_B T a^2}{3 N^2 b^3 \zeta} t . \tag{2.43}$$

Thus it follows that the reptation time is the longest characteristic time of this problem, above which only linear diffusion with an effective diffusion coefficient occurs. Whereas the behavior at large times may trivially be expected, a simple argument for the power-law behavior at small times may be helpful in the further discussion:
The movement along the tube is diffusive, hence the mean square distance traveled along the tube increases with t. We assume that at the small times under consideration almost all polymer segments remain in the initial tube, which follows a Gaussian distribution. Then, according to Eq. (2.38) if the chain moves a distance $\psi(t)$ along the tube, with $\langle \psi^2(t) \rangle \propto t$, the real mean square distance changes according to

$$\langle (\mathbf{r}_p(s,t) - \mathbf{r}_p(s,0))^2 \rangle \approx a \langle |\psi(t)| \rangle \approx a t^{1/2} . \tag{2.44}$$

Using the full Gaussian distribution and performing the actual integral for calculating the average in the above equation would even result in the correct prefactor to the power-law [39].

It is possible to include contour length fluctuations of the primitive path in the calculation. However, they are found to have no significant effect on the scaling and only a small effect on the disentanglement time, which vanishes for long chains.

In view of the later comparison with semiflexible polymers and due to the easier access to this observable in computer simulations, we are interested in the mean square displacement of the end-to-end vector of the actual polymer. Up to now we have considered the primitive path only, which is a reasonable description for the polymer movement only at times above some threshold value. Starting at very small times, we now discuss the additional effects that need to be considered when determining the MSD of the polymer. As the calculation is rather lengthy and does not result in any further insides, we only reason the final form of the results.

For very small times the contour of the polymer does not feel the constraints imposed by the surrounding obstacles. Consequently, we may use the results established for the dynamics of a segment of a free Rouse chain in dilute solution at times much smaller than the longest relaxation time, see Eq. (2.7). For small enough times it follows:

$$\langle (\mathbf{r}(s,t) - \mathbf{r}(s,0))^2 \rangle \approx \left(\frac{k_B T b}{\zeta} t \right)^{1/2} \tag{2.45}$$

As soon as the contour interacts with the obstacles, i.e., when the average displacement is comparable to a, the tube picture and interaction between different chains become relevant. This timescale is called the entanglement time τ_e. With the previous result it may be estimated by:

$$\langle(\mathbf{r}(s,\tau_e)-\mathbf{r}(s,0))^2\rangle \approx a^2 \tag{2.46}$$

$$\Rightarrow \tau_e \approx a^4\zeta/k_BTb\,. \tag{2.47}$$

When each polymer segment is affected by the tube, we may treat it as part of the primitive path and its motion is valid for the chain. However, there is an additional contribution caused by the Rouse motion of the polymer chain along the primitive path, which is still free to take place. This motion corresponds to the motion of the undulations indicated in Fig. 2.2c).

At times larger than the Rouse time, see Eq. (2.8), the polymer may be treated as its average contour and the dominant motion is linear diffusion. Thus the primitive path picture may be applied at times above τ_R.

As we have shown before, cf. Eq. (2.9) the mean square displacement of a Rouse chain increases with $t^{1/2}$. If the motion along the primitive path is dominated by this contribution it can be shown by a reasoning completely analogous to Eq. (2.44) that the mean square displacement increases with $t^{1/4}$. Taking prefactors into account, the behavior at intermediate times is given by [39]:

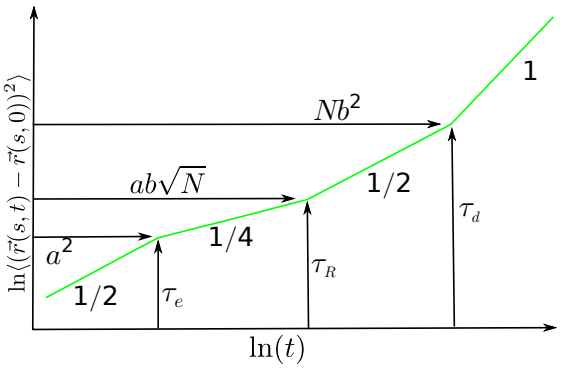

Figure 2.3: The power-laws for the time dependence of the mean square displacement occurring for a segment of a flexible polymer chain in a dense network are shown. The arrows give the crossover times and the corresponding values of Φ according to the theory of de Gennes [36] , Doi and Edwards [39].

$$\langle(\mathbf{r}(s,t)-\mathbf{r}(s,0))^2\rangle \approx a\left(\frac{k_BTb}{\zeta}t\right)^{1/4} \quad \text{for } \tau_e < t < \tau_R \tag{2.48}$$

Taking all these results together we may summarize the behavior of a flexible chain in a dense array of obstacles by the following set of power-laws:

$$\langle(\mathbf{r}(s,t)-\mathbf{r}(s,0))^2\rangle \approx \begin{cases} \left(\frac{k_BTb}{\zeta}t\right)^{1/2} & \text{for } t < \tau_e \\ a\left(\frac{k_BTb}{\zeta}t\right)^{1/4} & \text{for } \tau_e < t < \tau_R \\ a(\frac{k_BT}{Nb\zeta}t)^{1/2} & \text{for } \tau_R < t < \tau_d \\ \frac{k_BTa^2}{3N^2b^3\zeta}t & \text{for } \tau_d < t \end{cases} \tag{2.49}$$

For a better overview and comparison with the numerical data later, a graphical representation of the expected behavior is provided in Fig. 2.3.

With the solution to Eq. (2.37) it is also easily possible to calculate other observables like the correlation of the end-to-end vector $\mathbf{R}(t)$. Considering only the primitive path contribution it has been shown that [39]:

$$\langle \mathbf{R}(t) \cdot \mathbf{R}(0) \rangle = Nb^2 \sum_{k:odd} \frac{8}{k^2\pi^2} \exp(-k^2 t/\tau_d) \; . \tag{2.50}$$

Extension analogous to the segmental motion allows to include the fluctuations of the actual contour. In particular, yet unsurprisingly, it is found that the time dependence for the MSD of the end-to-end vector is identical to the one for the motion of a single chain segment.

Since the development of the original reptation theory, many alternative descriptions of dense systems of flexible chains based on the same picture and ideas have been put forward [28, 30, 44–46, 79–85]. These theories often differ in their mathematical approach, on numerical prefactors and sometimes give slightly different scaling predictions for the crossover times. However, the functional form is almost always very similar, if not identical to the one predicted by Doi and Edwards, keeping their theory not only the fundament, but also an important result on reptation [28, 30, 44–46, 80, 81].

With the fundamental processes and results clarified, we now turn to treating systems with rigidity.

2.2.3 The Doi-Edwards tube model for rigid rods

Using the same concepts as for the reptation of flexible chain, Doi and Edwards developed a theory for the diffusion of rigid rods in a densely crowded environment [38, 39, 86]. The basic assumptions are almost identical to the tube model for flexible chains. However, for rigid rods there is only global diffusion and rotation as there are no internal degrees of freedom in contrast to a Rouse chain. While this simplifies some aspects of the problem, it is still virtually impossible to give a full analytical solution to this problem. Nonetheless, several predictions for the dynamics are possible on a scaling level.

First, we discuss the meaning of a dense system and new problems arising in the study of (semi-)rigid objects in such a solution.
If, on average, all rods are free to rotate without interacting with another rod, the system may be described as a dilute solution. For this to occur, each rod requires a volume of about L^3, where L is the length of the rod. Thus only for densities above $\nu_1 \propto 1/L^3$ we expect a significant interaction between the rods and we call the system dense [39, 87]. However, our discussion is not valid for arbitrary densities $\nu > \nu_1$. While for the theoretical description we usually assume that each rod is a thin object of infinitesimal thickness, this simplification is not valid in experiments or computer simulations. Taking into account the finite diameter d of a stiff polymer chain results in an entropic effect known as the nematic transition [88].
A very dense system of any kind of elongated objects of diameter d exhibits an excluded volume interaction between these objects [88–92]. This interaction results in the alignment of the objects, and a nematic phase becomes the stable equilibrium conformation of the system. Such a nematic system violates several assumptions required for reptation theory and is indeed known to feature a completely different behavior [39, 89, 93, 94]. The critical density above

which the system becomes anisotropic has been found to be $\nu_2 \propto 1/L^2 b$ [88]. While both the nematic state and the isotropic-nematic transition are interesting physical problems, here we do not go into details as we focus on reptation processes in isotropic systems. Therefore, we always assume that we are using a solution with $\nu_1 \ll \nu \ll \nu_2$.

Thus, the density is supposed to be high enough to ensure that the radius of the effective constraining tube a is much smaller than L, as for the flexible chains. In contrast to a system of flexible chains, it is possible to derive a scaling law for the tube diameter a [39, 78]. Like for flexible chains, see Fig. 2.2 a), we consider the plane in which the rod lies. In contrast to the flexible case, such a plane always exists. The surrounding rods primarily intersect this plane as points. Given a typical distance $\xi_m = \sqrt{\frac{3}{\nu L}}$ between the rods, called the mesh size, the density of these intersection points is proportional to ξ_m^{-2}. Since the tube is defined as the largest cylinder around the rod of length L which does not intersect any of the obstacle points, the scaling of the tube diameter follows as:

$$a \propto \frac{\xi_m^2}{L} \ . \tag{2.51}$$

Note that the tube diameter is automatically smaller than the contour length if $\nu \gg \nu_1$.

For a rod in such a dense, isotropic solution, it is advantageous to split its movement into two parts. We define the orthogonal and parallel[4] contributions to the dynamics as the projections of the movement onto the end-to-end vector of the rigid rod. For any quantity $\mathbf{X}(t)$, we define $X_\parallel(t) := \mathbf{X}(t) \cdot \mathbf{e}_R(t)$ and $\mathbf{X}_\perp(t) := \mathbf{X}(t) - X_\parallel(t)\mathbf{e}_R(t)$, where $\mathbf{e}_R(t) = \mathbf{R}(t)/|\mathbf{R}(t)|$ is the normalized end-to-end vector of the rod for which $\mathbf{X}(t)$ is measured. Note that it is also possible to use $\mathbf{e}_R(0)$ in the definition. The two definitions give almost identical results for times much smaller than the longest rotational relaxation time τ_r as for those times the orientation of the polymer and thus $\mathbf{e}_r$ hardly varies. In contrast to a definition of parallelism and orthogonalism based on the orientation of the tube, this definition is easily accessible and well-defined even for a single configuration.
The rod is a stiff object and its rotation is hindered by the surrounding obstacles, i.e., the tube. Therefore it is reasonable to assume that $\mathbf{e}_R$ only marginally deviates from the orientation of the tube as long as the length L of the rod is much larger than the diameter a of the tube, as assumed for a dense system. We use this definition to approximate in a well-defined way the projection onto the tube orientation.
We employ the same splitting in the discussion of semiflexible chains. However, keep in mind that this procedure only gives a reasonable approximation to the tube orientation if the polymer and hence the tube have a rather straight conformation.
Consider a typical conformation of a flexible chain, e.g., the polymer in Fig. 2.2. Frequently, there are several regions of the tube where the orientation of the tube differs significantly from the orientation of the end-to-end vector of the polymer. Therefore splitting the contributions as described above does not give a suitable description of the movement in these regions. Even more importantly, if a segment of a flexible polymer diffuses out of the original tube, it may almost completely freely acquire a new orientation, which is impossible in the semiflexible to stiff regime. Hence, caution is advised when approaching the semiflexible to flexible transition.

Similar to flexible chains, it is assumed that movement along the tube is free diffusion. In contrast, the orthogonal movement is supposed to be restricted to a distance comparable to

[4] Instead of parallel, the term tangential is frequently used.

the tube diameter. However, as $a \ll L$ the timescale of orthogonal diffusion is very small and usually neglected in the discussion. Thus, the diffusion constants in the two directions are [38]:

$$D_{\parallel} = 2\frac{k_B T}{\zeta L} , \tag{2.52}$$

$$D_{\perp} = 0 , \tag{2.53}$$

where ζ is the friction per unit length of the rod. The time τ_d to diffuse a distance equal to the contour length obviously follows as:

$$\tau_d = \frac{\zeta L^3}{2k_B T} . \tag{2.54}$$

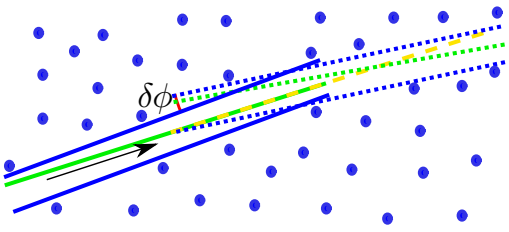

Figure 2.4: Basic idea for the scaling argument predicting the rotational diffusion of a rigid rod in a polymer network. After the polymer has moved at least half its length, the new tube is rotated by $\delta\phi$ to the original tube.

Given the diffusion of the center of mass of the rod, we are interested in quantifying the rotational diffusion.
There is a simple scaling argument to determine this quantity [38, 39]. While most of the rod is in the initial tube, its direction may only fluctuate around the tube axis and the average angular displacement is restricted by the tube radius. Mostly, the rod is not perfectly aligned with the original tube. Instead, it is tilted by an angle $\delta\phi$, which is on average proportional to a/L. The parallel diffusion along the direction of the rod then leads to the creation of a new tube, which is tilted by the same angle $\delta\phi$ relative to the original tube, see Fig. 2.4. In the new tube, the orientation of the rod fluctuates around the tube axis again and the process continues with a new, independent angular displacement leading to full rotational relaxation over large times.
The time τ_m for each of these steps may be estimated by the time for at least the major part, that is more than half of the rod, to move to a completely new tube. Therefore, this time is $\tau_m \approx (L/2)^2/D_{\parallel} \propto L^3\zeta/k_B T$. Taking these two parts together, the rotational diffusion coefficient D_r may be estimated as [38, 39]:

$$D_r \propto (\delta\phi)^2/\tau_m \propto \frac{a^2 k_B T}{\zeta L^5} . \tag{2.55}$$

If we restrict the rotation to the interval $[0 : 4\pi]$, it follows that the saturation time is proportional to the inverse of D_r. This is the longest relaxation time of the system, which is the disentanglement time for flexible chains. Thus for rigid rods $\tau_r \propto 1/D_r \propto L^5/a^2$, which is much larger than τ_d for a flexible polymer in a comparable system.
Up to this point we neglected the possibility that an obstacle forming the tube vanishs or newly appears during the process of the rod moving to a new tube. As the timescale in question is comparable to the time a rod needs to diffuse its own length, these processes are quite likely to occur. There may be an additional process changing the tube with timescale τ_m.

However, the alteration due to this process is of order a/L, too. Hence, both characteristic quantities are identical for the two processes. Consequently, the second process does not affect the functional form of our results, it only changes the numerical prefactors arising in the actual system [38, 39].

In a real system, especially in a polymer solution a completely rigid rod is impossible to realize. Therefore it is of great interest how finite stiffness influences the process of reptation.

2.2.4 The Odijk length and predictions for finite stiffness

Polymers with a finite, but significant stiffness cannot be adequately described by neither the completely flexible nor the rigid rod model of reptation. If a polymer moves out of its initial tube, the probability distribution for the orientation of the new region depends on the conformation of the polymer segments in the old part of the tube, but is not completely determined like for a rigid rod. Thus it is not surprising that experimental data for semiflexible polymers deviates from Doi-Edwards theories and their direct variants [55,95,96]. In principle, the existing approaches are combinations between the two previously discussed mechanisms.

As before, we assume that the solution is sufficiently dense to achieve a tube diameter $a \ll L$. Like for stiff polymers, a nematic transition may occur for semiflexible polymers, too. In this discussion we assume that the polymers are thin enough to avoid this transition. The system always is in an isotropic state.

Odijk introduced a new, fundamental concept suitable to cope with slightly bendable objects in form of an additional length scale [97]. The reasoning is: Consider a semiflexible polymer confined to a tube of radius a. Inside the tube the polymer is free and we may approximate the behavior of its segments as that of a free polymer. This means short sections of the polymer contour are supposed to exhibit orthogonal fluctuations according to Eq. (2.15). The orthogonal fluctuations of each section are restricted to be smaller than a^2, as the chain must stay inside the tube. Therefore, we may divide the polymer into several parts, a new one beginning where the polymer comes into contact with the tube. At each contact, the polymer is presumed to be deflected from the tube, such that the next part is free inside the tube and requires its own fluctuations to reach the tube again, see Fig. 2.5. The average section length L_e at which the contour comes into contact with the tube boundary may then be estimated by:

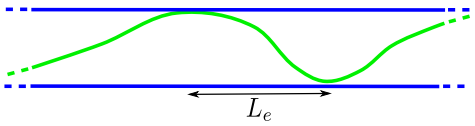

Figure 2.5: Excerpt of a semiflexible polymer (green) in a tube (blue) to visualize the concept of the Odijk length. At the contacts with the tube, the polymer is reflected back inside of the tube. The distance between contacts is L_e.

$$a^2 \propto L_e^3/l_p \tag{2.56}$$

$$\Rightarrow L_e \propto (a^2 l_p)^{1/3} \tag{2.57}$$

L_e is called the Odijk or entanglement length[5] and is a measure for the average distance between two neighboring contacts with the tube. Most theories, developed to treat the

[5] In the literature sometimes the name deflection length is an alternative term for the Odijk length.

reptation of semiflexible polymers, employ this quantity, although it is actually only known on a scaling level.

Like for the rigid rod, it would be interesting to derive a scaling relation for the tube diameter and thus for the Odijk length depending on the polymer properties and the mesh size $\xi_m = \sqrt{\frac{3}{\nu L}}$, where ν is the number density of the polymers. In fact, there are several contradicting predictions for the relation between these quantities.
Some works argue that the tube diameter should not be smaller than the typical distance between the chains [31, 40]. It is assumed to be identical to the average distance between the chains. This means:

$$a = \xi_m \quad \text{and} \quad L_e \propto \xi_m^{2/3} l_p^{1/3} \tag{2.58}$$

Several other works use a segment-based argument [78, 87, 98, 99]. There are different versions of this derivation of this scaling prediction, here we follow [78].
Assume that the tube is almost straight on lengths shorter or comparable to L_e. Remember that the orthogonal contour fluctuations on this range are smaller than a tube diameter and thus the segments of length L_e may be regarded as rigid rods. Consider the plane, in which this straight piece lies. As before, the surrounding chains are represented as point obstacles in this plane. The density of these point obstacles is proportional to ξ_m^{-2}, by definition of ξ_m. The tube diameter corresponding to the maximal radius a of a cylinder of length L_e in this plane is $a \propto \xi_m^2 / L_e$. Together with the definition of the Odijk length in Eq. (2.57), it follows that [78, 98]:

$$a \propto \xi_m^{6/5} l_p^{-1/5} \quad \text{and} \quad L_e \propto \xi_m^{4/5} l_p^{1/5} \ . \tag{2.59}$$

In this picture the tube diameter is smaller than the mesh size, as $l_p > \xi_m$. This occurs due to the variable distance of the obstacles to the polymer along its contour.
There are numerical works favoring both scaling predictions [29, 31]. In Sec. 4.1 we use our simulations to test these two scaling predictions for the Odijk length.

The reader is warned that none of these scaling laws is valid throughout all parameter regimes. Consider rather rigid polymers with $l_p > L(L/\xi_m)^4$. For these quite stiff objects it would imply $L_e > L$ which is physically meaningless. The distance between contacts along the polymer may not be larger then the length of the chain. Thus the original scaling predictions of Doi, Eqs. (2.51) and (2.55) should be preferred in this case [97]. Note, additionally, that it is not clear whether any of these scaling laws hold true. However, we employ these scaling laws later to compare the theoretical predictions with our results and find quite acceptable agreement.

For a system of semiflexible chains with a meaningful value of L_e, several different models for the reptation behavior have been put forward, which we compare to our data in Sec. 4.1.2. We do not give details on all the models, as this would go beyond the scope of this work. At least, we give the prediction for the longest relaxation time of the system for each model, due to the special significance of this observable. Especially, it is easily accessible in both simulations and experiments, and may be used for an easy first comparison later on.

The Odijk theory of reptation

After introducing the entanglement length, Odijk derived a scaling prediction for the rotation of polymer chains with $L_e < L \lesssim l_p$ [97]. It is basically a modified version of the original reptation theory for flexible chains, where the Odijk length replaces the segment length of the primitive chain. To move a distance L_e parallel to the tube, the polymer approximately requires a time $\tau_{L_e} \approx \zeta L L_e^2/k_BT$. Implicitly, it is thus assumed that the diffusion coefficients and, correspondingly, τ_d are as predicted in the Doi model for rigid rods, Eq. (2.52) and Eq. (2.54). Then an Odijk segment may acquire a new orientation with the average angular displacement in each step being proportional to $a^2/(LL_e)$. This follows from the assumption that each segment behaves like a rigid rod and rotates by an average angle of $\delta\phi \propto a/L_e$, cf. Sec. 2.2.3. As only one of the L/L_e segments changes direction, the average angular displacement is $(L_e/L)\delta\phi^2 = a^2/(LL_e)$, as claimed. From the step size and the required time follows Odijk prediction for the rotational diffusivity and, hence, the longest relaxation time [97]:

$$\tau_r \propto D_r^{-1} \propto \frac{\zeta l_p L^2}{k_BT} \quad \text{for } L_e < L < l_p \; . \tag{2.60}$$

Note that this scaling of the longest relaxation time may be derived without referring to the Odijk length, using an argument analogous to the Doi model for rigid rods, see Sec. 2.2.3. Consider again a polymer that has traveled at least half its length in a time proportional to L^3. The new tube may then deviate by an angle $\delta\phi$, which is now dominated by the tangent-tangent correlation instead of tube properties. This leads to $\delta\phi^2 \propto L/l_p$ such that the equilibration time is proportional to l_pL^2. Odijk assumed that for $L > l_p$ the flexible predictions of Doi and Edwards become valid.

The Doi model for semiflexible chains

In an alternative approach, Doi developed a different theory for semiflexible chains [100]. Assuming fixed obstacles, the basic equation of motion is supposed to be identical to those of the flexible Doi-Edwards theory, Eqs. (2.33) and (2.34) neglecting all orthogonal fluctuations. In contrast to the original theory, a dependence on the parts staying in the tube is introduced for the orientation of the chain parts diffusing out of the tube. For example, a new segment in the region $0 < s < -\Delta s$ is created according to

$$\mathbf{r}(s, t+\Delta t) = \mathbf{r}(0, t+\Delta t) - \int_s^{-\Delta s} \mathrm{d}s' \boldsymbol{\mu}(s', t) \; , \tag{2.61}$$

where $\mathbf{r}(s,t)$ is the position of the polymer segment at arc length s at time t. $\boldsymbol{\mu}(s,t)$ is a random variable of unit length representing the newly created tangent vector. It is drawn from the equilibrium distribution of the tangent vectors, which easily follows from the potential of the worm-like chain model, Eq. (2.10). An analogous equation holds for the case $L < s < L + \Delta s$, see [100] for details.

From the equation of motion Eq. (2.33), the diffusion coefficient of the center of mass may be calculated to be:

$$D_G = \frac{k_BT}{6\zeta L^3}\langle R^2 \rangle \; , \tag{2.62}$$

where $\langle R^2 \rangle$ is the average end-to-end distance of the polymer, see Eq. (2.16). In the limit of rigid rods, this equation is identical to the assumption of free one-dimensional diffusion as the dominant process.

To determine the internal dynamics of the chain, an approach analogous to the case of flexible chains is used, as the equation of motion is identical. We have to solve Eq. (2.37) with adjusted boundary and initial conditions. The initial condition is the tangent-tangent correlation of the worm-like chain model: $\Phi_{wlc}(s, s', t = 0) = \exp(-|s - s'|/l_p)$. For small values of Δs the boundary conditions follow from Eq. (2.61) as

$$\left.\frac{\partial \Phi_{wlc}(s, s', t)}{\partial s}\right|_{s=L} = -\Phi_{wlc}(s, s', t)/l_p \quad \text{and} \quad \left.\frac{\partial \Phi_{wlc}(s, s', t)}{\partial s}\right|_{s=0} = \Phi_{wlc}(s, s', t)/l_p \quad (2.63)$$

The solution to the differential equation with these boundary conditions directly determines the time correlation of the end-to-end vector as a special choice of s and s' [100]:

$$\langle \mathbf{R}(t) \cdot \mathbf{R}(0) \rangle = L^2 \sum_{k=1}^{\infty} \frac{2 L l_p \sin(\alpha_k)^2}{\alpha_k^2 (L^2 + l_p^2 \alpha_k^2 + L l_p)} \exp\left(\frac{8 \alpha_k^2 k_B T}{\zeta L^3} t\right) , \quad (2.64)$$

where the α_k are the positive roots of the equation $\alpha_k \tan(\alpha_k) = L/l_p$. The limiting cases of the longest relaxation time $\tau_r = \zeta L^3 / 8 \alpha_k^2 k_B T$ are in agreement with previous results. For flexible chains the Rouse time, Eq. (2.8), and for rigid chains the Odijk prediction, Eq. (2.60) are recovered.

Taking all possibilities for the density and stiffness from this and previous reptation theories together, Doi classified the scaling behavior of the longest relaxation time in dependence on the contour length of the polymer as follows:

- for $L < a$ one finds free rotation, thus $\tau_r \propto L^3$
- for $a < L < L_e$ the polymer behaves as a rigid rod, $\tau_r \propto L^5/a^2$
- for $L_e < L < l_p$ the Odijk prediction works, $\tau_r \propto L^2 l_p$
- for $L > l_p$ the flexible picture of de Gennes is valid $\tau_r \propto L^3$.

Note that the boundaries are not exact, and rather give the scaling of the crossover lengths between the different regimes.

As all these predictions deviate from the measured results for purely entangled solutions, Doi gave an additional scaling argument for such a system [100]. The aim of this model is to take into account the motion of the obstacles representing the surrounding polymers. The argument goes as follows:
Averaging a semiflexible chain over a suitable timescale allows treating it as an effective rigid rod. The length $\tilde{L}$ of this rod may be estimated by projecting the average length of the real polymer onto the orientation of the central segment. Then $\tilde{L} \propto l_p [1 - \exp(-L/2l_p)]$. The Doi -Edwards theory for rigid rods determines the relaxation time of this effective rod as:

$$\tau_r \propto L \tilde{L}^4 / a^2 . \quad (2.65)$$

Assuming that the scaling relation of the tube radius derived for rigid rods, Eq. (2.51), is valid for the polymers under consideration this finally leads to $\tau_r \propto L \tilde{L}^7 \nu^2$. In summary, this approach is just a slight modification of Doi's original rigid rod model [38].

Semenov's approach to reptation

An alternative calculational approach to the reptation problem was developed by Semenov [98]. The calculation employs the distribution function of the direction and position of a segment given arc length and time. This results in a differential equation similar to Eq. (2.37). The main result:

$$\tau_r = \zeta L^2 l_p/(4k_BT) \tag{2.66}$$

corresponds on a scaling level with the Odijk model for semiflexible chains, but is supposed to be exact including the prefactor [98]. As no new insight with respect to the processes involved in reptation may be gained from an explicit discussion of his calculations, we do not give any details here.
Semenov's work also include the first derivation of the scaling of the Odijk length and the tube diameter as presented in Eq. (2.59).

The reptation theory of Granek

Granek [40] employed a self-consistency approach in order to determine the exact dynamics of semiflexible polymers in dense solution for $a \ll L_e \lesssim l_p \ll L$. In analogy to the flexible model, it is assumed that stored length, i.e., undulations, may travel along the chain, affecting the diffusion along the tube. The effective diffusion coefficient originating in this process may be estimated as follows:
The length fluctuations of a semiflexible polymer are of order L^4/l_p^2, see Eq. (2.31). The time required to move such a distance is proportional to the equilibration time $\tau_{i,l}$ as given in Eq. (2.30). The contour undulations cause an effective diffusion with $D \propto \left(L^4/l_p^2\right)/(L^4/l_p) = 1/l_p$.
As the center of mass diffusivity scales as $1/L$, for polymers with $l_p > L$ the length fluctuations do not contribute significantly to the total diffusion along the tube. This differs from flexible chains, where the length fluctuations cause the dominant contribution at times below the rouse time.

Remember that the Odijk length is the average length between contacts with the confinement. Due to collisions with the surrounding chains, a polymer may only fluctuate freely up to a length L_e. The magnitude of the length fluctuations of each such segment may be estimated from the behavior of free semiflexible chains, Eq. (2.31) to be:

$$\Delta R_{L_e}^2 \propto \frac{L_e^4}{l_p^2} = \frac{L_e a^2}{l_p} \,, \tag{2.67}$$

where a is the tube diameter as before.[6] Assuming that the fluctuations in the different segments are independent, we may easily calculate the variance of the polymer length. There are L/L_e segments, each contributing the calculated fluctuations. If the solution is dense and there are enough segments, a Gaussian approximation becomes valid and the total variance is:

$$\Delta R^2 \approx (L/L_e)\Delta R_{L_e}^2 \propto \frac{L L_e^3}{l_p^2} = \frac{L a^2}{l_p} \,. \tag{2.68}$$

[6] Note that Granek uses a different definition for L_e, such that L_e in [40] corresponds to a here.

In the original argument, the average tube length $\bar{L} = L(1 - \frac{L}{6l_p})$ is used instead of L in Eq. (2.68). However, as this additional dependence does not change the scaling behavior we do not incorporate it here.

Analogously, the typical time for the fluctuations to reach this value follows from the free behavior, Eq. (2.30):

$$\tau_e \propto \frac{\zeta L_e^4}{k_B T l_p} \,. \tag{2.69}$$

This time is called the entanglement time in analogy to flexible chains. As it is the time required for a segment of length L_e to relax, we call this the Odijk time.

Similar to Odijk's approach, now the semiflexible polymer is replaced by an effective flexible chain, where each segment is of length L_e. This effective chain of L/L_e segments is supposed to behave approximately as a chain in dilute solution. The longest relaxation time is then the Rouse time, Eq. (2.8), of the effective chain:

$$\tau_R \propto (L/L_e)^2 \tau_e \propto L^2 L_e^2 / l_p \,, \tag{2.70}$$

as τ_e is the typical relaxation timescale of a single segment. Now, this flexible picture allows to argue similar to the Doi-Edwards theory. Yet, effective diffusion coefficients, like the one introduced above, are used.

Consequently, the predicted time dynamics are very similar to the flexible case as presented in Sec. 2.2.2. At small times $t < \tau_e$, a semiflexible behavior with a MSD proportional $t^{3/4}$ like in the free case, Eq. (2.32) is expected. In dependence on the stiffness a different time-ordering of the relaxation processes occurs. Therefore, two slightly different results are found for later times [40]:

- For $L \gg l_p^3/a^2$ the original Doi/Edwards dynamics, see Fig. 2.3 with a time dependence of, in that order, $t^{1/2}$, $t^{1/4}$, $t^{1/2}$, t for times larger than τ_e is found. However, the crossover times differ from the flexible case.
- For $L \ll l_p^3/a^2$ instead of the $t^{1/4}$ regime a regime proportional to t occurs and the crossover times appear in a different order. The scalings of the crossover times do not change.

For details on the derivation or the crossover times, see [40].

Calculations by Morse

Morse treated the topic of reptation with special focus on the viscoelasticity of an entangled polymer solution [20, 21, 87]. He predicted the occurrence of four distinct density regimes, where we are only concerned with the stiff case $l_p \gg L$ [87].

- At low densities $\nu \ll 1/L^3$ the polymers scarcely interact and the system is a dilute solution.

- At concentrations $1/L^3 \lesssim \nu \lesssim l_p^{1/2}/L^{7/2}$ the rotation is hindered by the surrounding. However, the average orthogonal contour fluctuations of order $\sqrt{L^3/l_p}$ are still smaller than the tube diameter. The latter is assumed to be $a \propto 1/\nu L^2$ as predicted by Doi for rigid rods, see Sec. 2.2.3. This regime with free contour fluctuations is called loosely-entangled.

- Consequently, in the density range $l_p^{1/2}/L^{7/2} \lesssim \nu \lesssim 4/(dL^2)$, where d is the diameter of the filaments, the contour fluctuations are restricted by the tube. In this regime the Odijk length becomes relevant, as the chain collides several times with the tube due to fluctuations. It is termed tightly-entangled regime.

- For high densities $\nu \gtrsim 4/(dL^2)$ the nematic phase appears, as already discussed in Sec. 2.2.3.

Morse's works focus on the tightly entangled regime. The primitive path picture known from previous models is modified in order to treat the primitive path as a semiflexible chain. Also, the approach includes the coupling of orthogonal and parallel contour fluctuations. As in previous arguments several timescales for diffusion over characteristic lengths are used. However, the diffusivity of the original polymer is employed in their derivation in contrast to the effective diffusivity used by Granek. These papers focus on providing quantitative results where possible [20, 21, 87].

As we are primarily interested in scaling laws and power-law descriptions of the dynamics, we do not discuss this model explicitly. Like in the approach by Granek, apart from the $t^{3/4}$ regime characteristic for free worm-like chains at small times, the predictions of this model correspond to models already discussed here with modified crossover times. The longest relaxation time is calculated to be [20, 21, 87]

$$\tau_R = \frac{6\zeta L^2 l_p}{k_B T} \,. \tag{2.71}$$

2.2.5 Constraint release models

The original derivation of reptation is for a chain in completely fixed obstacles [36, 37]. Yet, it is frequently assumed that the results of theories based on the reptation or tube model also hold for a purely entangled system [21, 31, 40, 42, 65]. In this case all objects move and the surrounding of each chain is subject to the same motion as the observed chain. The argument for the generalization is as follows:
The diffusion of a chain along the tube is essentially free. But if the observed polymer tries to move beyond the tube diameter in the orthogonal direction, it has to drag the tube along. The tube is composed of several chains, which then have to move together with the observed polymer. As a crude approximation there are $L/a \gg 1$ such polymers and hence the total friction for moving in the orthogonal direction is increased by the same factor. Additionally, each of the neighboring polymers is in a tube of its own and for movements larger than its respective tube diameter it has to drag along even more chains, increasing the effective friction further. Since this increases of the effective friction in the orthogonal direction, the orthogonal diffusion is assumed to be much slower than the diffusion along the tube. This separation of

timescales is supposed to justify the assumption that there is no orthogonal diffusion at scales larger than the tube diameter. Due to this reasoning, it is usually assumed that the tube acts as a fixed obstacle throughout the reptation process even in a purely entangled polymer solution.

However, in an entangled system all the chains move constantly and it is in principle possible that the tube deforms over time by an additional mechanism apart from classical reptation. None of the models discussed up to now includes such a constraint release mechanism independent from the diffusion of the observed polymer along the tube. Here we give a short overview over some possible constraint release mechanisms and on their expected significance for the dynamics.

Among the first discussed additional mechanisms are tube length fluctuations [79, 101, 102]. For a flexible polymer, the contour is usually coiled up inside the tube, reducing the average tube length to a value much shorter than the polymer contour length. Depending on how strongly the polymer is coiled, the tube length fluctuates around this average value. Due to the flexible nature of the chains, we may assume that the tube length obeys a Gaussian distribution with corresponding mean. In the classical reptation theory this effect is neglected and the tube length assumed to be constant. For several versions of the flexible reptation theory it is possible to take this additional effect into account [30, 44, 79, 101, 102]. It hardly affects the occurring power-laws in the relaxation of a single chain [30, 44, 102]. However, among other small changes, it most importantly leads to an increased dependence of the longest relaxation time τ_r on the length of the polymers in solution. While for the classical reptation theory it holds $\tau_r \propto L^3$, with this effect it approaches $\tau_r \propto L^{3.4}$ [101, 102]. As this higher dependence is expected from experiments, this modification was a major success of the reptation theory.
To our best knowledge, this effect has not yet been considered for semiflexible polymers. However, for polymers with $l_p \gtrsim L$ in dilute solution the average end-to-end distance is similar to the contour length of the polymer and the distribution exhibits a more pronounced peak [8, 16]. Hence, we expect the effect of tube length fluctuations in dense solution to be negligible as the end-to-end distance should not vary more strongly than in dilute solution.

Another possible description of constraint release is termed tube enlargement [41, 45, 46]. Due to the motion of the surrounding chains, the tube diameter around each chain is considered to increase during the reptation process of the chain leaving its original tube. The increase of the tube diameter is supposed to originate in the different lifetime of the surrounding chains. Consider a test chain confined in an array of other chains. The points of contact with the surrounding chains are distributed along the tube length of the obstacle chains. If the contact is close to the end of a chain's tube, the average time required for that chain to leave this region by reptation is much smaller than for a chain where the contact occurs close to the center of the tube. Effectively, the obstacles have a distributed life time, after which they vanish.
As soon as an obstacle has disappeared, it is assumed that the observed polymer explores the additional space up to the next obstacle leading to an increase of the tube diameter over time. To specify this increase of the tube diameter, usually a self-consistency argument is employed [41, 45].
Recall that according to classical reptation theory the longest relaxation time of a flexible chain is proportional to the inverse of the tube diameter square, cf. Eq. (2.41). Thus an in-

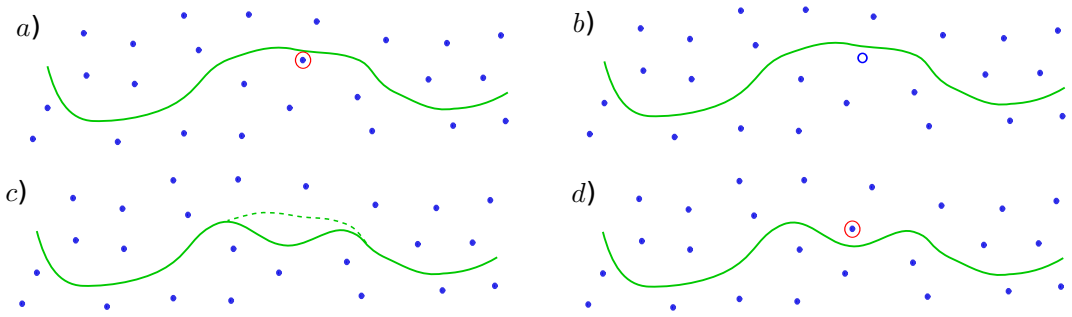

Figure 2.6: Two dimensional representation of the possible origin of convective constraint release. a) The primitive path (green) is confined by several obstacles (blue). Through reptation of an obstacle chain, e.g., the one in the red circle, the obstacle vanishes. The region blocked by the vanished obstacle, indicated by the small blue circle, is now available to the primitive path as shown in b). Through orthogonal fluctuations the primitive path may now acquire a new conformation in this region, shown in c). The old conformation is still shown as a dashed line. d) At a later time a new obstacle, marked by a red circle for better visibility, may appear. Thus a new tube conformation becomes fixed.

crease of the tube diameter is expected to accelerate relaxation. As the movement of the polymers are usually still modeled according to classical reptation theory, there is little effect on the relaxation dynamics. This mechanism is usually considered to be most relevant in polydispers systems, i.e., systems with polymers of different contour lengths, for which it was originally proposed [45]. For monodispers flexible chains at most a weak effect on the relaxation times is expected [41, 46].
Again, for semiflexible polymers this effect is much less studied. Experiments find no continuous dilation of the tube, but significant fluctuations of the tube width [33]. Recall that most predictions for the reptation of semiflexible polymers exhibit none or at most a much weaker tube width dependence, see the previous section. Also, note that a semiflexible polymer may not as easily as a flexible chain explore a newly vacated region orthogonal to its contour due to the bending stiffness. Thus we expect this process not to significantly alter the reptation dynamics of semiflexible polymers.

The last mechanism we discuss here is called convective constraint release. Actually, there are several different models for this type of mechanism, differing in the predicted contribution to reptation [44, 46, 65, 79–81, 103–105]. While similar to tube dilation in some sense, it is usually considered a separate mechanism.

The basic idea of this mechanism is sketched in Fig. 2.6. Consider a polymer confined by an array of surrounding chains, all subjected to reptation. For simplicity, assume that the primitive path of the polymer lies almost in a plane. As soon as one of the chains acting as an obstacle reptates out of this plane, the corresponding obstacle vanishes. The typical timescale for this is proportional to the reptation time τ_d of the surrounding polymers. The polymer and thus the primitive path may now explore a previously inaccessible region and thus the tube may acquire a new conformation. A new obstacle may emerge when a new polymer reptates into this vacated region, or the old one reptates back to slightly changing its location in the process. With the new obstacle the process yields a final state similar to the initial one. Especially the tube radius has returned approximately to its original value.
Each step of this process results in the reorientation of a segment of the tube in a time proportional to τ_d. In the easiest case, we now use the Doi-Edwards picture to represent the

tube like the primitive path as a Gaussian chain of L/L_e links [65, 79, 81, 103, 104]. Note that the entanglement length is slightly different for a flexible chain, but this is of no concern here. Assuming that the effective chain behaves almost like a free chain in dilute solution, the time required for the tube to relax by constraint release is given by:

$$\tau_{\mathrm{cr}} \propto (L/L_e)^2 \tau_d \,, \tag{2.72}$$

where τ_d is the reptation time of the surrounding polymers. If the solution is monodisopers, approximately $\tau_{\mathrm{cr}} \propto L^5 b^2/\xi_m^4$, which is much larger than τ_d.
Hence, this process of constraint release also modifies the reptation dynamics and derived quantities only weakly. However, consider a polydispers systems, where the observed polymer is of length L and the surrounding network polymers of contour length L_n. For simplicity, we assume that the segment length and mesh size are kept constant. Then $\tau_{\mathrm{cr}} \propto L^2 L_n^3 b^2/\xi_m^4$ which may be faster than τ_d for $L_n \ll L$. Again, this mechanism is relevant for polydispers systems [30, 46, 65, 81].

2.2.6 Results of previous Simulations

Numerical simulations play a major role to test the theoretical predictions and gain further insights in the occurring processes.

The first successful numerical test of the original Doi-Edwards theory was performed by Kremer and Grest [58, 59]. Based on a completely flexible chain model, each chain is represented by N beads connected to their neighbors by a suitable spring potential. The steric interaction is included as a repulsive Lennard-Jones potential between the beads. Several such chains are then simulated in a box with periodic boundary conditions. Consequently the simulated system corresponds to a purely entangled solution with all possible additional mechanisms of constraint release. In their extensive work, the power-laws predicted for the relaxation behavior by the classical reptation theory, cf. Eq. (2.49), were found to agree with the results of the simulations. Based amongst others on these results, reptation theory appears to be an appropriate description for the movement of single polymers in solution. Therefore this study still is among the most important numerical simulations for reptation.

In the course of time, several more simulational studies concerning the reptation of flexible polymers have been performed [34, 106–108]. With the basic description clarified, they often focus on specific topics. For example, some studies discuss in detail the significance of constraint release mechanisms and which are required in the theoretical modeling [28,30]. Another frequent topic is the viscoelastic properties of a solution of entangled polymers [30, 109, 110]. As we focus on semiflexible polymers, we do not discuss these studies.

For semiflexible to stiff polymers, there is less simulational data. Also, most existing simulations consider the movement of a single mobile chain in an array of fixed obstacles. The first attempts focused on the dynamics of a thin rigid rod in a dense environment of point obstacles, both in two and three dimensions [35, 42, 111]. In particular, simulations of rigid rods in fixed point obstacles agree with the Doi prediction for the scaling of the rotational relaxation time [35].

There is a more general simulation and accompanying theoretical analysis, which studies a semiflexible polymer with $l_p \gtrsim L$ [31, 32]. As we discuss an assumedly similar system in this thesis, here we shortly discuss the main results of this paper.

The simulation works in two dimensions, as before with fixed circular obstacles [31]. Apart from the standard worm-like chain bending potential, the single mobile chain is represented similarly as a chain in the simulations of Kremer and Grest [59].

As expected in the tube picture, the diffusion parallel to the chain is essentially free, one dimensional diffusion. Hence, the longest relaxation time is estimated as the time required to diffuse the effective tube length. Note the difference to the definition used in this thesis, as it does not ensure that orientational correlations decay. It is closely related to our τ_d, so that we use this symbol here for this prediction. The tube length is assumed to be shorter than the contour length due to the longitudinal fluctuations of the chain, which are approximated by the dilute case. In accord with the simulations the disentanglement time is [31, 32]:

$$\tau_d \propto \zeta L^3 \left(1 - \frac{L_e^{3/2}}{L^{1/2} l_p}\right) . \tag{2.73}$$

Starting with small times, the orthogonal fluctuations of the polymer dominate the behavior, as usual in the semiflexible case, cf. Sec. 2.1.3. As in previous studies, the relaxation behavior at times smaller than the entanglement time is free relaxation of a semiflexible polymer [31,32]. Especially, the predicted behavior at times $t < \tau_e$, the expected entanglement time τ_e, and the saturation value of the contour fluctuations correspond to the results of Granek [40]. τ_e is as in Eq. (2.69) and the contour fluctuations follow Eq. (2.32). From the tube picture, it is claimed that in the next time regime the chain may not explore lateral space outside the tube radius. Thus, the dynamics should be dominated by the longitudinal chain fluctuations. Using a scaling argument and in accord with the simulations it is found that mean square displacement of a segment in this time regime increases with $t^{1/2}$. The longest internal relaxation time until the chain is relaxed equals [31, 32]:

$$\tau_{i,l} = \zeta L^2 L_e^3 / k_B T l_p^2 . \tag{2.74}$$

For times up to the onset of free diffusion, $\tau_{i,l} < t < \tau_d$, no further increase of the segmental MSD is predicted. However, the simulations supposedly show a super-diffusive increase of the orthogonal MSD with $t^{3/2}$ in the regime $\tau_r < t < \tau_d$. To explain the super-diffusive behavior, the following argument is used [31,32]: The orthogonal fluctuations are proportional to the longitudinal fluctuations, in the form $\langle \delta r_\perp^2 \rangle \propto \langle \delta r_\parallel^2 \rangle^{3/2} / l_p$. Assuming that the parallel fluctuations correspond to free diffusion along the tube for times $t > \tau_{i,l}$, this leads to an increase $\langle \delta r_\perp^2 \rangle \propto t^{3/2} / l_p$.
A cautionary remark: If the contour fluctuations are defined as absolute deviations from the initial position, this argument is also valid for times $t > \tau_d$. However, at these times standard diffusion instead of a super-diffusive behavior is observed. Alternatively, if $\langle \delta r^2 \rangle$ measures the deviation of the contour length, i.e., as a relative quantity, it is bounded by the equilibrium value, which this argument neglects. Seeing this, we should not be surprised to find this argument failing in our simulations.

To summarize the main findings with respect to the occurring dynamics, see table 2.1 for the predicted kinetic exponents in the power-law description $\langle \delta r^2 \rangle \propto t^\alpha$ of the dynamics [31, 32].

	$t < \tau_e$	$\tau_e < t < \tau_r$	$\tau_r < t < \tau_d$	$\tau_d < t$
α	3/4	1/2	3/2	1

Table 2.1: Kinetic exponents for the diffusion of a single chain in a dense array of obstacles, according to [31, 32].

While the same argument as for the flexible picture holds, it is not yet clear whether the simplification of fixed obstacles results in the correct behavior for a purely entangled solution. In particular, all those simulations neglect possible additional effects of constraint release mechanisms.

There are some attempts to model a purely entangled solution of semiflexible polymers with constraint release, mostly focused on viscoelastic properties. They either take a two-dimensional approach with movable obstacles or on directly simulate a large number of polymers in a box [29, 112].
However, none of the latter simulations was capable of reaching sufficiently long times, i.e., only times significantly shorter than τ_r were achieved [29]. Thus, neither the full dynamics of the reptation process nor all its characteristic times could be clarified.
This work constitutes the first complete picture of the reptation of semiflexible filaments in a purely entangled solution.

3 Details on model, simulational technique and data acquisition

This chapter introduces the simulation used to acquire the data analyzed in this thesis. We discuss the model and details of the specific implementation. In addition, we specify the numerical parameters and the variables used in the dimensionless representation of the results. Then, we discuss the observables analyzed later and their explicit definitions. Using known results, we show that our simulation works correctly within the manageable accurateness. Thus, we only consider statistical errors in the following chapters.

3.1 Model and algorithm

To model each individual polymer, we employ the standard approach for semiflexible polymers, introduced in Sec. 2.1.3. This is the worm-like chain model, with the equation of motion given in Eq. (2.11). Solving such a stochastic differential equation numerically requires a suitable discretization scheme.

This discretization consists of the following two steps. Firstly, we use the discrete model for semiflexible polymers, where the polymer consists of N segments, each of constant length b, such that $L = Nb$. The segments are then represented by point-like objects, commonly referred to as a *beads*. All attributes like the friction of a segment and all forces acting on it are then ascribed to the corresponding bead. Thus the friction coefficient of each bead is given by ζb. As mentioned in Sec. 2.1.1, this discrete model is in accordance with the continuous model for times $t \gg \zeta b^3/k_B T$.
Secondly, we introduce the time step Δt, which represents the smallest unit of time accessible in the simulation. Time derivatives of any observables x may then be approximated by $\frac{\partial x}{\partial t} \approx \Delta x/\Delta t$, where Δx is the change of x in the time interval Δt. To achieve meaningful results and a stable algorithm, we have to choose Δt much smaller than all characteristic times in the model. Thus, we at least require $\Delta t \ll \zeta b^3/k_B T$.

Having clarified the general procedure, first we specify our system, as a set of discretized chains. The final simulation comprises M polymer chains, each described by N beads at positions $\mathbf{r}_{i,k}(t)$ at time t with $1 \leq i \leq N$. The index k, with $1 \leq k \leq M$, is used to determine the chain. The bending stiffness of each chain k of the polymers is included as the discretized version of the worm-like chain Hamiltonian [66, 67]

$$\mathcal{U}_{\mathrm{WLC},k}[\mathbf{r}_{i,k}(t)] = (l_p k_b T/b) \sum_{i=1}^{N-2} (1 - \mathbf{u}_{i,k} \cdot \mathbf{u}_{i+1,k}), \tag{3.1}$$

with $\mathbf{u}_{i,k} = \frac{\mathbf{r}_{i+1,k}-\mathbf{r}_{i,k}}{|\mathbf{r}_{i+1,k}-\mathbf{r}_{i,k}|}$ the normalized bond vector between beads i and $i+1$. To keep the discussion simple, we restrict our analysis to the case of homogeneous systems, where all polymers have the same persistence length.

Apart from this adjustment to the discretization, the equation of motion in the simulations requires some additional terms relative to Eq. (2.11). We have to include the connectivity of the chain, which is realized by the inextensibility constraint Eq. (2.12) in the analytical calculations. Also, as we are interested in a dense solution of polymers with steric interactions, some form of excluded volume interaction is required to keep the polymers from crossing each other.

To achieve the chain connectivity, two separate numerical approaches exist [113]. We may either realize the actual constraint by employing Lagrangian multipliers or incorporate a stiff spring potential. The former approach leads to a so-called bead-rod algorithm, the latter is called bead-spring.
Conceptually, the bead-rod algorithm has the advantage of only permitting moves which do not violate the constraints. In principle these moves may then be performed using a larger value for the time step than a bead-spring algorithm with the same bond length fluctuations. Yet there are several drawbacks to this approach. Obviously, but not of major concern, we have to perform additional calculations to determine the Lagrangian multipliers. Also, an additional pseudo-potential has to be introduced in order to achieve the desired tangent-tangent correlation [114–116]. The main problem arises from the fact that the constraints correspond to a position-dependent null-space in the diffusivity. Therefore special care has to be taken in solving the equation of motion for $\frac{\partial r}{\partial t}$. Because it is a stochastic differential equation, an additional term involving the local derivative of the diffusivity arises in the Ito-formalism. This expression cannot be calculated directly, and poses a major problem. Interpreting the equation of motion as a kinetic stochastic differential equation solves this problem [114, 117]. Numerically, this interpretation results in a special, well-known mid-step algorithm [118, 119]. Taking all this together, several more equations have to be solved, and most of them twice. This algorithm is a good choice if the bond length fluctuations are the limiting factor for the efficiency of the simulation.
The bead-spring approach is conceptually simpler, yet might suffer from trading off simulational efficiency for increased fluctuations. The numerical time step needs to be smaller than the relaxation time of the springs used for the bonds. We need to balance the required run time, increasing with smaller values of Δt, and the fluctuations of the bond length limiting the available time steps.
As we have to include a very strong, short-ranged force for the steric interaction, our choice of time step is rather limited by this potential than from the bond length. Since the steric interaction also occurs in a bead-rod algorithm, the advantages of the constraint-based approach do not apply here. In conclusion, a bead-spring approach is more suitable if the steric interaction is incorporated by a potential, as we do here.

Thus, in our model the connectivity of the chain is maintained by finitely extensible nonlinear elastic (FENE) springs, which are well established for the use in polymer simulations [31, 58, 59, 120, 121]. Explicitly, for each chain k the beads are connected to their next neighbors by

the potential:

$$\mathcal{U}_{\mathrm{FENE},k}[\mathbf{r}_{i,k}(t)] = \sum_{1\le i\le N-1} \begin{cases} -B\ln\left[1-(\frac{b-\tilde{r}_{i,k}}{r_m})^2\right] & \tilde{r}_{i,k} < b+r_m \\ \infty & \tilde{r}_{i,k} \ge b+r_m \end{cases}, \tag{3.2}$$

where $\tilde{r}_{i,k} = |\mathbf{r}_{i+1,k} - \mathbf{r}_{i,k}|$ is the distance to the next bead and $r_m = b/4$ the maximum allowed deviation. To keep the fluctuations in the bond length small, we choose the spring constant $B = 1000k_bT$, such that in the final simulation the deviation in bond length from the equilibrium value is below $0.05b$ at all times. Thus to good approximation the contour length L of a polymer fluctuates only slightly around its equilibrium value $L = Nb$.

The last interaction included in our model is the steric interaction. Abiding the standard set by previous studies [31, 58, 59], we employ the Weeks-Chandler-Anderson (WCA) potential [122], which is equivalent to the repulsive part of a Lennard-Jones potential. The potential acting on bead i of chain k is given by

$$\mathcal{U}_{\mathrm{WCA},i,k}[\mathbf{r}_{i,k}(t)] = \begin{cases} A \sum\limits_{\substack{1\le l\le M \\ 1\le j\le N \\ j\neq i \text{ for } k=l}} \left[(\sigma/\tilde{r}_{i,j})^{12} - 2(\sigma/\tilde{r}_{i,j})^6 + 1\right] & \tilde{r}_{i,j} \le \sigma \\ 0 & \tilde{r}_{i,j} > \sigma \end{cases}, \tag{3.3}$$

where $\tilde{r}_{i,j} = |\mathbf{r}_{i,k} - \mathbf{r}_{j,l}|$ is the distance between the beads. σ determines the range of the steric interaction. To achieve a fast algorithm we choose $\sigma = 0.9b$. In order to prevent the crossing of chains and the overlapping of different beads we use a strong potential by setting the parameter $A = 20k_bT$. Note that a large value of A, like the one used here, should be used even for the WCA potential to guarantee that the chains are subject a hard interaction. While at first glance this might seem superfluous for the behavior at the length and timescales of interest, it affects the behavior even in a simple colloidal system [123].

In an additional test, we implement a quadratic spring potential instead of the WCA potential used normally in our simulations. Using a stiff enough spring, we find no alteration of the results within the statistical error. Thus the exact form of the steric interaction does not significantly affect the results.

These are all interactions used in our model. To sum it up, the polymers resemble impenetrable pearls on almost inextensible strings. This systems is based on standard interactions, and is thus very similar to those used in previous studies on similar topics [31, 58, 59, 106].

Having determined all required potentials, we determine the time evolution of the system. The full Langevin equation, including all contributions, that is used in the simulation has the form:

$$m\frac{\partial^2\mathbf{r}_{i,k}(t)}{\partial t^2} + \zeta b\frac{\partial\mathbf{r}_{i,k}(t)}{\partial t} = -\frac{\delta\mathcal{U}_{\mathrm{total},i,k}[\mathbf{r}_{i,k}(t)]}{\delta\mathbf{r}(s,t)} + \boldsymbol{\eta}_{i,k}(t)\,, \tag{3.4}$$

where $\mathcal{U}_{\mathrm{total},i,k} = \mathcal{U}_{\mathrm{WCA},i,k} + \mathcal{U}_{\mathrm{FENE},k} + \mathcal{U}_{\mathrm{WLC},k}$. The three-dimensional Gaussian white noise $\boldsymbol{\eta}_{i,k}$ acting on bead i in chain k has average zero, and an amplitude determined by the Einstein relation in three dimensions:

$$\langle\boldsymbol{\eta}_{i,k}(t)\,\boldsymbol{\eta}_{j,l}(t')\rangle = 6\,\zeta\,\delta_{ij}\delta_{kl}\,k_BT\,\delta(t-t')\,. \tag{3.5}$$

As reasoned in Sec. 2.1.1, we keep the free draining approximation throughout this study. In contrast to the previously discussed equation of motion, Eq. (3.4) includes an inertia term, with m the mass attributed to a bead. This term is included for numerical reasons only. Our test yielded that an algorithm including the inertia term resulted in a more stable simulation. Especially the computational efficiency was found to be much higher, as larger time steps could be used with inertia. The chosen value of m is discussed later in this section.

We reformulate the second order differential equation as two first order equations in the independent variables $\mathbf{r}$ and $\mathbf{v} = \frac{\partial \mathbf{r}(t)}{\partial t}$. The two equation of motions are then discretized in time as described earlier. For the time evolution we use a semi-implicit Euler algorithm to integrate Eq. (3.4). First, all forces acting on the system in a given configuration are evaluated. Then the velocity of each particle is updated and finally the new position of the particle is calculated. Writing it down as an equation for bead i in chain k this corresponds to:

$$\begin{aligned} \mathbf{v}_{i,k}(t+\Delta t) &= (1-\frac{\zeta b \Delta t}{m})\mathbf{v}_{i,k}(t) + \mathbf{f}_{i,k}(\mathbf{r}_{i,k}(t),t)\frac{\Delta t}{m} \\ \mathbf{r}_{i,k}(t+\Delta t) &= \mathbf{r}_{i,k}(t) + \mathbf{v}_{i,k}(t+\Delta t)\Delta t \ , \end{aligned}$$

where $\mathbf{f}_{i,k} = -\frac{\delta \mathcal{U}_{\mathrm{total},i,k}[\mathbf{r}_{i,k}(t)]}{\delta \mathbf{r}(s,t)} + \boldsymbol{\eta}_{i,k}(t)$ are the potential and stochastic forces acting on the bead.

To achieve the required densities, the chains were simulated inside a cubic simulation volume with edge length $\hat{A}$ and periodic boundary conditions. To avoid interactions of the two ends of the same polymer, which would allow reptating along the already existing tube, we choose $\hat{A} = 1.35L$. For a discussion of this choice, see Sec. 3.4. Given the simulation volume $V = \hat{A}^3$, we use the mesh size $\xi_m = \sqrt{\frac{3V}{ML}}$ to characterize the density of the polymer network.

In addition to the second order scheme, we use the following two procedures in order to achieve a fast algorithm.
We employ uniformly distributed random numbers instead of Gaussian distribution random numbers for the noise. Within the statistical errors both distributions amount to the same behavior at times $t \gg \Delta t$ [59, 113]. The creation of random numbers is among the most expensive tasks in terms of computational time in our simulation. Generating Gaussian distributed random numbers requires in most implementations the calculation of a logarithm. In our computer systems, this slows down the random number generation and thus the simulation by up to a factor 8 compared to using uniformly distributed random numbers. Thus, we employ a maximally equidistributed combined Tausworthe generator [124] to create uniformly distributed noise with zero mean and an appropriate scaling to achieve the desired second moment as given in Eq. (3.5).
Moreover, we employ a cell linked-list algorithm to speed up the calculations of the excluded volume forces [125]. As each bead may intersect with any other beads the steric interaction is the numerically most expensive calculation of this simulation. The obvious approach of simply determining the distance of each bead to all other beads requires $MN(MN-1)/2$ distance calculations. For systems with many chains M and acceptable discretization N this quickly becomes sumptuous. Therefore we employ a pre-sorting which limits the number of particles that have to be checked for collisions. The basic idea of this procedure is depicted for the analogous two-dimensional case in Fig. 3.1. First, the accessible volume is rasterized into

several identical, small, cubic cells of edge length greater or equal σ. Then for each bead it is determined in which cell it is located, which requires only some $3MN$ calculations. We may now determine all collisions and thus contributions from the steric interaction by considering cells. For a bead in a given cell it suffices to calculate the distance to the other beads in that cell and all cell directly around it. All beads in cell further away automatically have a distance grater than σ, even if the particle is close to the boundary of its cell. Thus we only have to check a significantly smaller volume for collisions, leading to an increase in efficiency.

With these methods our algorithm becomes fast enough to allow us to reach times above the terminal relaxation time in our study of reptation.

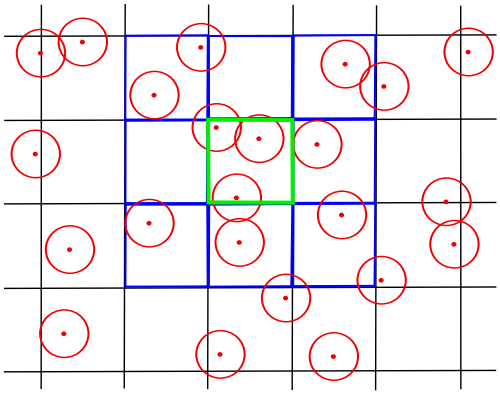

Figure 3.1: Two-dimensional representation of the employed sorting algorithm. For objects (red dots) in the green square, only objects in the green and blue squares have to be checked for possible collisions if the lattice spacing is larger than the interaction range (circles).

Like in any numerical simulation, all parameters and expressions are dimensionless in the actual calculation. For converting to and back, respectively, from this dimensionless system there is some freedom of choice on how to define the transformation. As commonly used, we choose the units in a way that $k_bT = 1$ and $\zeta = 1$ in all our simulations.
The final degree of freedom is used to define the length scale for the system. In many polymer simulations with excluded volume interactions the range σ of this potential is used as unit of length [58, 59, 106]. This is motivated by the analogous role in the study of colloidal systems, from which also the form of the potential has been adopted. We believe that this choice is not beneficial in our system due to the following reason. Our main focus resides in simulating slender filaments, where the diameter of the chain does not influence the dynamics. We show in Sec. 3.4 that we actually reach this limit. Consequently our value of σ does not need to be related to the actual diameter of the chain, but is rather arbitrary. Also, the properties of a semiflexible polymer are completely described by l_p and L at all times $t > \zeta b^3/k_BT$, as established earlier. As we choose $\sigma = 0.9b$ this lower timescale depends on σ. However, again this timescale is irrelevant and only serves as a lower boundary for the validity of our model. Likewise, no other relevant characteristics of our system intrinsically depends on σ. In conclusion, using σ as the unit of length introduces an additional, almost arbitrary length scale as a main parameter.
To avoid this problem we use the easily measurable contour length as our basic length scale and give all other lengths in multiples of L. With these three choices, all other quantities may be expressed in dimensionless form, e.g., ξ_m/L is used for the density of the system.
Also, we may easily derive a meaningful basic timescale with this unit of length. Expecting a diffusive behavior on the relevant timescales, we define a timescale τ in dependence on the basic length scale L for the presentation of our numerical results:

$$\tau = \frac{\zeta L^3}{6k_BT}\,. \tag{3.6}$$

This corresponds to the time the center of mass of a chain takes to diffuse its own contour

ξ_m	0.075	0.086	0.10	0.12	0.13	0.14	0.15	0.17	≥ 0.21
ϵ	138.9	138.9	104.2	104.2	104.2	104.2	69.5	104.2	69.5

Table 3.1: For each mesh size used in this thesis, the aspect ratio used to generate the data is given in this table.

length; Assuming free diffusion along the tube, after a time τ the chain should on average have moved to a completely new tube and thus $\tau_d \approx \tau$.

For later reference, an actin filament with a contour length of $L = 10\mu$m and a diameter of 5nm in a solution with a viscosity of 0.1Pa s at a temperature of $20°C$ has $\tau \approx 1.5\ 10^4$s.

Like the range of the steric interaction, two more parameters, the time step and the mass of a bead, are primarily numerical parameters. That means that their chosen values should not affect the results of our simulations on the timescales of interest. As usual in Brownian dynamics simulations, the mass is set to a value much greater than the actual mass of a corresponding segment of a real polymer [58, 59]. However, over-damped dynamics at all relevant timescales are ensured. This increases the numeric stability and allows for bigger time steps, making the simulation more efficient in terms of computational times. We used two different sets of masses and time steps to determine the behavior of the system at the different timescales. The small time behavior $t/\tau \lesssim 1$ was simulated using the values $m = 3\ 10^{-6}$ and a time-step $\delta t = 1\ 10^{-6}$, while the behavior at times $t/\tau \gtrsim 0.1$ is determined using the values $m = 3\ 10^{-4}$ and $\delta t = 2\ 10^{-5}$. To ensure the validity of the larger values, we checked that in the time $0.1 \lesssim t/\tau \lesssim 1$ both results agree within the statistical errors.
For b and N, respectively, we do not use fixed parameters. Instead we use b to adjust the range σ of the steric interaction thus fixing $N = L/b$. The used values of $b = \sigma/0.9$ are relevant for the aspect ratio, which is defined as the ratio of the chain radius to its length $\epsilon = 2L/\sigma$. We show in Sec. 3.4 that the value of ϵ for $\epsilon \gtrsim 70$ has almost no effect on the results of our simulations. Hence, for a shorter notation later on we do not explicitly give ϵ for each set of data. However, the value of ϵ may be determined from the mesh size ξ_m according to Table 3.1. Apart from the simulations discussed in Sec. 3.4 to determine the effect of ϵ on the results, we employ this unique assignment of ϵ.

3.2 Creation of initial conditions

In the first tests of our simulation, we employ an ordered initial condition, with all polymers aligned in one direction. This is certainly not an equilibrated configuration. To reach such a state, we need to simulate this system over a time of at least τ_r, the longest rotational relaxation time of the system. As this is also the longest relaxation time of all processes in the system, this procedure is too inefficient for productive use.

In order to construct an initial condition, which *ab initio* is close to equilibrium, we employ an approach motivated by the Monte Carlo algorithm. The initial configurations for the Brownian dynamics are generated by randomly placing chains with decreased range of the excluded volume one after the other in the simulation box. To simplify the procedure, a hard

core repulsion with infinite potential is assumed. More specifically, we apply the following procedure: Starting with an empty simulation box, we repeat steps a) to d) for placing chains of beads with diameter 0.6σ until the desired number of chains is present in the simulation volume:

(a) The first bead for a new chain is placed at a random position inside the simulation box.

(b) If there is no overlap with another bead already in the box, a second bead is placed at an arbitrary position on a sphere with radius b around the first bead. If this second beads overlaps with a previously placed bead, a new position on the sphere is generated and tested for overlap. This procedure is iterated until there is no overlap or 20 positions have been rejected, in which case the generation of the current chain is started anew by returning to step (a).

(c) With equal probability either end of the already existing part of the chain is chosen and a new bead is appended at this end. It is placed at a distance b to the existing bead currently ending the chain. The direction of the new bond vector is determined relative to the outermost, already existing bond vector at this end of the chain. For this, a polar angle is randomly chosen from the equilibrium distribution following from the worm-like chain potential Eq. (3.1). The azimuthal angle is drawn from a uniform distribution, and thus the position of the new bead is fixed. The newly placed bead is checked for an overlap with all previously placed beads and accepted only if there is none. Otherwise the current position is discarded and the procedure returns to the beginning of step (c). Once 20 attempts have been discarded in a row, the complete chain is discarded and the algorithm is reset to step (a).

(d) Step (c) is repeated until the required number of beads is attached to the chain such that is has contour length L.

The decreased range of the steric interaction is employed to make this procedure more efficient.

Before we are able to use this configuration, we have to increase the diameter of the chains to its designated size. This is accomplished by using a modified version of the standard Brownian dynamics simulation for short times. This version is identical in every aspect except for starting with a low value for the range of the excluded volume interaction of 0.6σ and increasing its value by 0.04σ every 5000 time steps. Thus, starting with a system containing the desired number of smaller chains, all beads are inflated simultaneously until the designated diameter σ is reached.

As this procedure might introduce tensions in the system during the inflation phase, a final equilibration step is required. However, with this method an equilibration over a time $\tau \approx \tau_d \ll \tau_r$ is expected to suffice and may easily be performed using the standard simulation.

To ensure that the initial configurations generated by this procedure are equilibrium configurations, we recorded 10 to 50 time-series for the various mean-square displacements with an offset of 0.2τ between each series in all productive runs, see Fig. 3.2 for an example. Within the statistical errors, no deviation between the curves measured at different times up to $0.5\tau_r$ apart were found. We conclude that our initial conditions correspond to completely equilibrated systems.

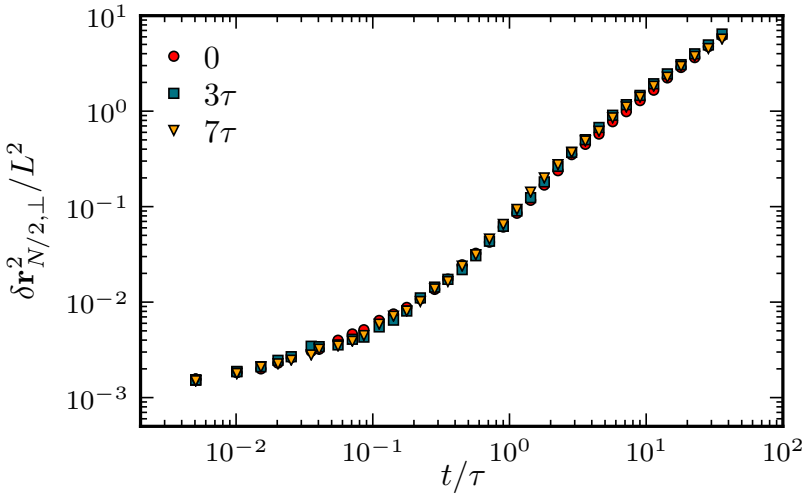

Figure 3.2: Time series of three different measurements of the orthogonal mean square displacement of the center monomer $\langle \delta r^2_{N/2,\perp}(t) \rangle$ starting from an initial configuration generated as detailed in Sec. 3.2. The data is averaged over all chains in the simulation box. For the system employed here the parameters are $l_p/L = 2$, $\epsilon = 70$ and $\xi_m/L = 0.11$. The measurements were started at times 0 (red), 3τ (blue) and 7τ (yellow). No significant deviations between the different curves are visible. The statistical errors are about symbol size.

3.3 Observables

In our simulation almost all information about the system is accessible as the position of each bead is known in every time step. In this thesis we focus on the dynamics of single chains in the melt. To evaluate the occurring processes, we employ several of the standard observables known from previous studies on polymers in dilute or dense solution, most of which have already been discussed in Chapter 2. Because we are interested in semiflexible polymers, we split most observables in orthogonal and parallel contributions, as introduced in Sec. 2.2.3.

Throughout this thesis, we average observables over the M individual chains of each simulation, assuming that the movements of the different polymers are almost uncorrelated in the isotropic polymer network. As the polymers interact only locally via repulsion, this assumption seems to be justified. Additionally, we employ a time average over 20–200 measurements, each initiated with a time offset of $\tau/5$ to the previous one. This is primarily used to reduce the statistical error in the case of low density networks. Thus the angular brackets used to denote averages are to be understood as averages over both all chains k and the measurements at different times. For all figures presented in this thesis, the statistical errors are about symbol size.

We define the end-to-end vector of a discrete chain k of N beads as $\mathbf{R}_k(t) = \mathbf{r}_{N,k}(t) - \mathbf{r}_{1,k}(t)$. As for free polymers, see Sec. 2.1, we can determine the internal relaxation from the length fluctuations of this vector. We evaluate:

$$\delta R^2(t) = \langle [|\mathbf{R}_k(t)| - |\mathbf{R}_k(0)|]^2 \rangle \,. \tag{3.7}$$

In principle, this may be seen as the parallel part of the relaxation of the end-to-end vector, as the projection from $\mathbf{R}$ on its direction equals the length. The longest internal relaxation time $\tau_{i,l}$ is determined from this observable. Obviously, the rotational relaxation of the polymer does not contribute to δR^2.

The rotation of a polymer is separately described using the mean square displacement of the normalized end-to-end vector. Thus we define the rotational MSD $\delta \mathbf{e}_R^2$ as:

$$\delta \mathbf{e}_R^2(t) = \langle [\mathbf{e}_{R,k}(t) - \mathbf{e}_{R,k}(0)]^2 \rangle \,. \tag{3.8}$$

where $\mathbf{e}_{R,k}(t) = \frac{\mathbf{R}_k(t)}{|\mathbf{R}_k(t)|}$ is the normalized end-to-end vector of chain k. In turn, this corresponds more or less to the orthogonal part of the end-to-end vector relaxation. From this observable, the longest rotational relaxation time τ_r is determined.
Recall that for small times the dominant contribution to the relaxation behavior of wormlike chains in the weakly bending limit is given by the orthogonal fluctuations, cf. Sec. 2.1.3. Thus for times much smaller than the longest internal relaxation time $\tau_{i,l}$, we expect identical dynamical behavior of δR^2 and $\delta \mathbf{e}_R^2$.

Apart from these two observables for the relaxation of the end-to-end vector, we also are interested in the spatial diffusion of each polymer through the network of surrounding chains. For flexible chains it is common to analyze the movement of an individual segment, while for semiflexible to stiff filaments usually only the center of mass motion is considered. In order to capture all possible crossovers and to achieve a discussion as complete as possible, we consider both quantities.
To minimize effects from the chain ends, we choose to observe the mean square displacement of the center bead, in this context frequently called center monomer. Following the literature [31] we denote this quantity by $g_1(t)$. Analogously, the mean square displacement of the center of mass is called $g_3(t)$. For a better understanding of the underlying processes we follow the standard procedure of splitting the diffusion in a parallel and an orthogonal component relative to the orientation of the polymer at the initialization of the measurement. We define:

$$g_{1,\parallel}(t) = \langle \big[\big(\mathbf{r}_{N/2,k}(t) - \mathbf{r}_{N/2,k}(0) \big) \cdot \mathbf{e}_{R,k}(0) \big]^2 \rangle \tag{3.9}$$

$$g_{1,\perp}(t) = \langle \big[\mathbf{r}_{N/2,k}(t) - \mathbf{r}_{N/2,k}(0) \big]^2 \rangle - g_{1,\parallel}(t) \tag{3.10}$$

$$g_{3,\parallel}(t) = \left\langle \left[\frac{1}{N} \left(\sum_{i=1}^{N} \mathbf{r}_{i,k}(t) - \sum_{i=1}^{N} \mathbf{r}_{i,k}(0) \right) \cdot \mathbf{e}_{R,k}(0) \right]^2 \right\rangle \tag{3.11}$$

$$g_{3,\perp}(t) = \left\langle \left[\frac{1}{N} \left(\sum_{i=1}^{N} \mathbf{r}_{i,k}(t) - \sum_{i=1}^{N} \mathbf{r}_{i,k}(0) \right) \right]^2 \right\rangle - g_{3,\parallel}(t) \,. \tag{3.12}$$

We expect to be capable to extract the reptation or disentanglement time τ_d from these measurements.
For times larger than the longest internal relaxation time, the contour fluctuations can be neglected and hence we expect that both observables g_1 and g_3 become identical at times $t \gg \tau_{i,l}$. Due to an increase of that time, we find the separate discussion of both observables still worthwhile. For times $t \ll \tau_{i,l}$ the value of g_1 is dominated by fluctuations of the individual segment. As these are related to the contour fluctuations [40], we expect identical dynamics as for δR^2 in this time regime.

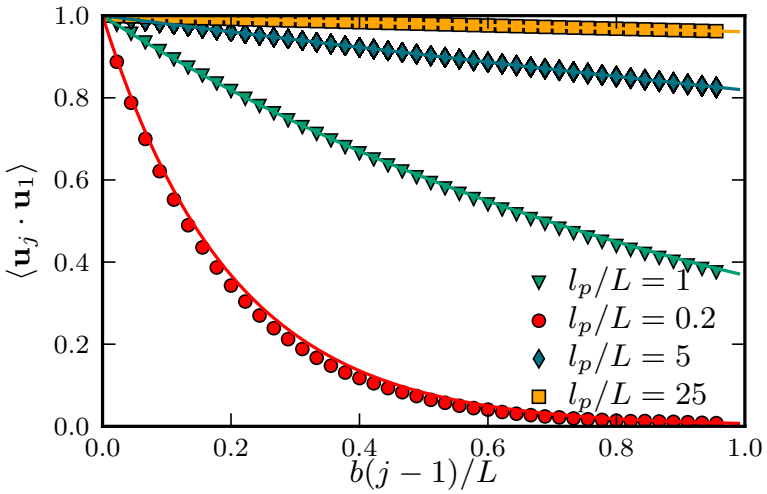

Figure 3.3: Tangent-tangent correlation of a polymer in a network with mesh size $\xi_m/L = 0.14$ for different values of the stiffness l_p/L. The solid lines give the theoretical predictions. The distance along the polymer is measured in beads j. Errors are about symbol size.

3.4 Consistency checks and discussion of aspect ratio

We perform several tests to ensure the reliability of our simulations. First, we test some static quantities, and then the dynamics of the system. Finally, the influence of purely numerical parameters like the mass and the aspect ratio on the long time behavior is examined.

One of the most fundamental relations of the worm-like-chain model is the tangent-tangent correlation, as introduced in Sec. 2.1.3. For a discrete chain the normalized bond vectors $\mathbf{u}$ need to obey $\langle \mathbf{u}_j \cdot \mathbf{u}_1 \rangle = \exp(-b(j-1)/l_p)$ for $1 \leq j \leq N-1$ with high precision. Due to the equipartition theorem this prediction should also hold in a dense polymer solution, in accord with expectations from earlier works [97]. As required, our simulations agree very well with this law both for a dilute polymer system and a dense polymer network, see Fig. 3.3 for an example. For rather flexible chains with $l_p/L \lesssim 0.2$ a very slight deviation may be observed. It is probably due to the excluded volume interaction, which constrains the range of available angles between neighboring bonds. As we primarily use chains of higher stiffness this deviation is of no concern.

With respect to the dynamical properties, we first determine the internal relaxation dynamics of the polymers in a dilute solution using our simulation. A comparison with the theoretical prediction, see Fig. 3.4, shows that they agree well with the analytical calculations for the worm-like chain model in the weakly bending limit, see Sec. 2.1.3. Recall that the theoretical prediction does not incorporate excluded volume effects, which are included in the simulations. As expected, they do not cause significant differences in the dynamics for semiflexible filaments. Thus we conclude that our simulations produces correct results for the dynamics of semiflexible polymers in dilute solution.

In this thesis, we are interested in reptation, which depends on the topology of the system. Consequently it is of utmost importance to prevent chain crossing. In order to ensure this

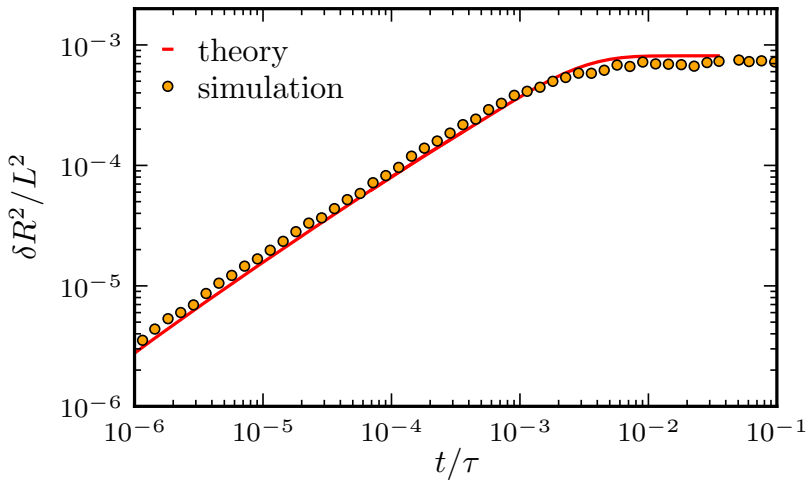

Figure 3.4: Time evolution of δR^2 determined from the simulation as compared to the theoretical prediction of the weakly-bending limit for the worm-like chain model. The data is for a system with $l_p/L = 5$ in a rather dilute solution with $\xi_m/L = 0.34$. The deviations from the expected behavior are comparable to the statistical error.

condition we employed a specialized scenario, see Fig. 3.5. Two initially stretched chains are positioned in the box to form a cross, one along the x-axis, the other parallel to the y-axis, such that the center of both chains is on the z-axis. Initially, the shortest distance between the chains is set to 1.5σ. This system is now simulated with our standard algorithm as introduced in Sec. 3.1, except for an additional spring force acting on the outermost beads of both chains. The force has a magnitude of $10k_BT/b$ and pulls the chains one against the other parallel to the z-direction. This system is simulated for 5τ without the chains actually crossing each other. Thus we conclude that both the excluded volume and the connectivity interaction are chosen suitable to prevent chain crossing.

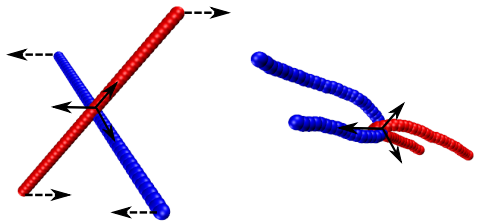

Figure 3.5: Setting used to test for chain crossing. The initial configuration is shown on the left, a typical snapshot of a state during the simulation on the right. The coordinate system is given by the black arrows, the pulling forces are indicated by the dashed arrows.

As an added precaution, we checked in all of our simulations whether the distance between any two beads decreased below 0.7σ or the bond length increases above $1.2b$. As expected due to the strong potentials, this never happened in any simulational setting used throughout this study.

The time required to simulate a system depends strongly on the total number of beads present in the simulation, given by MN. To realize a small mesh size a high number density $\nu = M/V$ is necessary. Additionally we need thin chains to avoid the nematic transition and thus a good discretization with large N. To keep the run times of the simulations at acceptable times below 14 days, we thus have to restrict the system size. Having said that, it is also of paramount importance to avoid artifacts arising from the finite size of the system. For

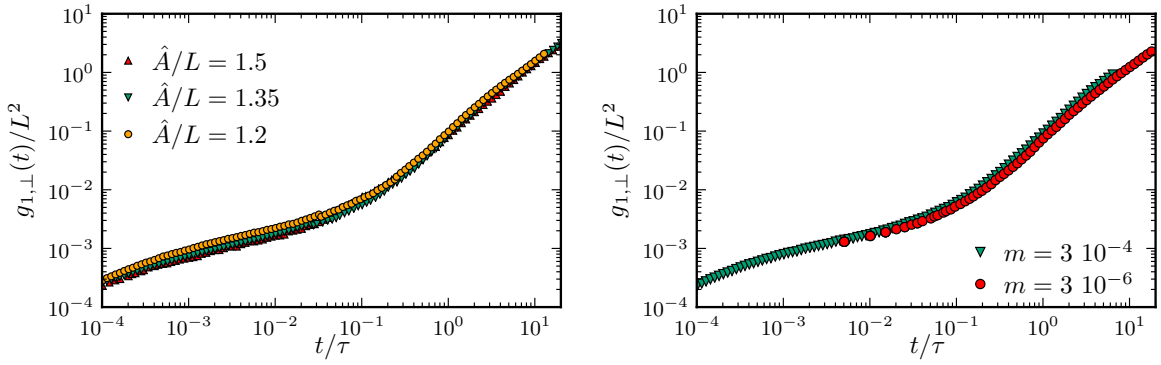

Figure 3.6: Left: Orthogonal diffusion of the center monomer in a polymer network with $\xi_m/L = 0.086$ and $l_p/L = 5$ resulting from simulations with different size of the cubic simulation box. The legend in the figure gives the corresponding values of the edge length for each simulation. No significant differences are found. Right: $g_{1,\perp}(t)$ in a polymer network with $\xi_m/L = 0.086$ and $l_p/L = 1$ determined from two simulations with different values for the mass of a bead. Only deviations of the order of the statistical error (symbol size) occur.

example, if the edge length $\hat{A}$ of the cubic simulation box would be smaller than L, it would be possible for one end of a polymer to come into contact with the other end due to the periodic boundary conditions. By continuously sliding along the same tube, results for the reptation behavior could be erroneous.
To check for any artifacts of that kind, stemming from the finite size of the simulation cell, we employ an exemplary system with $l_p/L = 1$ and density $\xi_m/L = 0.086$. We modify the simulation and the generation of initial condition to describe systems with edge lengths $\hat{A} = 1.5L$ and $\hat{A} = 1.2L$. The results are compared to the standard value on the left of Fig. 3.6 for a typical observable. Neither increasing nor decreasing the edge length results in any significant deviations for any of our observables.
This result could be expected due to the following reasoning: As long as $\hat{A}$ is several mesh sizes larger than the contour length, when the polymer vacates a part of its original tube, the mesh may rearrange in that region. Even if the polymer approaches this region rather directly from the other side, it already acquires a new configuration in the time required for this move. Thus both ends of the polymer experience almost independent conditions, comparable to a much larger system.
In conclusion, we find that the results are not affected by our choice of $\hat{A}$.

To increase the numerical stability, the mass of each bead is set to a large value compared to a segment of real polymers, see Sec. 3.1. We already found that the single filament dynamics of our simulations are correct in the dilute case. However, since several polymers interact in dense solution, an additive effect of the mass might be possible. As an additional test for any effects due to the increased inertia in the simulation, we prolonged the short time simulation, which uses a smaller mass and time step, see Sec. 3.1, to simulate up to 7τ for a system with $\xi_m/L = 0.086$ and $l_p/L = 1$. We find that the data for both simulations agrees reasonably well, see Fig. 3.6 (right).
Note that for a system with even larger mass, the long time dynamics were found to slow down significantly, in spite of no deviations occurring in the dilute system. Thus the interaction of many different chains indeed increases the requirement on the allowed values of inertia. For

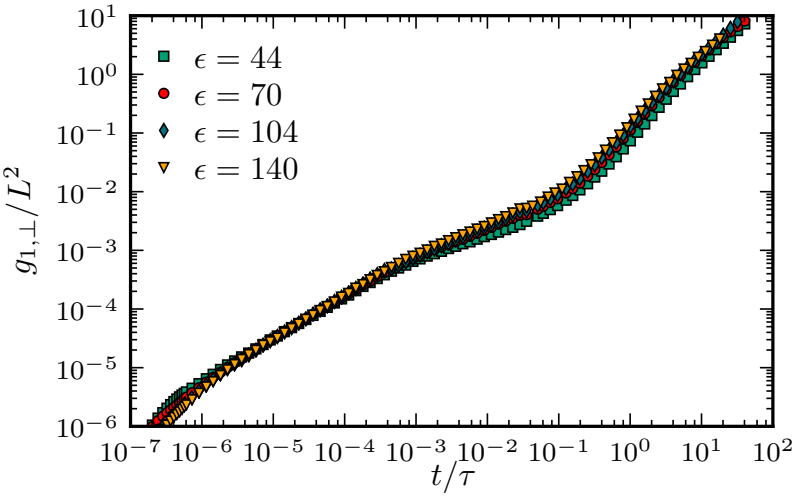

Figure 3.7: Orthogonal diffusion of the center monomer in a polymer network with $\xi_m/L = 0.17$ and $l_p/L = 25$ determined from simulations using different values for the aspect ratio.

our simulations any remaining effects of the mass are below the statistical errors.

Finally we want to determine the consequences of the achievable aspect ratios. These are much smaller than for typical actin filaments, which have $\epsilon \approx 10^3$. For this we use two different systems. One has a stiffness of $l_p/L = 25$ and a mesh size of $\xi_m/L = 0.17$, the other has $l_p/L = 1$ and $\xi_m/L = 0.12$. Both systems are realized several times with different aspect ratios, in such a way that the fraction of volume occupied by the chains also changes. As can be seen in the examples given in Fig. 3.7, and Fig. B.1 in the appendix, the results for all systems with $\epsilon \geq 70$ are almost indistinguishable throughout all observables. As there is no further dependence on the aspect ratio, we conclude that we have reached the slender filament limit in our simulation, such that only the topology is relevant for the dynamics. Due to this observation, ξ_m suffices to uniquely describe the system, whereas the aspect ratio or the occupied volume fraction are irrelevant for the dynamics of the isotropic polymer network. Especially, we may assume that without restriction our simulational results are valid for filaments of a much higher aspect ratio.

3.5 Nematic transition

As already mentioned in Chapter 2, depending on the diameter of the chains an isotropic-nematic transition may occur in our system. This phase transition in a solution of semiflexible to stiff polymers is of physical interest of its own. Experimentally, this transition may be observed, e.g., in dense actin solutions in vitro [94, 126]. Due to the complicated competition between the entropic contributions of global orientation and internal conformation, several attempts to analyze this topic from a theoretical point of view have been discussed [88–91, 127–131]. As other methods like Monte Carlo simulations are more efficient in studying this problem, we do not attempt to contribute to this discussion. However, we may use this

transition as an additional test for our simulations.

For rigid rods an approximate calculation for the phase boundary is possible. In good accordance with simulational results a nematic phase is found for systems with [88, 89, 132]

$$\nu V_c \epsilon \gtrsim 4 \,, \tag{3.13}$$

where V_c the volume occupied by a single chain.

For semiflexible polymers the situation is more complex. In the transition from the cylindrical rigid rod to a flexible, almost spherical coil the elongated shape of the chain gets lost. Thus, if still possible, the transition requires higher densities in dependence on the stiffness [89, 127, 132]. Qualitatively, some statements may be made. Starting from rigid rods, initially the critical density is expected to change very little with decreasing stiffness l_p/L. At some value $l_p/L \approx 5$ the stiffness is expected to significantly affect the position of the phase boundary [89]. Finally, at $l_p/L \approx 0.5$ the flexibility should overcome the orientational entropy and a phase transition should require much higher values of $\nu V_c \epsilon$ [89, 127, 132].

To compare our data with these predictions, we employ the standard nematic order parameter S as commonly used in the literature [128, 129, 131]. S, with $0 \leq S \leq 1$, quantifies the orientational ordering, where $S = 1$ corresponds to a completely ordered system. To calculate S we assume that each polymer k is oriented along its end-to-end vector $\mathbf{R}_k$. As before, the direction of polymer k is then given by the unit vector $\mathbf{e}_{R,k} = \mathbf{R}_k/|\mathbf{R}_k|$. For the whole solution we then define the second rank tensor Q as:

$$Q_{ab} = \frac{1}{M} \sum_{k=1}^{M} \frac{1}{2} \left(3 e_{R,k,a} e_{R,k,b} - \delta_{ab}\right) \,, \tag{3.14}$$

where the indices $a, b \in x, y, z$ denote the components of the tensor Q and vectors $\mathbf{e}_{R,k}$. δ_{ab} is the Kronecker delta. From this, we may finally determine S, which is the largest eigenvalue of Q.

We simulate each system for 15τ to 20τ, while recording the value of S. A typical time trace is shown on the left in Fig. 3.8. We can not ensure that the system has reached equilibrium at the end of the simulation. However, usually S only performs small fluctuations around some value at the end of the simulation. We assume that this value is the equilibrium value and use it for the further discussion.

By varying the aspect ratio, we can test our simulations against the prediction of Eq. (3.13). For a polymer with $l_p/L = 25$ we find that the nematic transition occurs roughly at $\nu V_c \epsilon \approx 5$, see the center picture of Fig. 3.8. We assume that the slight increase above 4 is due to the finite stiffness. Comparing our data to the results of previous Monte Carlo simulations and theories including bending stiffness shows good agreement indeed [89, 131].

To quantify the effect of the persistence length, we use a setting with $\epsilon \approx 70$ and determine the critical density for two types of polymers, one with $l_p/L = 1$ and the other with $l_p/L = 25$. From previous studies and the accompanying theories we expect that the critical density should roughly double when decreasing the persistence length in this way [89]. Again, we find good agreement with our simulational data, see right of Fig. 3.8. Thus we conclude that

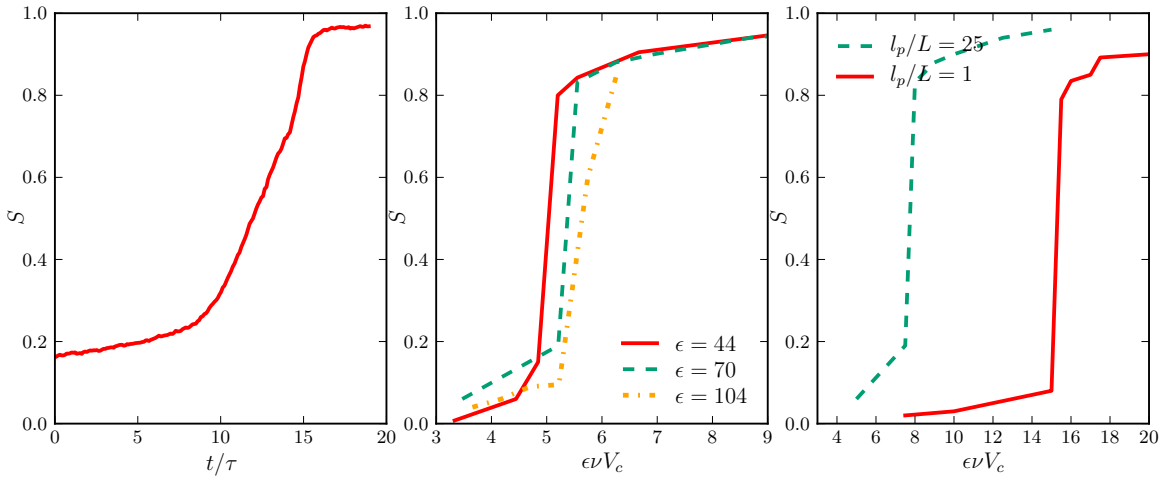

Figure 3.8: Left: We show a typical time trace of the order parameter in a single simulation, here for a system with $\epsilon = 70$, $\xi_m/L = 0.075$ and $l_p/L = 5$. Center: Varying the density ν for fixed ϵ allows to examine the dependence of S on $\nu V_c \epsilon$ for a system with $l_p/L = 25$. Right: For smaller l_p/L the phase transition occurs at higher values of $\nu V_c \epsilon$. Here given for a system with $\epsilon \approx 70$.

our simulations and excluded volume interactions work as required for a thorough study of polymer systems with steric interactions.

From the numerical point of view, we may interpret the occurrence of the nematic interaction in a different way. The polymers in our simulations may be considered to have an increased diameter compared to reality. In order to simulate the actual aspect ratio, while keeping the chains from crossing, we would need a much steeper potential. This in turn requires a significantly smaller time step in order to achieve a stable algorithm. As we have already ensured that the aspect ratio has no relevance for the observables of interest, we may employ the more efficient version with increased chain diameter.

Thus we could treat the nematic transition as a numerical artifact limiting the available densities. We reformulate Eq. (3.13) to express the density in terms of the mesh size. To calculate the volume of each chain, we assume a cylindric volume for a polymer chain, $V_c = \pi L(\sigma/2)^2$. The requirement to avoid the nematic transition is then found to limit the range of accessible mesh sizes in the form:

$$\xi_m/L \gtrsim \sqrt{\frac{2.35}{\epsilon}} \tag{3.15}$$

While this equation is derived from Eq. (3.13) for rigid rods, it serves as an approximate boundary for semiflexible chains, too.

In the remainder of this study we are interested in the isotropic phase only. Therefore, we attempt to adjust the aspect ratio such that the nematic transition does not occur while keeping the runtime at acceptable times below 14 days. This condition results in the employed values of aspect ratio for the various densities as given in Table 3.1. To ensure the isotropy we additionally check that the standard order parameter stays below 0.25 throughout the whole data acquisition time. In summary, due to this effect we are limited to mesh sizes with $\xi_m/L \geq 0.075$.

4 Analysis of simulational data for power-laws and scaling of crossover times

In this chapter we analyze the results of our simulations on semiflexible to stiff polymers in dense solution with respect to the power-laws describing the relaxation behavior and the corresponding crossover or saturation times. We discuss our findings and compare them with existing predictions and previous simulational studies where applicable, see Chap. 2. As the flexible case with $l_p < \xi_m$ has already been studied extensively [58, 59], we focus on semiflexible to stiff polymers with $l_p \gg \xi_m$. Note that at $l_p = \xi_m$ it also holds $L_e \propto \xi_m$, such that this condition may analogously be considered as a restriction of the Odijk length $L_e \gg \xi_m$.

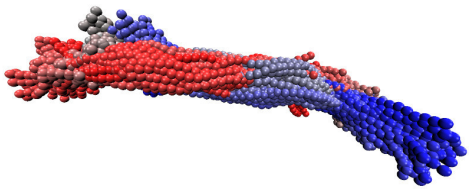

Figure 4.1: Time evolution of a single chain in a system with $\xi_m/L = 0.10$ and $l_p/L = 1$. The figure is a superimposition of configurations acquired every 2.5 $10^{-4}\tau$ over a time interval of 0.1τ. The color indicates the time of the measurement, red corresponds to $t = 0$, blue to $t = 0.1\tau$. A tube-like structure like reported in experiments [33, 43, 50–55] is clearly visible.

For a first visual impression, Fig. 4.1 shows superimposed images of a single filament. A tube like structure as known from experiments and previous simulations is clearly visible [31, 33, 43, 50–54]. This observation is usually considered to assert that the tube picture is valid for purely entangled system. Yet, in the following detailed analysis, we find a much richer dynamics than predicted by theories or reported from simulations with fixed obstacles.

4.1 Internal relaxation of polymers

To get a first impression of the dynamics of single filaments in a network of identical polymers, we start by discussing contour fluctuations as an observable for the internal relaxation. This is comparable to some of the original questions discussed by de Gennes [36] when introducing the reptation picture: How does a small undulation of contour length move along a polymer in a tube? How strong are the resulting fluctuations and what is the relaxation time of this process?

It is advantageous to start with this observable, as it is likely not affected by diffusion or rotation. In return, knowledge of this process allows to easily evaluate the effect of these fluctuations in the following discussions of other observables.

As introduced earlier, we employ the mean square displacement of the length of the end-to-end vector $\delta R^2(t)$ to determine the internal relaxation behavior, following the standard approach for free semiflexible to stiff filaments [6, 9, 19, 40, 61, 133].

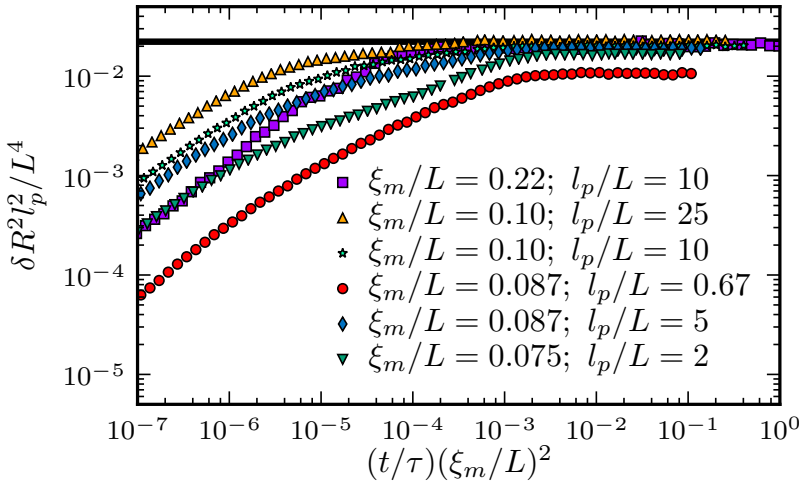

Figure 4.2: Saturation regime of $\delta R^2/L^2$, scaled by l_p^2/L^2 shown for various densities and stiffnesses, see legend. The solid line give the predicted saturation value in dilute solution, see (2.31). The scaling law $\delta R^2 \to L^4/45l_p^2$ holds even for polymers in dense solution, no dependence of the saturation value of δR^2 on the mesh size is found. For better visibility of the common saturation regime, times have been rescaled by $(\xi_m/L)^2$. The deviation of the curve with $l_p/L = 0.67$ occurs due to the breakdown of the weakly bending approximation. The saturation value of this curve corresponds to the equilibrium value in dilute solution, too.

4.1.1 The saturation value of internal fluctuations

Remember the fact that the tangent-tangent correlation is unchanged in a network, as established in Sec. 3.4. Then it would be surprising if the saturation value of $\delta R^2(t)$ of a polymer in a network should deviate from the value in dilute solution. Thus in the weakly bending case introduced in Sec. 2.1.3, i.e., for $l_p/L \gtrsim 1$, we especially should find a scaling $\delta R^2 \propto L^4/l_p^2$ [6, 9, 19, 40, 61, 133]. Indeed, in our simulations we find no dependence of the saturation value on the mesh size and good agreement with the predicted scaling relation, see Fig. 4.2. In particular, this holds for systems where the expected tube diameter is much smaller than the typical orthogonal fluctuations of the filament. While this might have been expected for a system in equilibrium, as detailed initially, it is still a very relevant observation. Some previous works endorse this fact to derive scaling laws [97], yet several other theoretical predictions based on the tube picture are contrary to this observation [31, 32, 40, 87] due to the following argument:
In the semiflexible case, δR^2 is dominated by the orthogonal fluctuations of the contour, which in the tube picture are supposed to be limited to the tube diameter. Hence it is often claimed that in a dense solution the contour fluctuations are limited to a value much smaller then in dilute solution. Also, simulations based on fixed obstacles are supposedly in accord with this expectation [31].
However, this is obviously not the case in our purely entangled system. Like for semiflexible polymers in dilute solution, we find in Fig. 4.2:

$$\delta R^2(t \to \infty) = \frac{L^4}{45 l_p^2} \,. \tag{4.1}$$

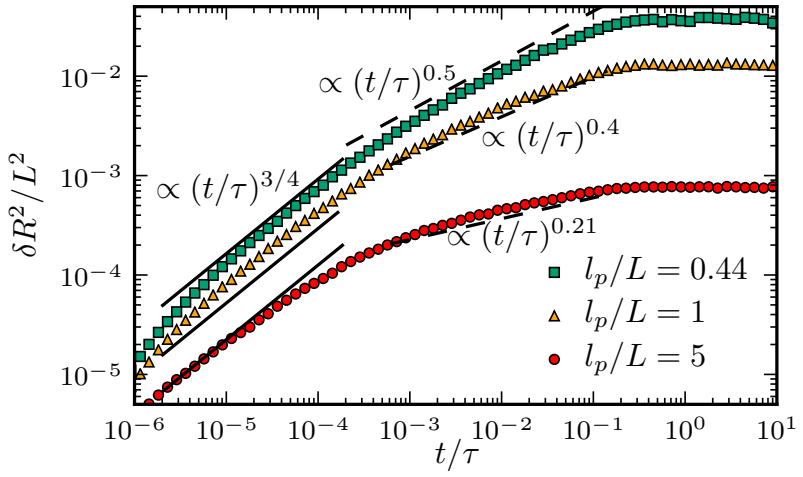

Figure 4.3: Typical examples for the length fluctuations of single polymers in networks of different stiffness, here for a mesh size $\xi_m/L = 0.086$. As a guide to the eye, the continuous lines are proportional to $t^{3/4}$, whereas the dashed lines are rough estimates of the power-laws in the intermediate regime with the individual behavior as given in the picture.

4.1.2 The boundaries of the intermediate regime and the Odijk length

This insight for the saturation value raises the interesting question how a polymer relaxes at times above the Odijk time, when its orthogonal fluctuations should be confined by the tube. Some typical relaxation curves measured in our simulations are shown in Fig. 4.3. We find that the dynamics of the system exhibit three relevant different scaling regimes before it saturates. Note that the behavior at very small times, $t/\tau < 10^{-6}$ in Fig. 4.3 is due to inertia and we neglected this part here, and in the following discussions of the other observables.
As expected and predicted previously [40], at small times we find the familiar $t^{3/4}$ regime known from free polymers, see Sec. 2.1.3. If the system is dense enough, it is followed by an intermediate regime where the contour fluctuations increases approximately with some power-law t^{α_i}. We call α_i the exponent of internal relaxation and find that value of α_i depends on the characteristics of the system. Finally, at times above the still unknown longest internal relaxation time $\tau_{i,l}$, we have already shown that $\delta R^2(t)$ saturates to the same value as in a dilute system.

To characterize the dynamics and especially the intermediate regime, we first analyze the crossover times. We start by scrutinizing the lower bound of the intermediate regime. The initial $t^{3/4}$ regime is supposed to be free relaxation, per definition of several segments with a contour length of approximately L_e each, see Sec. 2.2.4. Thus the lower crossover time is expected to be the entanglement time τ_e, for which holds $\tau_e = \frac{\zeta L_e^4}{k_B T l_p 4.73^4}$ according to Eq. (2.30). The corresponding value of $\delta R^2(\tau_e)$ is supposed to be $\frac{L L_e^3}{l_p^2}$, see Granek's argument in Sec. 2.2.4. Hence, the crossover is governed by the Odijk length L_e. Remember that there are different predictions for the scaling of L_e with mesh size and persistence length, see Sec. 2.2.4. We may now use this crossover to determine the correct scaling of L_e in a dense

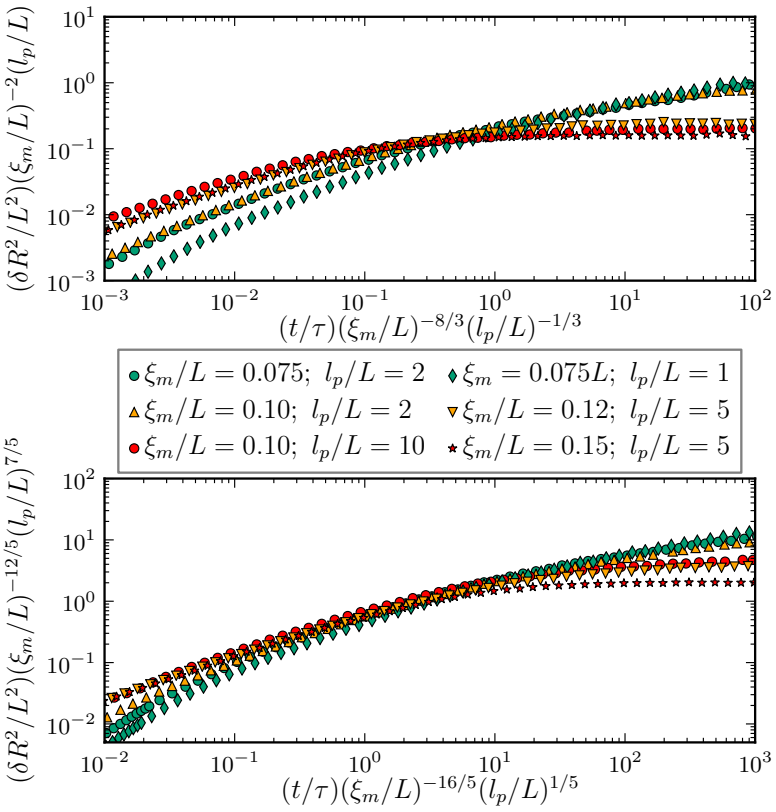

Figure 4.4: Length fluctuations of single polymers in networks with different characteristics. The time has been rescaled by the entanglement time τ_e and accordingly the amplitude by $\delta R^2(\tau_e)$. In the upper figure we follow the prediction $a \propto \xi_m$, whereas the lower is for $a \propto \xi_m^{6/5} l_p^{-1/5}$. We find a significantly better data collapse using the latter scaling relation for the tube diameter a.

solution of purely entangled semiflexible filaments.

If we follow the simple argument that $a = \xi_m$, the crossover time should scale as $\tau_e/\tau \propto (\xi_m/L)^{8/3}(l_p/L)^{1/3}$. The amplitude at this time should scale as $\delta R^2(\tau_e)/L^2 \propto (\xi_m/L)^2(l_p/L)^{-1}$. In contrast, based on the Semenov scaling prediction $a \propto \xi_m^{6/5} l_p^{-1/5}$, it follows $\tau_e/\tau \propto (\xi_m/L)^{16/5}(l_p/L)^{-1/5}$ and $\delta R^2(\tau_e)/L^2 \propto (\xi_m/L)^{12/5}(l_p/L)^{-7/5}$. Due to the different sign of the l_p dependence of τ_e it should be easy to assess the success of both scaling laws. By rescaling several relaxation curves for different densities and stiffnesses accordingly, we find that the first scaling assumption does not give a good data collapse, see the upper part of Fig. 4.4. Using Semenov's prediction $a \propto \xi_m^{6/5} l_p^{-1/5}$, and consequently $L_e \propto \xi_m^{4/5} l_p^{2/5}$ results in a good data collapse at the crossover time, see Fig. 4.4 bottom. We employ this scaling law throughout the rest of our analysis.

Also, Fig. 4.4 is in accord with the predictions of free fluctuations up to the scale of the Odijk length, as claimed by existing theories, see Sec. 2.2.4. In summary, the $t^{3/4}$ regime and the lower crossover time are as expected [40]. In particular, they agree with Semenov's prediction

for the tube diameter, similar to some previous studies [21, 29], and we find:

$$\tau_e \propto \frac{\zeta \xi_m^{16/5}}{k_B T l_p^{1/5}} \quad \text{and} \quad \delta R^2(\tau_e) \propto \frac{L \xi_m^{12/5}}{l_p^{7/5}} \ . \tag{4.2}$$

From this result we may conclude some important properties of the crossover time and the following intermediate regime. If the Odijk length becomes longer than the contour length, i.e., for stiff polymers with $a^{2/3} l_p^{1/3} > L$, it especially follows that the intermediate regime should vanish. As in previous simulations with fixed obstacles [31], our simulations are in agreement with this prediction, see appendix, Fig. B.2. This effect may easily be interpreted: the fluctuations of the polymer are too small to cause continuous interactions with the confinement.
With the established scaling of the tube diameter, we may reformulate the condition on the Odijk length to get a critical stiffness in dependence on the density of the system. We define a critical persistence length:

$$l_{p,c} \propto L^5 / \xi_m^4 \ . \tag{4.3}$$

Then, for polymers with $l_p > l_{p,c}$ the Odijk length becomes longer than the contour length and the intermediate regime vanishes. The critical persistence length can be interpreted as a critical density using the definition of the mesh size. The critical number density $\hat{\nu}$ is found by substituting $\xi_m = \sqrt{3/\nu L}$ and solving for ν. With this, the condition $l_p < l_{p,c}$ is equivalent to assuming a tightly-entangled regime, as defined by Morse, see Sec. 2.2.4, yet as a condition on the stiffness instead of the density.

We have successfully identified the lower crossover time with the entanglement time and may now turn to analyzing the longest internal relaxation time $\tau_{i,l}$ for systems with $l_p < l_{p,c}$. This poses an interesting problem, as to our best knowledge, there are no theoretical prediction for $\tau_{i,l}$ in accordance with our hitherto findings. The few existing theories predicting the internal dynamics of a chain in a dense solution usually assume that the orthogonal fluctuations are bounded by the tube diameter [31, 32, 40, 87]. Thus, if contour fluctuations at times $t > \tau_e$ are incorporated at all, only parallel contour fluctuations are considered for the further relaxation of $\delta R^2(t)$. As these fluctuations are sub-dominant to the orthogonal ones, see Sec. 2.1.3, the predicted saturation value of $\delta R^2(t)$ is much smaller than in dilute solution, a clear contradiction to our data, see Sec. 4.1.1.
Thus, instead of testing a given scaling prediction, we attempt to find the correct dependence of the saturation time $\tau_{i,l}$ on ξ_m and l_p by optimizing the data collapse at this crossover. First, we test the mesh size dependence for various values of the persistence length independently. For each value of stiffness used, we find the best data collapse when rescaling the time by $(\xi_m/L)^2$, see Fig. 4.5. Thus, the longest relaxation time increases with the density of the network. This is a reasonable result: If the chain is more strongly confined due to the smaller mesh size, it is more difficult to explore lateral space, which is required to saturate the contour fluctuations.

Having established the density dependence, we may scrutinize the influence of the persistence length on $\tau_{i,l}$. An analogy to the scaling of $\tau_{i,l}$ in dilute solution, cf. Sec. 2.1.3 suggests a behavior of roughly $\tau_{i,l} \propto l_p^{-1}$. Also theories considering the longitudinal fluctuations predict a similar dependence in densely entangled networks, see Sec. 2.2.6.

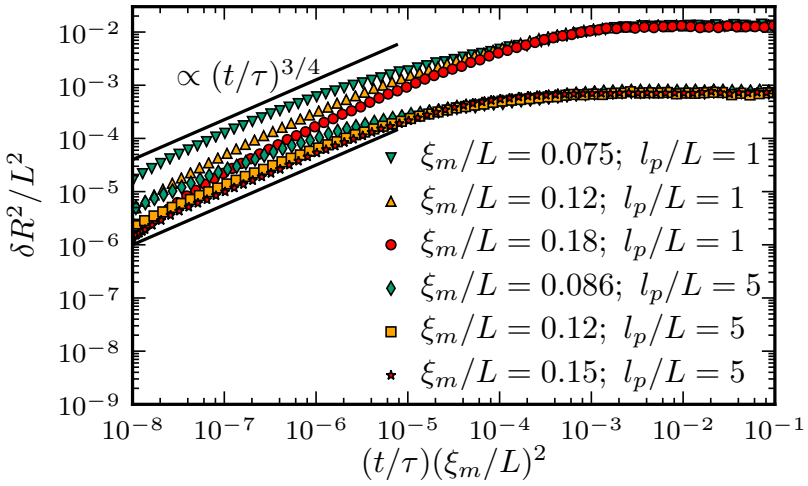

Figure 4.5: Two examples with different stiffness for the contour length fluctuations of single polymers in networks of various densities. The time has been rescaled by $(\xi_m/L)^2$. For each set of curves for a given stiffness we find good data collapse for the longest relaxation times.

Surprisingly we find that the dependence of $\tau_{i,l}$ on the persistence length does not obey the expected scaling. Indeed, the saturation time rather lacks any l_p dependence, cf. Fig. 4.6 for a typical example.

In conclusion, we find in Figs. 4.5 and 4.6 the following dependence for the longest relaxation

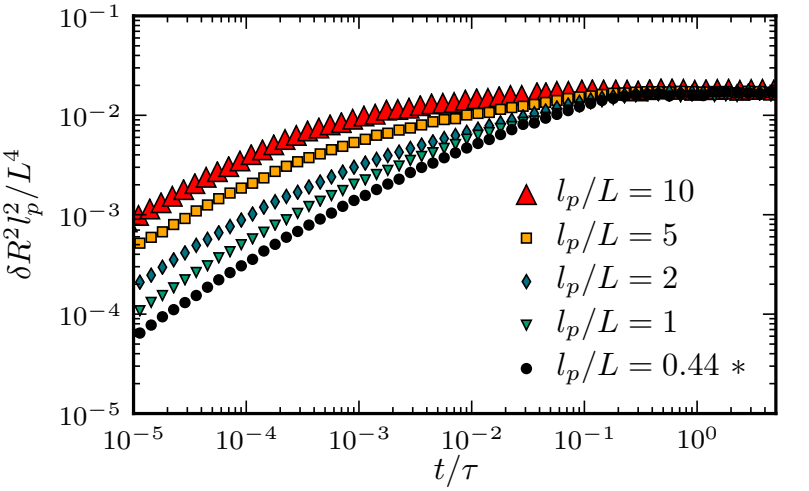

Figure 4.6: Length fluctuations of single polymers in networks with $\xi_m/L = 0.086$. For better visibility of the agreement of saturation times, $\delta R^2/L^2$ has been rescaled with $(l_p/L)^2$ to achieve a data collapse of the saturation value. As the weakly bending limit is not valid for the polymer marked with $*$, the values of $\delta R^2/L^2$ of this data set have only been rescaled by l_p/L. The time has *not* been rescaled. We find a good data collapse for the longest relaxation times.

time, where the additional terms follow from dimensional analysis:

$$\tau_{i,l} \propto \frac{\zeta L^5}{k_B T \xi_m^2} \ . \tag{4.4}$$

To our best knowledge, this result has not been predicted previously by any theory based on a tube model. Also, our results significantly deviate from previous simulations based on fixed obstacles [31], which exhibit a completely different scaling, see Eq. (2.74). We attribute the divergence of our results from previous studies to the neglect of constraint release in those studies. In Chap. 5 we discuss the results of some additional simulations, performed in order to identify the dominant processes responsible for the newly found scaling of $\tau_{i,l}$.

Before scrutinizing the behavior in the intermediate regime, it might be worth to comment on experimental data. Also in experiments the largest relaxation time is often seemingly found to be τ_e. This is not necessarily a contradiction to our results, as it may easily be explained by the large ratio $\tau_{i,l}/\tau_e$. It holds:

$$\tau_{i,l}/\tau_e \propto \frac{L^5 l_p^{1/5}}{\xi_m^{26/5}} \ , \tag{4.5}$$

which may be several orders of magnitude for systems with small ξ_m/L. Thus for dense networks, it is very likely that $\tau_{i,l}$ is significantly above the hitherto experimentally accessible times, which are typically of the order 10^2s [33].

4.1.3 Varying power-law behavior in the intermediate regime

After we have established the boundaries of the intermediate regime in the previous discussion, we analyze the behavior in this regime. We find that to good approximation this regime may be described by an power-law $\delta R^2 \propto t^{\alpha_i}$, see Fig. 4.3. The exponent of internal relaxation α_i is found to depend on all characteristics of the system.

From the previous analysis, we may draw some easy conclusion on how α_i depends on the mesh size and stiffness before turning to simulational results. From Fig. 4.6 it follows that α_i decreases strongly with increasing stiffness. On the other hand, Fig. 4.5 suggests that the mesh size dependence is rather weak over the range of available mesh sizes.

Assuming a pure power-law, we may easily calculate the behavior of α_i from our previous results. Obviously this yields:

$$\alpha_i = \frac{\ln \delta R^2(\tau_{i,l}) - \ln \delta R^2(\tau_e)}{\ln \tau_{i,l} - \ln \tau_e} = \frac{\ln \frac{\delta R^2(\tau_{i,l})}{\delta R^2(\tau_e)}}{\ln \frac{\tau_{i,l}}{\tau_e}} \tag{4.6}$$

From the ratio of the two timescales limiting the intermediate regime, Eq. (4.5), the saturation value Eq. (4.1) and the crossover value as given in Eq. (4.2) it follows:

$$\alpha_i \approx \frac{3 \ln \frac{l_p}{L} + 12 \ln \frac{\xi_m}{L}}{26 \ln \frac{\xi_m}{L} - \ln \frac{l_p}{L}} \ . \tag{4.7}$$

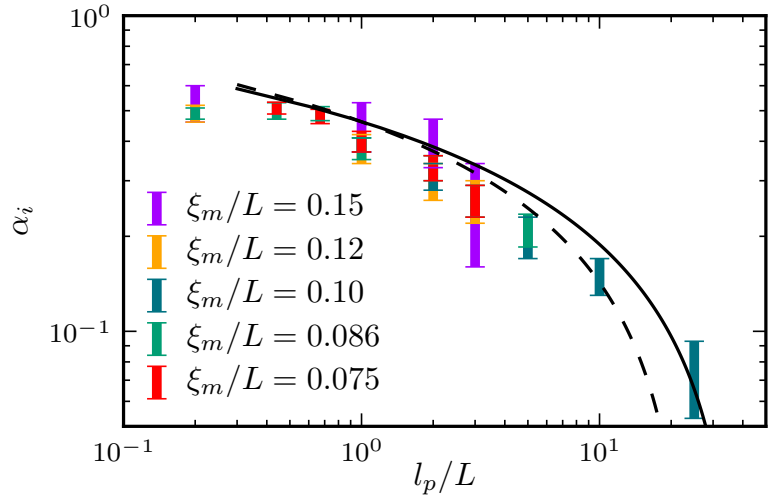

Figure 4.7: Fitted values for the scaling exponent α_i in the intermediate regime of the length fluctuation relaxation in dependence on the stiffness for systems of various densities as given in the legend. In the flexible limit the familiar result of de Gennes with $\alpha_i \approx 0.5$ is recovered. The black continuous line is the prediction according to Eq. (4.8) for $\xi_m/L = 0.086$, the dashed line is for $\xi_m/L = 0.12$. The curves agree well with the measured values.

As we only consider polymers with $\xi_m \ll l_p$ and $l_p < l_{p,c}$ such that the intermediate regime exists, we may assume that $26 \left|\ln \frac{\xi_m}{L}\right| \gg \left|\ln \frac{l_p}{L}\right|$. Thus we may neglect the second term in the denominator. This leads to the simplified expression:

$$\alpha_i \approx \frac{6}{13} + \frac{3 \ln \frac{l_p}{L}}{26 \ln \frac{\xi_m}{L}} . \tag{4.8}$$

To extract α_i from our simulational data, we perform a fit with a function $c(t/\tau)^{\alpha_i}$ for various values of the stiffness l_p/L using c and α_i as fitting parameters. Please note that due to the difficulty involved in determining small slopes over a limited range, these results should be taken with a grain of salt. In Fig. 4.7 we compare our prediction, Eq. (4.8), with our numerical results. We find that our solution agrees very well with our data. Note that our derivation of Eq. (4.8) is only valid for semiflexible polymers with $l_p/L \gtrsim 1$, as we employ the saturation value of δR^2 following from the weakly bending limit. Thus a small deviation from the measured values in the regime $l_p/L \ll 1$ is to be expected and does no affect the validity of our result in the remaining parameter regime.

Having established the accuracy of our calculation, some more properties are gained from the result. As expected, α_i varies strongly with l_p and quickly converges to zero for $l_p \to l_{p,c}$. For systems close to $l_{p,c}$ the mesh size significantly affects α_i, cf. Fig. 4.7. However, as the slope of the intermediate regime is very small for those systems, this effect is hard to observe. The strong decrease of α_i close to the transition $l_p \approx l_{p,c}$ also is the reason why it is almost impossible to unambiguously observe the vanishing of the intermediate regime. Nevertheless, our findings explains the difficulty in characterizing the existence of this intermediate regime in previous studies assuming a constant slope [31].

In contrast, for polymers with $l_p \ll l_{p,c}$, the mesh size dependence of α_i indeed is found to be almost negligible, see Fig. 4.7. Also the influence of the persistence length becomes weaker and α_i converges to 0.5. Recall that this is the behavior expected for flexible chains, see Sec. 2.2.

This is an import result, as thus our data is in agreement with reptation theory for flexible chains. The intermediate scaling regime of $t^{1/2}$ is an hallmark of reptation in those systems, see Sec. 2.2.2, and has already been predicted by de Gennes [36]. Later this predictions was confirmed by simulations of freely jointed chains [58, 59]. Thus our results are in agreement with the well-established boundary cases of flexible chains and rigid rods, which lack an intermediate regime [38].

It is interesting to compare our results to the results of previous simulational studies. Using a tube model and simulations of a filament moving in two dimensions through an array of fixed point-like obstacles a system-independent $t^{1/2}$ regime has been reported for semiflexible filaments with $l_p/L \gtrsim 1$ [31, 32].[1]
We assume that this difference to our data arises from the use of fixed obstacles, which do not completely correspond to a purely entangled system as considered in our simulations. Consequently, we assume that additional constraint release mechanism, cf. Sec. 2.2.5 dominate the behavior in purely entangled networks. We elaborate on this topic in Chap. 5.

To our best knowledge there is no theory predicting a similar complex behavior for the internal relaxation. However, as our description incorporates a smooth transition from flexible chains with $\alpha_i = 0.5$ to rigid systems with $\alpha_i = 0$, we think our model is favorable to other descriptions.
This concludes the discussion of the internal dynamics and allows us to clarify how they affect the polymer interaction and thus the global dynamics of each filament.

4.2 Rotational relaxation

In systems of flexible chains, the rotational relaxation is usually not explicitly studied. For these polymers the orientation of new tube segments is uncorrelated to the existing parts. Hence it suffices for the polymer to leave its original tube to achieve full rotational relaxation. In other words, for flexible filaments the rotational relaxation time is identical to the reptation time τ_d required to diffuse a distance equal to the tube length, see Sec. 2.2.2. For semiflexible to stiff chains, the orientation may only change by a comparatively small amount in the same time, as the direction of a segment is influenced by the other segments. Thus, for those systems the rotational relaxation is expected to be much higher than the reptation time. In fact, it is supposed to determine the longest relaxation time of the whole system, which we also call the terminal relaxation time. After the longest relaxation time all correlations and stresses are decayed and the diffusion of each chain becomes linear diffusion with an effective diffusion coefficient. Therefore this timescale and the characteristics of rotation are of primary interest for entangled polymer networks.

[1] Curiously the vanishing of this regime in the stiff limit is not explained by that theory.

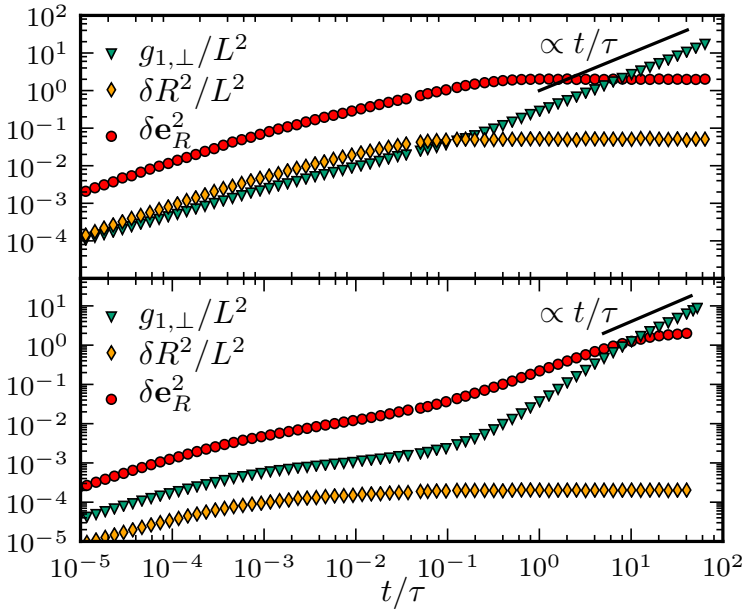

Figure 4.8: For two polymer networks the internal relaxation $\delta R^2/L^2$ [diamonds], the orthogonal part of the diffusion of center monomer $g_{3,\perp}/L^2$ [triangles] and the rotational MSD $\delta \mathbf{e}_R^2$ [circles] are given. The system in the upper plot has a mesh size of $\xi_m/L = 0.15$ and a stiffness of $l_p/L = 0.2$, whereas in the lower figure the parameters are $\xi_m/L = 0.10$ and $l_p/L = 10$. Upon saturation of the rotational MSD the diffusion becomes linear in time. The internal dynamics always relax at smaller times.

4.2.1 The terminal relaxation time

As discussed earlier, the longest relaxation time of the whole system is expected to stem from rotational relaxation. Especially it is expected to coincide with the transition to linear diffusion of the center of mass or of individual monomers, which we scrutinize in Sec. 4.3.

As expected and used in previous discussions of reptation [40, 97, 100], we find that for all considered polymer systems with $\xi_m \lesssim l_p$ the saturation of the rotational MSD coincides with the crossover to free diffusion of the polymer, see Fig. 4.8. Note that for this observation it is irrelevant whether the center monomer or the center of mass motion are considered.
Also, for all of the semiflexible systems we simulated, we always found the internal relaxation time to be smaller than the rotational relaxation time, i.e., $\tau_{i,l} < \tau_r$. We conclude that the rotational relaxation is indeed the dominant process for determining the longest relaxation time for all polymers with $\xi_m \lesssim l_p$.
While the longest relaxation time may also be determined from measuring the diffusion of a polymer segment or of the center of mass, we believe it is advantageous to extract this time from the rotational diffusion. Usually, it is significantly easier and more precise to fit a saturation event than a crossover from some sub-diffusive regime to free diffusion due to the more pronounced curvature in the saturation event.

There are several contradicting predictions for the rotational relaxation time of entangled

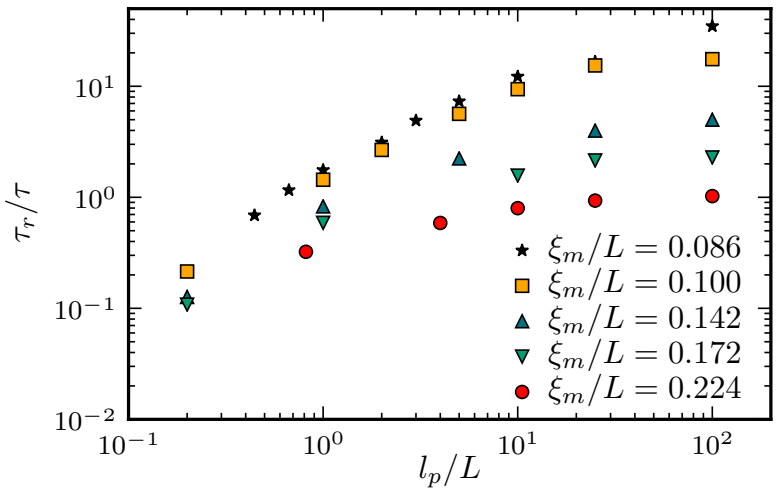

Figure 4.9: Fitted values for the longest relaxation time τ_r in dependence on the stiffness l_p/L for systems with various mesh sizes, see legend. The terminal relaxation time is found to vary strongly with both characteristics of the system.

semiflexible filaments, although all of them are based on the reptation theory or a tube model, respectively [21, 31, 40, 96–98, 100]. These often predict the rotational diffusion coefficient, which is completely analogous to our approach, as it is directly proportional to the inverse of the saturation time.
Most notably, the predictions vary in the scaling of τ_r with the persistence length from no dependence to a linear increase with l_p. See Sec. 2.2.4 for a short overview of important predictions. Experimentally, it has been found that the longest relaxation time for relatively stiff polymers in an array of fixed obstacles is proportional to the stiffness l_p/L [55].

Here, we report the existence of two distinct regimes of the rotational relaxation time in dependence on the persistence length and the mesh size. We determine values for the saturation time τ_r by performing a least-square fit of the measured curves of $\delta\mathbf{e}_R^2$ with $2 - 2\exp(-t/\tau_r)$. We show in Sec. 4.2.2 that this functional form indeed provides a good fit in the relevant time regime. We restrict our discussion to the case $\xi_m < l_p$ to avoid difficulties stemming from the crossover $\xi_m \gtrless l_p$. For numerical reasons we are limited to stiffnesses $l_p/L \leq 100$.

The terminal relaxation time is found to depend on both density and stiffness of the polymer system, see Fig. 4.9. Also, the dependency on either quantity seems to depend on the other. However, by rescaling the stiffness with $(\xi_m/L)^2$ and the values of τ_r with $(\xi_m/L)^4$ we find that the data for the longest relaxation times collapses onto a single master curve, see Fig. 4.10. Therefore we formulate the following scaling law:

$$\tau_r = \tau(\xi_m/L)^{-4}\hat{\tau}_r(x), \tag{4.9}$$

where we introduce the dimensionless scaling variable x with:

$$x = l_p\xi_m^2/L^3\ . \tag{4.10}$$

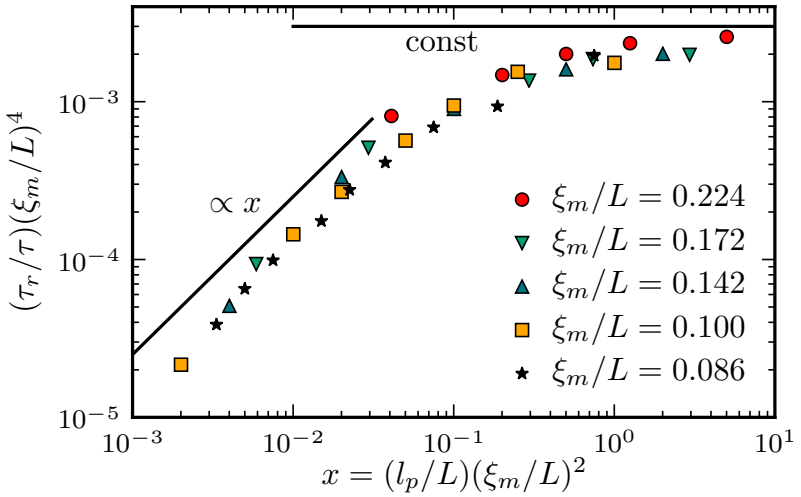

Figure 4.10: Fitted values for the longest relaxation time τ_r in dependence on the scaling variable $x = (l_p/L)(\xi_m/L)^2$ for various values of the mesh size. By rescaling τ_r with $(\xi_m/L)^4$ the different curves collapse onto a master curve. From the master curve we can follow the scaling laws of τ_r in the different regimes. For dense networks and rather flexible chains we find a linear dependence on x, but it strongly decreases for systems with $x > 0.1$. For values above $x = 1$ the x-dependence (or, correspondingly, the l_p-dependence) of τ_r vanishes completely.

$\hat{\tau}_r(x)$ is the scaling function with asymptotic behavior (as long as $l_p > \xi_m$, i.e., $x > (\xi_m/L)^3$):

$$\hat{\tau}_r(x) \propto \begin{cases} x & \text{for } x \lesssim 0.1 \\ \text{const} & \text{for } x > 1 \end{cases} . \tag{4.11}$$

For the reader's convenience we also give the full expression of τ_r, which is:

$$\tau_r \propto \begin{cases} \frac{\zeta l_p L^4}{k_B T \xi_m^2} & \text{for } x \lesssim 0.1 \\ \frac{\zeta L^7}{k_B T \xi_m^4} & \text{for } x > 1 \end{cases} . \tag{4.12}$$

To gain insights about the nature of the crossover and the behavior in the two asymptotic regimes, we are interested in an interpretation of our newly found scaling parameter x and especially of the crossover value $x = 1$. For this, we introduce a critical persistence length $\hat{l}_p$, which we find to determine the dominant rotational mechanism. We define:

$$\hat{l}_p/L := (\xi_m/L)^{-2} . \tag{4.13}$$

With this definition we may rewrite the important scaling variable x as a ratio of l_p to this critical value:

$$x = l_p/L(\xi_m/L)^2 = l_p/\hat{l}_p . \tag{4.14}$$

To elucidate the meaning of $\hat{l}_p$, recall that even in a dense solution the orthogonal fluctuations $\delta r_\perp^2$ of each polymer correspond to the free value $\delta r_\perp^2 \propto L^3/l_p$, as shown in Sec. 4.1.1. Hence, in a system with $x = 1$ or analogously $l_p = \hat{l}_p$, it holds $\delta r_\perp^2 \propto L^3/\hat{l}_p = \xi_m^2$, i.e., the orthogonal fluctuations of each chain are comparable to the mesh size of the system. This finding suggests

that the terminal relaxation time τ_r for $x > 1$ should correspond to a stiff limit, whereas contour fluctuations become relevant for $x < 1$.

Using the established relation $\xi_m \propto \sqrt{aL}$ [78,98], with tube diameter a, we find that our result for $x > 1$, see Eq. (4.12), is identical to the prediction of Doi for rigid rods, see Sec. 2.2.3. This is consistent with our interpretation of $x > 1$ as a stiff limit.
In contrast, for the large and highly relevant regime $\xi_m < l_p < 0.1\hat{l}_p = 0.1(L/\xi_m)^2$ we find: $\tau_r \propto l_p L^4/\xi_m^2$, see Eq. (4.12). To our best knowledge, this is a completely new scaling behavior, which is not explained by existing arguments. Our interpretation of x leads us to believe that contour fluctuations give the dominant contribution to rotation in the regime $x < 0.1$. Based on this interpretation, we construct a scaling argument clarifying the underlying mechanism and the observed behavior: As established previously, the contour fluctuations equal their equilibrium value. Thus, after a time $\tau_{i,l}$ parts of the polymer have explored a distance of L^3/l_p in its lateral direction, which is significantly larger than the mesh size or tube diameter in the regime $x < 0.1$. The average angular deviation $\langle \delta\theta^2 \rangle_{\text{bend}}$ resulting from those orthogonal fluctuations is proportional to L/l_p. The time required to achieve rotational relaxation through several steps of this type is then given by $\tau_{i,l}/\langle \delta\theta^2 \rangle$. Hence we find:

$$\tau_{i,l}/\langle \delta\theta^2 \rangle \propto \frac{\zeta L^5}{k_B T \xi_m^2} \frac{l_p}{L} \propto \tau_r \ , \tag{4.15}$$

which agrees with our finding for τ_r and establishes a direct relation between the two relaxation times. Thus we propose that the exploration of orthogonal space due to contour fluctuations is the dominant process for rotation. This interpretation is further supported by a finding established in Sec. 4.2.2. In the regime with $x < 0.1$ the onset of the terminal regime of $\delta \mathbf{e}_R^2$ coincides with the longest internal relaxation time. This is consistent with assuming that $\tau_{i,l}$ is the basic timescale for the dominant mechanism in that regime.
Note that our argument is based on the fact that the orthogonal fluctuations are larger than the tube diameter, which hints at a major role of constraint release in this regime.

In the literature a change of the dominant rotational diffusion process at $l_p/L = 1$ has been proposed [40, 97]. This leads to a sharp change in the l_p dependence of τ_r at that boundary. The change in behavior is usually included to cope with the varying strength of the orthogonal fluctuations. In contrast, in the relevant regime $x < 0.1$ our scaling prediction for τ_r is found to be valid for all systems with $l_p \gtrsim \xi_m$. Especially no difference in the l_p-dependence for $l_p/L \gtrless 1$ is found, see Fig. B.3 in Appendix B.

Having clarified the longest relaxation time of the rotational relaxation as the longest timescale in the system, we continue with analyzing the time evolution of the rotational MSD $\delta \mathbf{e}_R^2$. As there are different regimes for the scaling of τ_r, we also expect to find a different behavior of $\delta \mathbf{e}_R^2$ for stiff and semiflexible polymers. Therefore, we discuss the two cases separately.

4.2.2 Contour fluctuations dominate for semiflexible chains

We start by discussing the time evolution of the rotational mean square displacement $\delta \mathbf{e}_R^2$ of semiflexible chains with $x < 0.1$. Before going into details, shortly recall the rotational relaxation of a free semiflexible polymer chain in dilute solution. Up to the saturation time

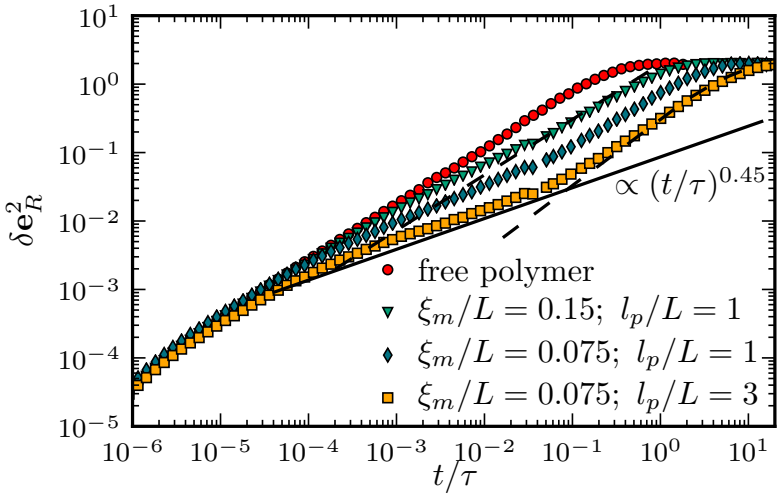

Figure 4.11: Rotational MSD for different systems with possible power-laws. Dashed curves show fits with $2 - 2\exp(-t/\tau_r)$. The solid line is a guide to the eye with a possible power-law to give an impression of the occurring behavior.

of internal fluctuations, the rotational MSD is dominated by the orthogonal fluctuations of the end segments of the polymer contour and hence increases with $t^{3/4}$. At larger times the polymer rotates like a rigid rod, which follows a $2[1 - \exp(-t/\tau_r)]$ behavior [39].

For a dense system, we expect an analogous segmentation of the dominant processes. First, the orthogonal contour fluctuations should dominate, later the global rotation takes over. As there appear two distinct regimes in the relaxation of δR^2 before it saturates, see Fig. 4.3, a corresponding additional regime should appear in $\delta \mathbf{e}_R^2$.

Indeed, in our simulations of tightly entangled networks we find that the dynamics of the rotational MSD may be separated into three regimes, see Fig. 4.11. At very small times the rotational diffusion of a single polymer in a network is identical to the free case, see Fig. 4.11, until the first contact with the surrounding mesh occurs. In the following intermediate regime the contour fluctuations are not yet saturated and we expect them to still dominate the rotational diffusion. Due to the intermediate regime appearing in the internal relaxation behavior, this no longer corresponds to free rotation. In conclusion, we expect the rotation to be dominated by the orthogonal contour fluctuations for the first two regimes. As these likewise give the dominant contribution to the contour length fluctuations δR^2, see Sec. 2.1.3, we expect that $\delta \mathbf{e}_R^2 \propto \delta R^2/L^2$ in these two regimes.

As soon as the contour fluctuations saturate at time $\tau_{i,l}$, we may treat the chain as an effective rigid rod and expect to recover the familiar $2-2\exp(-t/\tau_r)$ behavior, as predicted by existing theoretical models [97,98,100]. However, our newly found scaling of τ_r as discussed previously for the case $\xi_m < l_p \lesssim 0.1\hat{l}_p$ has to be used. Taking these parts together and assuming that the global rotation and local orthogonal fluctuations of chain segments are independent, we thus predict:

$$\delta \mathbf{e}_R^2(t) = c\delta R^2(t)/L^2 + 2\left(1 - \exp(-t/\tau_r)\right) \ , \tag{4.16}$$

where c is a proportionality parameter, which we use for fitting. Note that we are not concerned with the exact form of the parameter c, which includes the stiffness-dependency

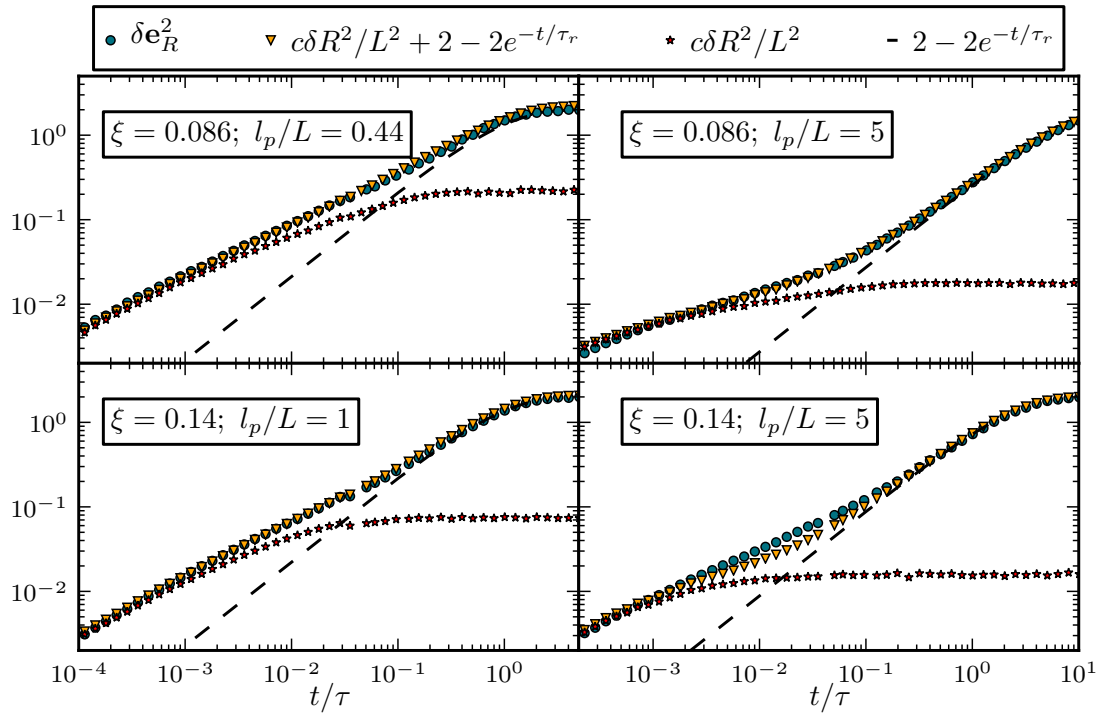

Figure 4.12: Examples for the correlation of rotational MSD $\delta \mathbf{e}_R^2$ and the length fluctuations δR^2 for networks with characteristics as given in each plot. For each system we compare the time evolution of $\delta \mathbf{e}_R^2$ to a function $c\delta R^2 + 2 - 2\exp(-t/\tau_r)$, where c is a fit parameter with values of $c = 0.13$ (top left), $c = 0.52$ (top right), $c = 0.13$ (bottom left), and $c = 0.48$ (bottom right). We find that $\delta \mathbf{e}_R^2$ is to good approximation identical to $c\delta R^2 + 2 - 2\exp(-t/\tau_r)$. The dashed lines give the rigid rod rotation contribution of $2 - 2\exp(-t/\tau_r)$ alone, to allow an easier identification of the onset of the final regime. For all systems considered, it becomes the dominant contribution at times $t \gtrsim \tau_{i,l}$.

relating $\delta R^2(t)$ and the orthogonal fluctuations. As can be seen in Fig. 4.12, our prediction is found to be correct. The $2 - 2\exp(-t/\tau_r)$ behavior becomes dominant at times $t > \tau_{i,l}$ after the polymer has equilibrated completely. This is no trivial observation, as this process is much slower than in dilute solution. As discussed in Sec. 4.2.1 this suggest that the rotation is coupled to contour fluctuations. Would rotation dominantly depend on diffusion along the tube, then the onset of the final regime would depend on that process, which exhibits a completely different scaling dependence.

Finally the discussion of $\delta \mathbf{e}_R^2$ becomes trivial for times $t \ll \tau_{i,l}$, as in this case we may with high accuracy approximate $\delta \mathbf{e}_R^2 \propto \delta R^2/L^2$. Thus the behavior of $\delta \mathbf{e}_R^2$ and the lower crossover time are identical to those found for the length fluctuations. Thus, the constraint release mechanism creating the intermediate regime in the internal fluctuations also affects rotation and especially the terminal relaxation time.

Note that when approaching the regime $x > 0.1$ we find that some small deviations between our prediction and the curves determined in our simulations occur, see the lower right part of Fig. 4.12 for an example. Usually these first become relevant close to $\tau_{i,l}$, i.e., before the crossover to the $2 - 2\exp(-t/\tau_r)$ behavior. As these deviations initially affect a rather small

time regime we do not attempt to explicitly study this intermediate transition to the stiff polymer behavior. To achieve this it would be necessary to study even smaller mesh sizes, on which we were numerically limited due to the available computational time.
We expect that in this range $\hat{l}_p < l_p < l_{p,c}$, i.e., $(L/\xi_m)^2 < l_p/L < (L/\xi_m)^4$ the behavior of the two limiting cases mix. This is in agreement with the few cases of our data where the transition may clearly be spotted, see lower right of Fig. 4.12. For small times, where the contour fluctuations dominate, we expect a behavior similar to the flexible case, which changes to the stiff dynamics at later times. By the definitions of the boundaries of this regime, see also Sec. 4.2.3, the crossover time τ_c must be located in the range $\tau_e < \tau_c < 9\frac{\zeta L \xi_m^2}{2k_B T}$. Due to the strong decrease of α_i with l_p the exact crossover is hard to determine. To avoid problems stemming from this transition, we skip the transition at $x \gtrsim 0.1$ and turn to discussing the stiff case $l_p > l_{p,c}$ or $x \gtrsim (\xi_m/L)^2 \gg 1$, respectively.

4.2.3 A mesh size dependent intermediate regime for stiff chains

We want to determine the behavior of $\delta \mathbf{e}_R^2$ for single chains in a network in the limit of stiff polymers with $l_p > l_{p,c}$. Like for the semiflexible chains, we may separate the dynamics of $\delta \mathbf{e}_R^2$ into three regimes, see Fig. 4.13: free rotation at small times, followed by an intermediate regime, and finally the expected $2 - 2\exp(-t/\tau_r)$ behavior of rigid rods.
The discussion may be simplified by noting that τ_r does not depend on l_p for $x > 1$. Thus we expected that for a fixed mesh size $\delta \mathbf{e}_R^2$ converges to a universal relaxation curve independent of l_p, which is indeed found in our simulations, see Fig. 4.13. Of course, this is only valid for times above the longest internal relaxation time, where contour fluctuations dominate the rotational diffusion. However, in the stiff limit the orthogonal fluctuations are smaller than the initial tube diameter and the longest internal relaxation time is identical to the case of free polymers in the dilute regime. In particular, $\tau_{i,l}$ is extremely small for these stiff polymers and may be neglected.
A stiff polymer in dense solution may undergo free rotation up to some crossover time $\tau_{r,c}$. To estimate this crossover time, consider a rigid rod of length L in an initial tube of diameter $a \propto \xi_m^2/L$, see Sec. 2.2.3. The rod undergoes free rotational diffusion until its angular deviation from the tube axis causes contact with the confinement. This first contact occurs at

$$\langle \delta\theta^2 \rangle \propto d^2/L^2 \propto (\xi_m/L)^4 \, . \tag{4.17}$$

The average time required to reach this angular displacement may be determined from $D_{\mathrm{rot}} t = \langle \delta\theta^2 \rangle$, where D_{rot} is the rotational diffusion coefficient in dilute solution. Hence the crossover time of first contact with the tube due to rotation should be:

$$\tau_{r,c} \propto \tau (\xi_m/L)^4 \, . \tag{4.18}$$

By rescaling our data accordingly, cf. Fig. 4.14 we find that this simple model is in agreement with our data.

At the second crossover, the rotational diffusion changes from the sub-diffusive intermediate regime to the expected $2 - 2\exp(-t/\tau_r)$ behavior, with τ_r as discussed previously. The crossover time between those two regimes may be determined by a simple argument. It follows from Doi's scaling argument for the longest relaxation time, see Sec. 2.2.3, which we

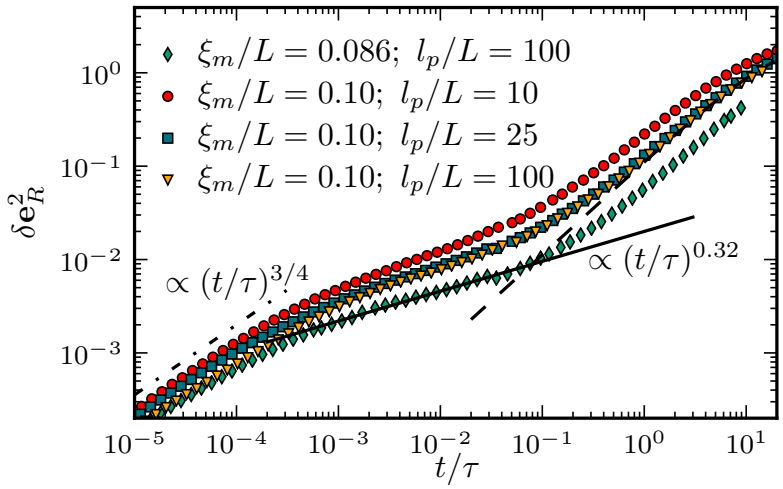

Figure 4.13: Examples for the rotational MSD of stiff chains in dense polymer networks. Like in the semiflexible case, we may identify three distinct regimes. An initial regime $t/\tau \lesssim 10^{-3}$dominated by free contour fluctuations (dashed-dotted line), is followed by an intermediate regime, where we find a mesh size dependent power-law. The solid line gives an example of the behavior in this regime. Finally, $\delta \mathbf{e}_R^2$ follows the $2 - 2\exp(-t/\tau_r)$ behavior (dashed line) expected for rigid rods. While for a constant mesh size there is a clear difference between the curves with $l_p/L = 10$ and $l_p/L = 25$, hardly any deviations between the results for $l_p/L = 25$ and $l_p/L = 100$ are visible. Thus, with increasing persistence length, $\delta \mathbf{e}_R^2$ converges to a l_p-independent relaxation curve for all times above the internal relaxation time.

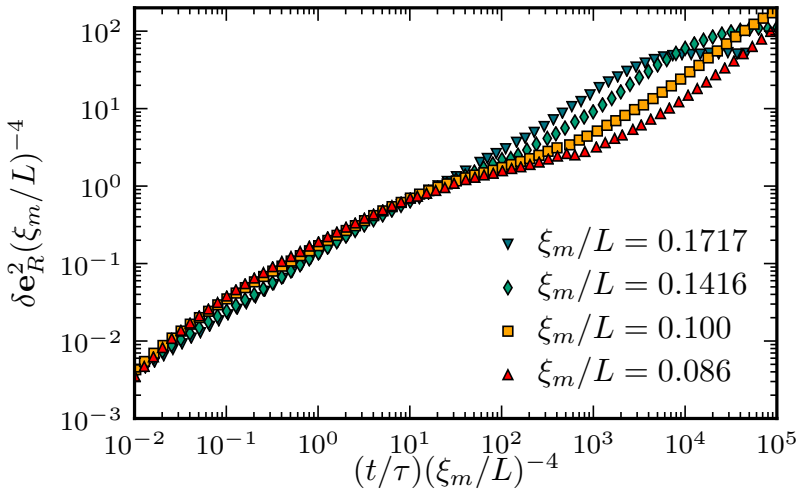

Figure 4.14: Rotational relaxation of single filaments in polymer networks with a stiffness of $l_p/L = 100$ for different mesh sizes. By rescaling the time and the amplitude with $(\xi_m/L)^4$ we find that the crossover from the regime of free rotational diffusion to the intermediate regime collapse.

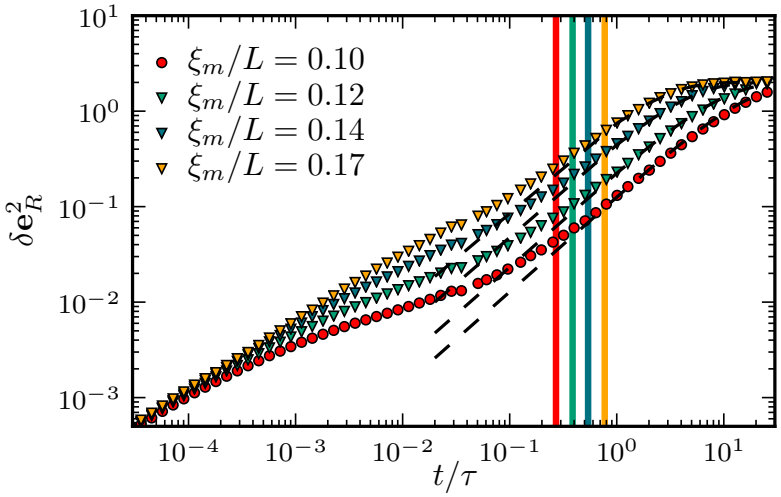

Figure 4.15: Examples for the rotational MSD of single chains in networks of stiff polymers with $l_p/L = 25$ for different mesh sizes. The horizontal bars give the times $T_{3\xi_m}/\tau$, where the color of the bar corresponds to the color of the rotational MSD with the same mesh size. The dashed lines represent fits of $2 - 2\exp(-t/\tau_r)$ to each curve, where τ_r is the fitting parameter. We find that the crossover from the sub-diffusive regime to the $2 - 2\exp(-t/\tau_r)$ behavior of $\delta \mathbf{e}_R^2$ occurs close to those time, i.e., at the intersection of a bar with the curve of the same color.

know to be in accord with our results, see Sec. 4.2.1. It is based on the assumption that the polymer has to move a distance comparable to the mesh size before it has sufficiently left its initial tube to acquire a new orientation. Thus we expect the exponential regime to start at the time required for a polymer to diffuse a distance proportional to ξ_m parallel to its end-to-end vector. As we show in Sec. 4.3.1, the parallel diffusion is essentially free. On average, the time to travel a distance x in one dimension is then given by $T_x = x^2 \zeta L / 2 k_B T$. We assume that $x = c\xi_m$, where c is a numerical fitting parameter. In Fig. 4.15 it can be seen that with $c = 3$ this prediction results in times very close to the crossover. Thus the crossover time is found to be:

$$\tau_{r,c} \approx 9 T_{\xi_m} = \frac{9 \zeta L \xi_m^2}{k_B T} \,. \tag{4.19}$$

Between these crossover times we report the existence of an intermediate regime, whose behavior depends only on the mesh size. We find that $\delta \mathbf{e}_R^2$ strictly increases even during this intermediate regime, see Fig. 4.13 for some examples.
This contradicts the standard reptation picture where the tube stays fixed around the rod, and thus limits the accessible angles until the polymer has moved far enough out of the tube. This is comparable to the intermediate regime in the semiflexible case, and probably also relates to a form of constraint release, as discussed earlier.
To quantify the behavior in the intermediate regime of $\delta \mathbf{e}_R^2$ in the stiff case, we analyz systems with $l_p/L = 100$ and various mesh sizes. Using a least square method we fitted $\delta \mathbf{e}_R^2$ with a function ct^β in the time interval $\tau_{r,c} < t < 2T_{\xi_m}$, where c and β are dimensionless fit parameters. One might argue that the stiffness should be adjusted to the mesh size for this measurement to compensate the increase of the critical persistence lengths with smaller mesh

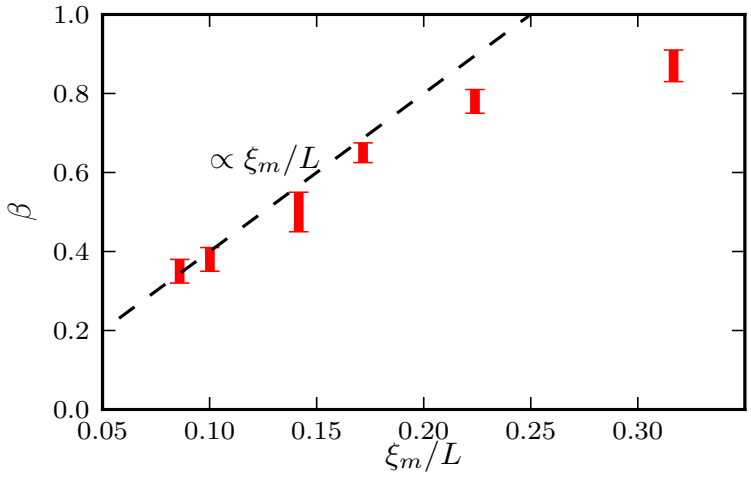

Figure 4.16: Dependence of the exponent in the intermediate regime on the mesh size ξ_m/L for polymers with a stiffness of $l_p/L = 100$.

size. Unfortunately, in order to ensure numerical stability, we could not increase the stiffness above $l_p/L = 100$. However, as discussed previously $\delta\mathbf{e}_R^2$ converges to an l_p-independent curve in the stiff limit. As we avoid the transition at $x = 1$ we are confident that our results correspond to the true exponent characterizing the behavior in the stiff limit.

In Fig. 4.16 we present the fitted values for the exponent β. For dense networks with $\xi_m/L \ll 1$ we find that β decreases approximately linearly with the mesh size. For less dense networks the dependence on ξ_m/L decreases and we assume that it converges to the value 1 of free rotation.

To sum it up, two different processes may determine the crossover time to the $2-2\exp(-t/\tau_r)$ behavior found for all sets of parameters. For very stiff polymers it is determined by the time required to diffuse a distance of about $3\xi_m$ parallel to the polymer contour. When decreasing the stiffness, as soon as the internal relaxation time $\tau_{i,l}$ becomes longer than this diffusion time, the contour fluctuations completely dominate and determine the crossover time. Depending on the type of crossover, there occurs a different intermediate regime, but in all cases the rotational MSD strictly increases at all times $t < \tau_r$ in contrast to the predictions of the reptation theory, see Sec. 2.2.4. We attempt to identify the relevant constraint release mechanisms causing these recurring deviations from standard theory in Chapter 5.

4.3 Diffusion

Finally, we analyze the diffusion of a chain. We frequently employ the previous results on the relaxation dynamics to achieve a better understanding of the relevant processes. As discussed in the methods, see Sec. 3.3, we separate the diffusion of each chain into a parallel and an orthogonal component with respect to the orientation of the polymer at the start of the measurement, $t = 0$. First, we analyze the basics of the parallel diffusion and then complement the discussion by scrutinizing the orthogonal part.

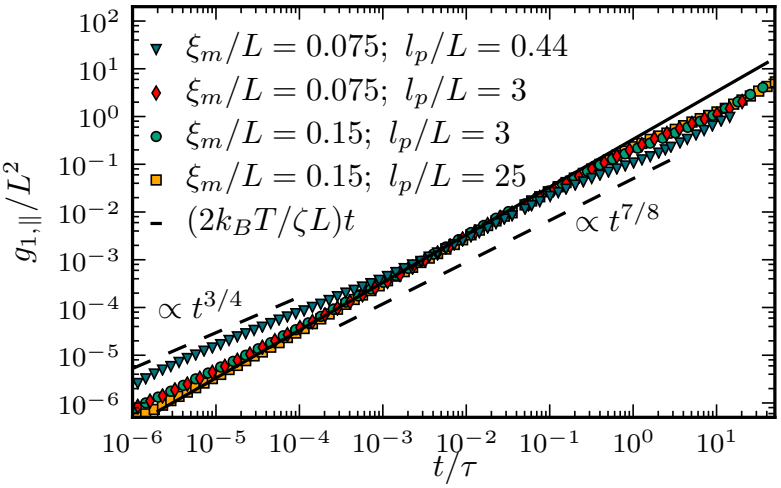

Figure 4.17: Examples for $g_{1,\parallel}$ of a chain in polymer networks of different characteristics. The solid lines gives the theoretical prediction for the free one-dimensional diffusion of a single polymer of length L. Additional possible scaling laws as expected from the longitudinal relaxation are given by the dashed lines.

4.3.1 Free diffusion along the polymer

In Fig. 4.17 the parallel diffusion of the center monomer, $g_{1,\parallel}$ measured in our simulations for several different systems is shown. We may separate $g_{1,\parallel}$ into roughly four regimes. At very small times, $t/\tau \lesssim 10^{-4}$ in Fig. 4.17, we find a regime with $g_{1,\parallel} \propto t^{3/4}$, which seems to primarily depend on the persistence length. Next, the most notable feature of $g_{1,\parallel}$, is a large intermediate regime, where the parallel diffusion is almost unaffected by both the flexibility and the mesh size of the system. The behavior in this regime is found to be close to linear diffusion. It is followed by a short crossover regime, occurring in the range $10^{-1} \lesssim t \lesssim 10^{1}$ for the different parameters in Fig. 4.17. We explain this regime in Sec. 4.3.2 when discussing the super-diffusive regime appearing in the orthogonal diffusion. In particular, we show that his regime ends at time τ_r. In agreement with the definition of the terminal relaxation time, the last regime at times $t > \tau_r$ is found to exhibit linear diffusion with a diffusion coefficient proportional to the inverse of the longest relaxation time. Here, we focus on the behavior before the short crossover regime, i.e., on the range $t/\tau \lesssim 1$ in Fig. 4.17.

The dynamics at intermediate times are usually associated with the sliding along the initial tube of the polymer. Thus they are expected to be equivalent to free diffusion of a rigid rod with identical length [39, 40, 97]. We find that our data on $g_{1,\parallel}$ agrees very well with free one-dimensional diffusion, see Fig. 4.17. Hence, in the intermediate regime it holds:

$$g_{1,\parallel} \approx \frac{2k_BT}{\zeta L} t \,, \tag{4.20}$$

as used previously for determining T_{ξ_m} in Sec. 4.2.3.

Instead of free diffusion, some theories predict an increase with $t^{7/8}$. This behavior originates in the tangential relaxation of worm-like chains, and is known from theoretical predictions

for polymers in dilute solution [9,134]. Also, it has been reported for the reptation of chains through a 2-dimensional system with fixed obstacles [31]. Our data seems to fit better with the free diffusion, see Figs. 4.17 and 4.18, although for chains with $l_p/L < 1$ it is hard to unambiguously distinguish between the two proposed power-laws. For these chains it is possible that the behavior becomes slightly sub-diffusive. This seems to affect a small range of flexibilities only and is a relatively small difference. For simplicity we always assume linear diffusion in this time regime for all arguments throughout this paper.
From this result, we derive the reptation time τ_d, which is defined as the time required to move out of the original tube. Note that we have not yet found any process associated with this timescale for our system. Also, none appear in the further discussions. As the value of τ_d thus serves only as a comparison to the flexible case, we do not make the effort to use an evolved description of the tube length. See Sec. 2.2 for models employing more details in this derivation. Here, due to the semiflexible nature of the filaments, we approximate the tube length by the contour length L and it follows:

$$\tau_d \approx \frac{\zeta L^3}{2k_B T} \,. \tag{4.21}$$

In accordance with previous models [31, 40] and motivated by the familiar $t^{3/4}$ power-law, we attribute the initial regime at very small times to contour fluctuations. This view is substantiated by the observations that the $t^{3/4}$ behavior vanishes when observing the center of mass diffusion. Note that in every other aspect, i.e., at all later times, the parallel diffusion of the center of mass $g_{3,\parallel}$ is identical to $g_{1,\parallel}$, see Fig B.4 in the appendix. In the limit of small times, $g_{3,\parallel}$ directly exhibits a linear diffusion at very small times, which for $g_{1,\parallel}$ appear later in the intermediate regime. In other words, $g_{3,\parallel}$ exhibits free diffusion in one dimension for all times below the short crossover regime.

As shown in Sec. 4.1 the fluctuations of the polymer contour are modified by the presence of the surrounding network. To test whether this affects $g_{1,\parallel}$, we compare our measurement in dense networks with the corresponding results in dilute solution, see Fig. 4.18. We find that for all times below the short crossover regime the parallel diffusion in a network is identical to the case of a dilute polymer system for the full range of flexibilities $l_p \gg \xi_m$ and densities $0.075 \leq \xi_m/L \leq 0.3$ studied here. For rather flexible polymers, see lowest part in Fig. 4.18 we find a very small, but systematic deviation between the dilute and dense simulation in the form of a decreased diffusivity in the dense case. We attribute this decrease to collisions at the confinements of the tube corresponding to an increased effective friction coefficient. As the orthogonal fluctuations decrease linearly with the stiffness, this only occurs for almost flexible polymers.

In conclusion, we find free diffusion along the tube corresponding to the dynamics in dilute solution including the effects of contour fluctuations on $g_{1,\parallel}$. It is followed by a crossover regime, which is explained in the next section. Finally, linear diffusion at times $t > \tau_r$ dominates as expected.

A major point in this analysis is the complete lack of an intermediate $t^{1/2}$ regime, cf. Fig. 4.17, as famously occurs in the reptation of flexible polymers [39,59]. Recent simulations in two dimensions with fixed obstacles reported a similar regime for polymers with $l_p/L \approx 1$ [31]. Here, we exclusively find a $t^{1/2}$ regime in the flexible limit, $l_p < \xi_m$, see Fig. B.5 in the appendix

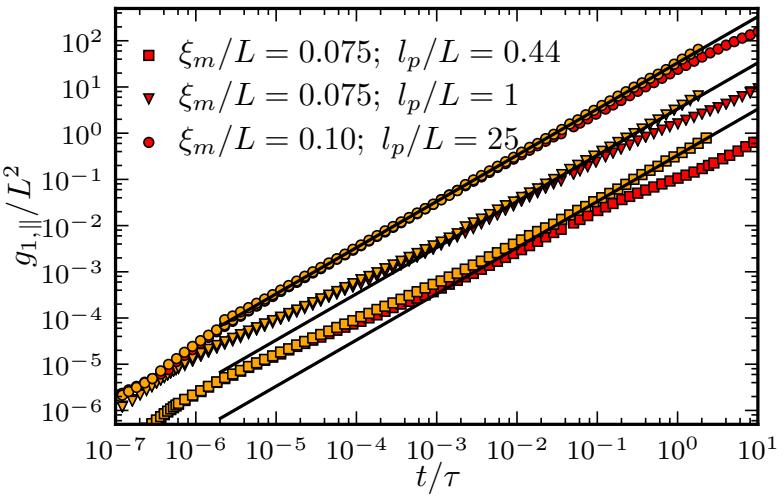

Figure 4.18: Comparison of $g_{1,\parallel}/L^2$ for various dense networks in red with the results for free polymers of identical stiffness in dilute solution in yellow. The characteristics of the networks are given in the legend. For better visibility the values of $g_{1,\parallel}/L^2$ for $\xi_m/L = 0.075$, $l_p/L = 1$ (triangles) and $\xi_m/L = 0.10$, $l_p/L = 25$ (circles) have been shifted in amplitude by a factor of 10 and 100, respectively. We find that the results are essentially identical up to the crossover at about $10^{-1}\tau$. The solid lines give the prediction for free one-dimensional diffusion of the polymer $\frac{2k_BT}{\zeta L}t$.

for an example. Our result is in accordance with previous studies in the flexible parameter regime [59]. A detailed analysis of the effects of fixing the obstacles, which eliminates all types of additional constraint release, follows in Sec. 5.1.

4.3.2 Orthogonal diffusion and a super-diffusive regime

The orthogonal part of the diffusion $g_{1,\perp}$ allows a more detailed analysis of the occurring processes. As can be seen in Fig. 4.19, the orthogonal part of the diffusion may be segmented into four major regimes, which depend on both the stiffness and the mesh size. At very small times, we expect free contour fluctuations. According to the tube picture and consequently predicted by all theories based on it, once the chain is in contact with the tube, it no longer diffuses orthogonally until it has traveled a distance long enough to tilt its direction. Thus, in the following regime both $g_{1,\perp}$ and $g_{3,\perp}$ should be constant [31, 100]. In contrast to this prediction we shall see in our simulations that for all parameter sets used both observables always increases in the regime following the free dynamics. Before the diffusion becomes linear in t at late times, a super-diffusive regime occurs, which has only recently been found in simulations [31].

To simplify the more complicated dynamics of these observables, we divide the discussion into several segments. First, we analyze the behavior in the two regimes at large times, $t/\tau \gtrsim 0.1$ in Fig. 4.19, where the diffusion of the center monomer and the center of mass are identical, see Fig. B.4 in the appendix. Also, we find that the behavior and scaling laws in this regime are valid for semiflexible and stiff polymers alike. Then we first discuss the dynamics in the

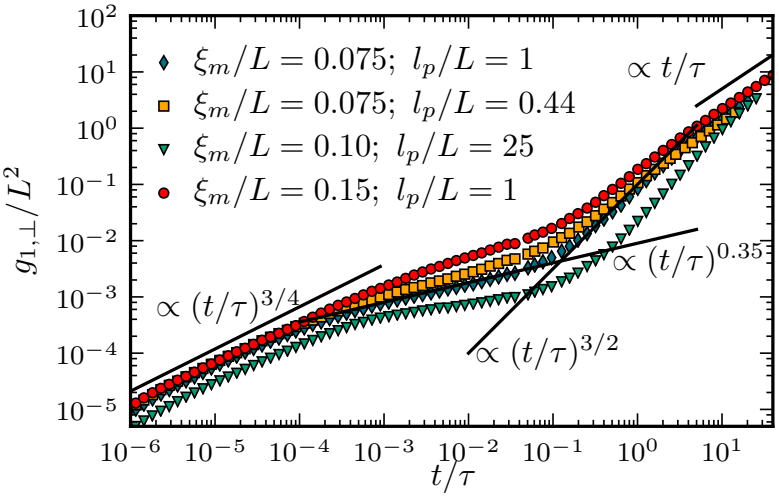

Figure 4.19: Examples for $g_{1,\perp}$ of a chain in polymer network of different characteristics. The solid lines give possible scaling laws for each regime.

two small times regimes $t/\tau \lesssim 0.1$ for stiff polymers, as they only differ trivially for the two observables. Finally we discuss the semiflexible parameter regime with $\xi_m \ll l_p \ll \hat{l}_p$. Here we explicitly have to distinguish between $g_{1,\perp}$ and the center of mass diffusion $g_{3,\perp}$.

We start with the expected observation that for late times $t > \tau_r$, analogous to the parallel diffusion and for all sets of parameters studied, the chains diffuse linearly in time. See the discussion of the longest relaxation time in Sec. 4.2.1 for more details.

The final diffusive regime is preceded by a super-diffusive regime, e.g., in the range $0.1 \lesssim t/\tau \lesssim 10$ in Fig. 4.19. This super-diffusive regime has already been found in recent simulations of a chain in two dimensions surrounded by fixed obstacles [31]. It has been claimed that this super-diffusive regime universally follows a $t^{3/2}$ scaling and a scaling argument relating it to tangential contour fluctuations has been given, see Sec. 2.2.6. However, in our simulations we find that the exponent in the super-diffusive regime is not universal, see Fig. 4.19. Motivated by the given scaling argument we compare the orthogonal diffusion with the length fluctuations and the parallel diffusion of a chain, see Fig. 4.20. We find clear evidence of a super-diffusive scaling even if δR^2 is saturated and in spite of the parallel diffusion lacking a suitable $t^{1/2}$ scaling regime. We conclude that the scaling argument given in Ref. [31] does not hold for polymers of finite length.

Here we propose a different mechanism as the origin of the super-diffusive regime. Consider a chain moving in a polymer mesh at a time $t > 0$. As previously established for the tube sliding motion, the chain diffuses freely along the parallel direction with respect to its current normalized end-to-end vector $\mathbf{e}_R(t)$. Hence the total diffusion increases at any point in time with approximately $t\mathbf{e}_R(t)$. However, we are only interested in the orthogonal component relative to the orientation at $t = 0$. The projection on the orthogonal direction may be written as $[\mathbb{1} - \mathbf{e}_R(0) \otimes \mathbf{e}_R(0)]$. Then the contribution to orthogonal diffusion is given by $t[\mathbf{e}_R(t) - \mathbf{e}_R(0)(\mathbf{e}_R(t) \cdot \mathbf{e}_R(0))]$. This expression contains a term proportional to the correlation of the end-to-end vector, and thus the rotational relaxation. Hence the movement along the

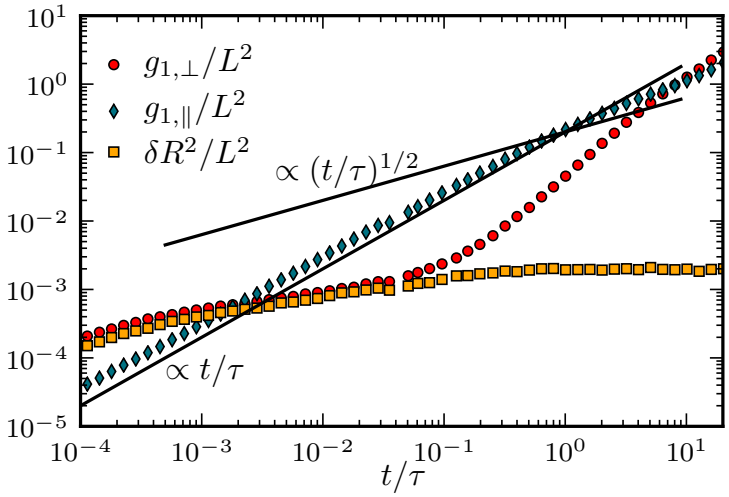

Figure 4.20: Example for a polymer network with $l_p/L = 3$ and $\xi_m/L = 0.075$, where the contour length fluctuations saturate at the onset of the super-diffusive regime. Thus an increase of $g_{1,\perp}$ may not be explained by the contour fluctuations. Also, the parallel diffusion does not follow a $t^{1/2}$ scaling, especially not during the full super-diffusive regime. As a guide to the eye both a $t^{1/2}$ and a linear scaling are given. The super-diffusive regime may not be explained as suggested previously [31].

tube gives a contribution to the orthogonal diffusion, which increases as the tube rotates. This tube rotation argument may easily be reformulated to a more suitable expression and we predict:

$$g_{1,\perp} \propto t\delta\mathbf{e}_R(t)\,. \tag{4.22}$$

As can be seen in Fig. 4.21, this scaling law very precisely results in the observed power-law in the super-diffusive regime. We find similar good agreement for all sets of parameters considered, both in the semiflexible and stiff regime.

Note that the orthogonal and parallel contribution of the tube sliding motion depend on each other, as they are projections of the same process. Thus, if the orthogonal part increases, the parallel projection decreases accordingly. This is required as at times $t > \tau_r$, when all orientational correlation is lost, the diffusion becomes isotropic and there is no difference between the parallel and orthogonal directions. In this way our tube rotation picture explains the short parameter dependent crossover-regime occurring in the parallel diffusion, see Sec. 4.3.1. It corresponds to the super-diffusive regime of the orthogonal diffusion, except that the parallel contribution of the free tube sliding motion decreases with proceeding rotation.

Our tube rotation argument is further affirmed by the fact that the crossover time, where $g_{1,\perp}$ changes to the super-diffusive regime, coincides with the onset of the $2 - 2\exp(-t/\tau)$ regime in $\delta\mathbf{e}_R(t)$, see Fig. 4.22. Importantly this is true independent of the specific process determining this onset. Explicitly the regimes starts at $\tau_{i,l}$ in the semiflexible and at $9T_{\xi_m}$ in stiff case, compare Sec. 4.2.2. Like for the process of rotation, see Sec. 4.2, this clearly hints that the dynamics in the regimes at shorter times than the super-diffusive regime behave completely differently in those two cases.

Before we turn to discussing these regimes, for the reader's convenience we shortly summarize

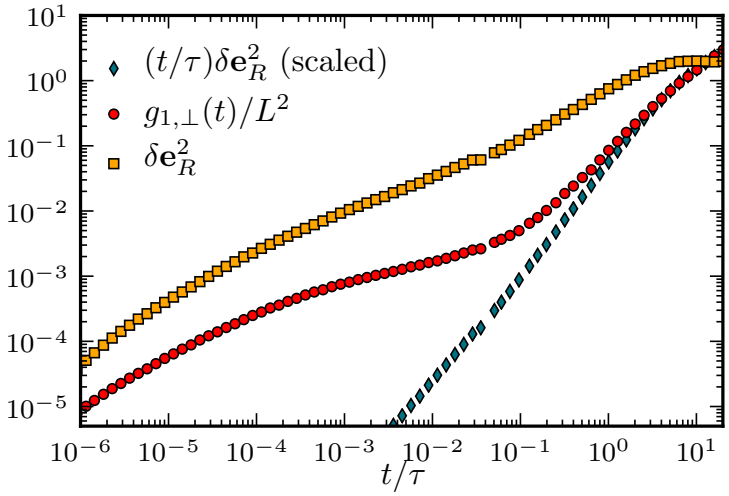

Figure 4.21: Possible explanation of the super-diffusive regime by tube rotation. The red circles give the orthogonal part of the center monomer diffusion, and the diamonds show the prediction according to the tube rotation argument, which has been scaled for better comparison of the two curves. We find a good agreement between the two curves throughout the full super-diffusive regime.

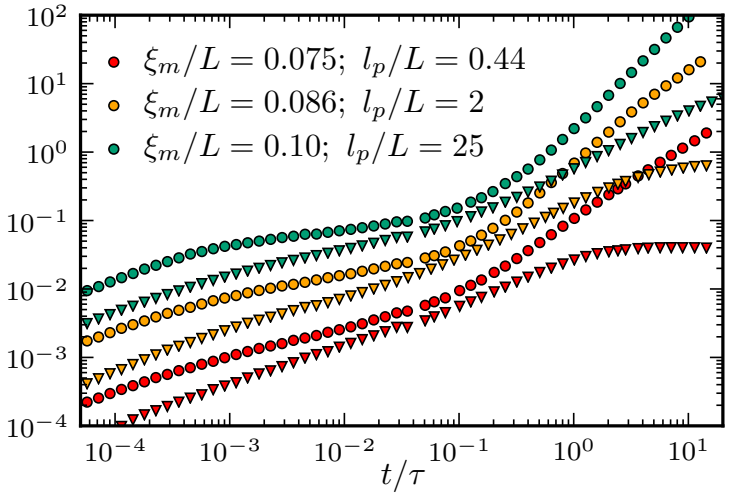

Figure 4.22: For several systems the rotational MSD $\delta\mathbf{e}_R(t)$ (triangles) and $g_{1,\perp}/L^2$ (circles) are given. See color code and legend in the figure for mesh size and stiffness of the systems. For better visibility the curves of $g_{1,\perp}$ for $\xi_m/L = 0.086$, $l_p/L = 2$ and $\xi_m/L = 0.10$, $l_p/L = 25$ have been shifted in amplitude by a factor of 10 and 100, respectively. Also, the rotational MSD has been scaled to allow easier comparison of the crossover times. We find that the onset of the super-diffusive regime in $g_{1,\perp}$ coincides with the onset of the $2 - 2\exp(-t/\tau)$ regime in $\delta\mathbf{e}_R(t)$.

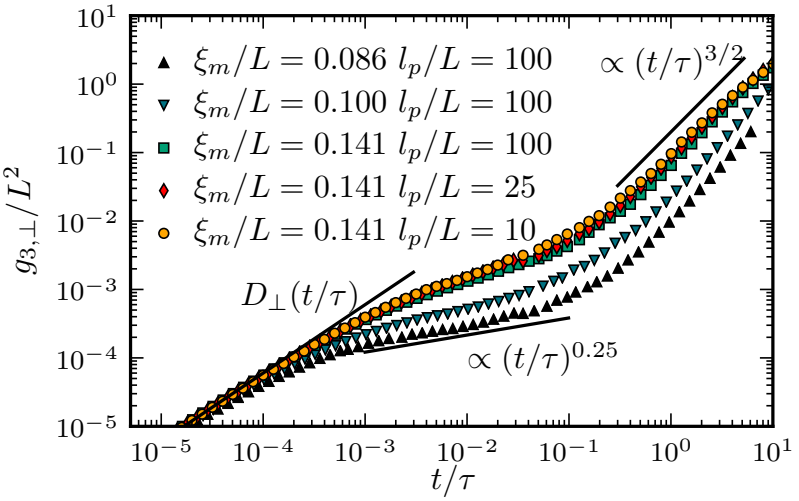

Figure 4.23: Orthogonal diffusion of the center of mass for polymers in networks of different characteristics. The black lines give the prediction for free diffusion at very small times $t < 10^{-3}$, as well as possible scaling laws to allow for an easier identification of the different regimes.

our findings for the two late time regimes of the orthogonal diffusion of polymers in a dense mesh. At times $t \gg \tau_r$ we find the expected diffusive regime. For times $\tau_{i,l} \ll t \ll \tau_r$ in the semiflexible parameter regime and times $T_{3\xi_m} \lesssim t \ll \tau_r$ in the stiff case, a super-diffusive regime occurs. We propose that in all cases this super-diffusive regime results from the projection procedure and only expresses the rotation of the polymer, or analogously its tube, when observing the diffusion.

Short time diffusion of stiff chains

Since we find it is the easier case, we continue by discussing the small time regimes appearing in the diffusion of stiff filaments. Remember that the diffusion of the center monomer and the center of mass only vary up to the internal relaxation time. This timescale is well below the times of first interaction with the boundary for polymers with $l_p > l_{p.c}$. Therefore, we do not need to distinguish between those two observables on the timescales relevant for the diffusion through a network. Thus, while discussing the stiff case, please consider all following propositions to be equally valid for both $g_{1,\perp}$ and $g_{3,\perp}$, even if not stated explicitly.

In Fig. 4.23 we present results for the center of mass diffusion for stiff chains in a network. We find that the stiffness has only negligible effect on the diffusion, whereas a significant effect of the mesh size may be observed.

As expected and similar to the rotational MSD in the stiff case the polymers diffuse freely at very small times, cf. Fig. 4.23. The crossover time t_c of first contact may be estimated analogously to the discussion for the rotational MSD. Consider a rigid rod of length L in an initial tube of diameter $d \propto \xi_m^2/L$. The rod undergoes free diffusion up to contact, thus: $D_\perp t_c = d^2$. It follows: $t_c \propto \tau(\xi_m/L)^4$. Note that this is the same scaling as derived for the

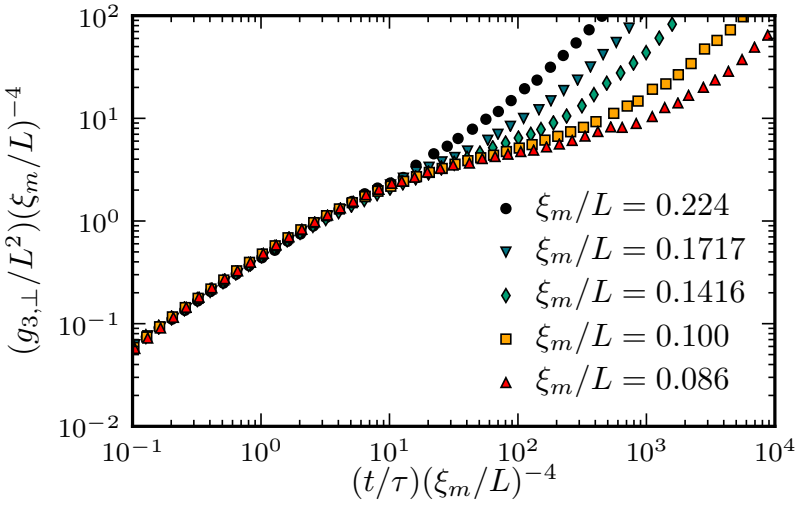

Figure 4.24: Orthogonal diffusion of the center of mass of polymers with a stiffness of $l_p/L = 100$ in networks of different mesh sizes. By rescaling the time and the amplitude with $(\xi_m/L)^4$ we find that the crossover from the regime of linear diffusion to the intermediate regime collapse.

crossover time of first contact of the rotational MSD, i.e., $t_c \propto \tau_{r,c}$. As can be seen in Fig. 4.24 this simple prediction works well with our data.

Finally, in the intermediate regime after the free diffusion but before the super-diffusive regime, i.e., in the range $\tau_{r,c} < t < T_{\xi_m}$, we find an almost purely mesh size dependent behavior, cf. Fig. 4.23. A similar dependence is found in the analysis of the rotational relaxation of stiff filaments, Sec. 4.2.3. Obviously for a stiff chain or rigid rod, rotation and orthogonal movement are tightly coupled. To increase the angular displacement, at least a part of the rod has to explore a previously un-accessed region orthogonal to the initial orientation. Thus the orthogonal diffusion and the rotational relaxation should be proportional to each other at small times, while most of the chain resides in the initial tube:

$$g_{3,\perp} \approx g_{1,\perp} \propto \delta \mathbf{e}_R^2 \,. \tag{4.23}$$

Indeed, we find that the behavior of $g_{3,\perp}$ in this regime is completely identical to the intermediate regime observed in $\delta \mathbf{e}_R^2$, cf. Fig. 4.25. Thus, it may be described by ct^β, where c is a fitting parameter and the mesh size dependent β is given in Fig. 4.16.

Short time diffusion of semiflexible chains

Let us now take a closer look at the diffusion dynamics of semiflexible polymers with $x \ll 1$. In this regime the orthogonal contour fluctuations interact with the surrounding chains before any other contact due to diffusion or rotation occurs. Seeing this, we should not be surprised to find sever differences between the center of mass diffusion $g_3(t)$ and the center monomer diffusion $g_1(t)$.

For the center monomer diffusion, as expected and predicted by all existing theories, for very small times the familiar $t^{3/4}$ power-law governing the free fluctuations in semiflexible to stiff

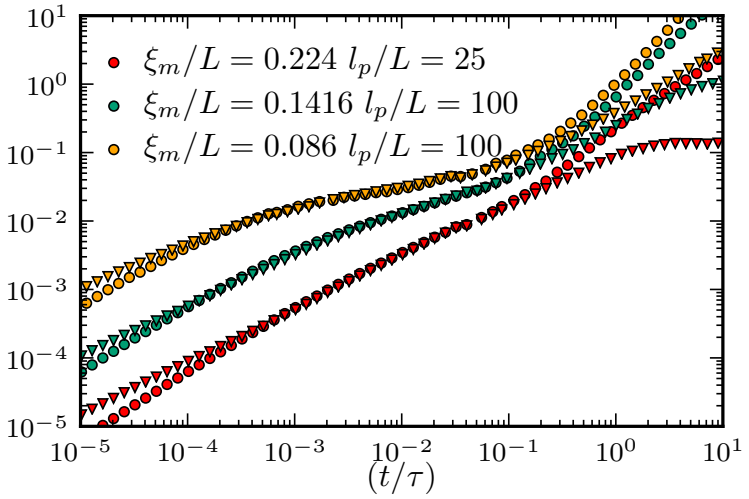

Figure 4.25: Orthogonal diffusion of the center of mass $g_{3,\perp}/L^2$ (circles) of single polymers in networks of different characteristics, see legend, compared to $\delta \mathbf{e}_R^2$ of the same polymers (triangles). We find that in the regime $\tau_{r,c} < t < T_{\xi_m}$ both curves behave similarly. For better visibility of this relation, we use $3\delta \mathbf{e}_R^2$ in the plot.

polymers appears, see Fig. 4.19. The intermediate regime after the free fluctuations and before the onset of the super-diffusive regime shows a clear increase with time. Expecting the contour fluctuations to be dominant, we look for a correlation between δR^2 and $g_{1,\perp}$. In a dilute solution of semiflexible chains, for small times an approximately direct proportionality $g_{1,\perp} \propto l_p/L\delta R^2$ between the two observables is known to hold [40]. In a dense network, we need to consider that only segments of length L_e may fluctuate freely. Assuming that identical mechanisms govern the contour fluctuations in dense networks we thus expect:

$$g_{1,\perp} \propto l_p L_e / L^2 \delta R^2 \ . \tag{4.24}$$

As can be seen in Fig. 4.26, scaling δR^2 accordingly indeed results in a good data collapse of $g_{1,\perp}$ with the length fluctuations up to time τ_i, l. We assume that the deviations in the amplitude for the curves with $l_p/L < 1$ in Fig. 4.26 are due to the fact that the weakly bending approximation is not sufficiently fulfilled. Thus, in the power-law description of the intermediate regime of $g_{1,\perp}$ the same exponents α_i occur as for the intermediate regime of the internal fluctuations discussed in Sec. 4.1. Also, this shows that the super-diffusive regime follows directly onto the regime dominated by fluctuations, i.e., the crossover time to the super-diffusive regime is $\tau_{i,l}$.

For the center of mass diffusion $g_{3,\perp}(t)$ of semiflexible polymers in a network with $x \ll 1$, consistent with the results for $g_{1,\perp}(t)$ and in agreement with all predictions, we find free diffusion at very small times up to the time of first contact with the tube τ_e, see Fig. B.6 in the appendix. Remember that in this parameter regime this timescale is governed by fluctuations as established earlier.
Analogous to all previous observables the regime of free diffusion is followed by an intermediate regime, where $g_{3,\perp}(t)$ increases sub-diffusively, see Fig 4.27. Like before, we fit the data for different systems in this regime with a power-law ct^γ for a more quantitative analysis. We

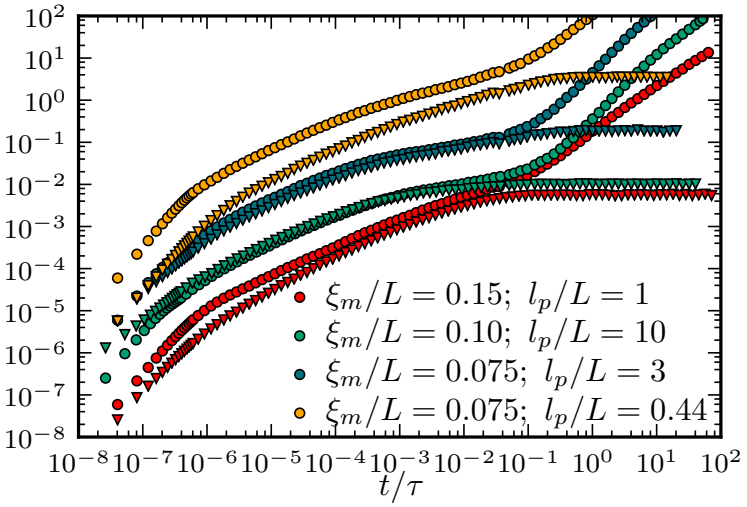

Figure 4.26: Examples for the connection of $g_{1,\perp}/L^2$ (circles) with $l_p L_e \delta R^2/L^4$ (triangles) of single chains in polymer network of different characteristics as given in the legend. For better visibility, the curves for $\xi_m/L = 0.10;\ l_p/L = 10$, $\xi_m/L = 0.075;\ l_p/L = 3$ and $\xi_m/L = 0.075;\ l_p/L = 0.44$ have been shifted by a factor of 10, 100 and 1000, respectively.

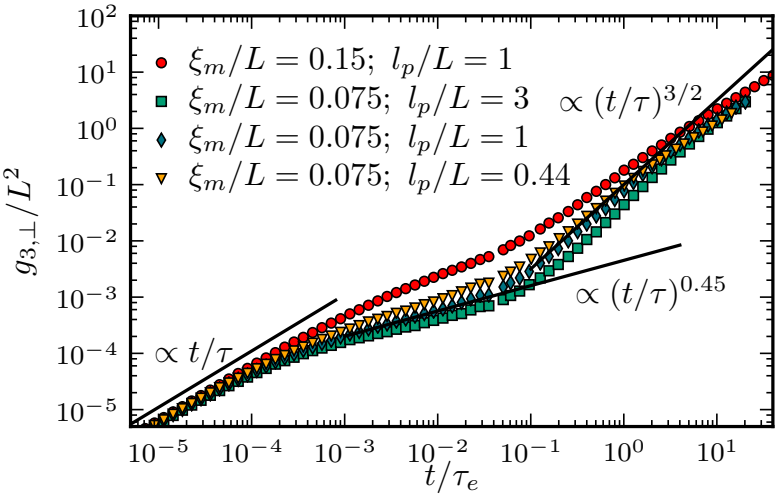

Figure 4.27: Some typical examples for $g_{3,\perp}/L^2$ measured in our simulations are shown. The continuous lines give examples of the possible power-laws describing the behavior in the different regimes.

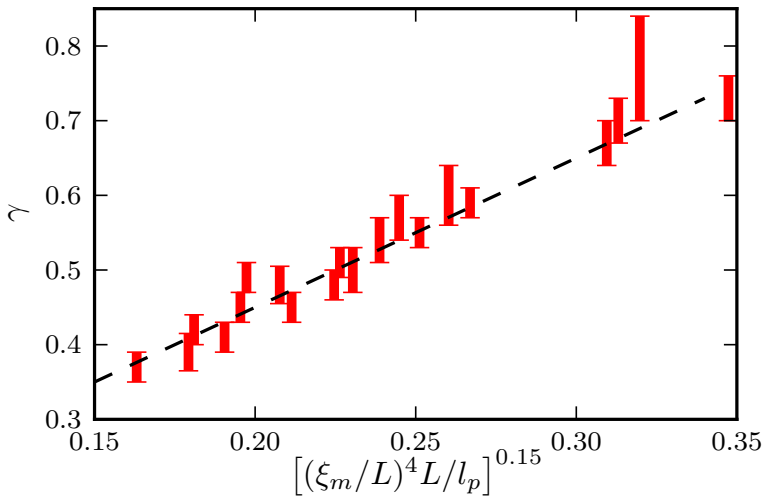

Figure 4.28: Shown are the fitted values for γ in dependence on $y = \left[(\xi_m/L)^4 L/l_p\right]^{0.15}$. The dashed line shows the proposed linear relation between γ and y.

find that the behavior in this regime depends on both stiffness and mesh size for polymers in a network with $x \ll 1$, cf. Fig 4.27. To good approximation the exponent γ depends almost linearly on the single parameter $\left[(\xi_m/L)^4 L/l_p\right]^{0.15}$, see Fig. 4.27. Interestingly this scaling parameter may be reformulated as $(\xi_m/L)^4 L/l_p = (\xi_m^4/l_p)/\tau$, i.e., the ratio of the time required for a segment of length ξ_m to relax due to fluctuations and the diffusive timescale τ. This observation might help to shed some light on the underlying process allowing the polymers to explore a region larger than the initial tube. We leave the justification of this scaling behavior for later work.

5 Evaluating the significance of constraint release

Having found several discrepancies between our results and both existing theoretical predictions and previous simulations, it is interesting to analyze those differences and take a closer look at the source of those discrepancies. A hint for the possible origin may be found in the intermediate regime.

The point is most apparent for the orthogonal diffusion of the center monomer. In the tube picture of standard reptation theory the tube stays fixed and is only renewed by the chain leaving it at either end [36,39]. Therefore, each segment of the polymer chain is completely confined to the tube. Thus, at intermediate times the orthogonal diffusion of the center monomer should exhibit a plateau.

These predictions have been confirmed by previous simulations with semiflexible filaments or rigid rods [31, 35]. However, these simulations are based on single polymers moving through an array of fixed obstacles [31, 35]. While they are therefore close to the original theoretical model, it is not clear how this description relates to systems without fixed obstacles.

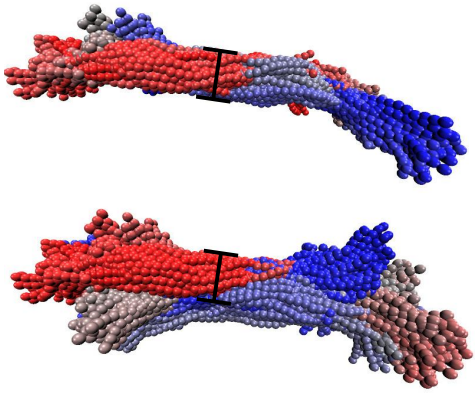

Figure 5.1: Comparison of the apparent tube width after different times in a system with $\xi_m/L = 0.10$ and $l_p/L = 1$. Similar to Fig. 4.1, a superimposition of configurations acquired during a time interval is shown. The upper figure shows configurations collected over 0.1τ, the lower is for an increased interval of 0.3τ. The color indicates the relative time of the measurement. In the lower part, the polymer seems to occupy a tube with a larger diameter. For better visibility of this enlargement, the black lines gives the apparent tube width resulting from the shorter time interval.

In a purely entangled polymer mesh no chains are completely fixed. All chains are constantly moving and the surrounding of each chain is permanently changing, in contrast to a system with fixed obstacles. In our simulations for this type of system we do not find a constant plateau in the intermediate time regime for any observable. This effect may easily be visualized. Fig. 5.1 shows superpositions of several configurations of a single chain during a time interval of 0.1τ and 0.3τ, respectively. Both pictures are for the same chain, yet in the lower figure the observed period of time is larger by a factor of 3. It is apparent that in the larger time interval the chain has explored a broader region with respect to the orthogonal direction. Note that it has not left its initial tube yet. Thus, the apparent tube width and orthogonal fluctuations increase in time. In other words, the tube constraint relaxes. Taking a closer look, we can see in Fig. 5.1 that the occupied region of the tube changes over time. Consider the lower part of Fig. 5.1. Initially the polymer is in the red region, which may be seen as the initial tube. At later times, shown in gray and blue, the

polymer is in a region shifted downwards relative to the initial tube. This means that the tube is not dilated, but rather moves and in that process changes its conformation over time. This additional process relaxes the constraint posed by the surrounding polymers, and treated as a tube in reptation theory.

Recall that there is only a weak argument claiming the validity of the fixed obstacle assumption for such systems, see Sec. 2.2. The additional movement of the tube due to the changing surrounding creates constraint release, which may alter the observed dynamics. These effects are not yet included in the theories for dense solutions of semiflexible polymers, see Sec. 2.2. While they are present in our simulations, previous studies with fixed obstacles would not have captured these effects. Consequently, we assume that this constraint release is responsible for the deviations between our data and both existing predictions and simulational results.

5.1 Constraint release significantly alters reptation

As a first test for the relevance of constraint release on the dynamics of single chains in a network, we want to eliminate all constraint release. To achieve this, we employ a modified version of our original simulation, see Chap. 3. We freeze $M-1$ of the polymers, such that they become fixed obstacles without any dynamics. Then, the single remaining test chain is allowed to move through this three-dimensional fixed porous network using the same algorithm as before. As initial condition, we use three independent, equilibrated configurations resulting from the original simulations. In particular, the frozen polymer networks surrounding the test chain are in different configurations.
For the single moving chain we record the familiar observables using a time average over 400 measurements, each initiated 0.1τ after the previous one. To check for artifacts which might result from accidentally chosen special configurations of the network, for each set of parameters we compare the results gained for the independent initial conditions to each other. All of the independent runs for a parameter set show identical features and at most deviate slightly in the amplitude. The data presented in the following is the average over the time-averaged data of the independent runs. As before, the errors are about symbol size.
Systems with fixed obstacles have already been studied elsewhere [31, 35, 111]. Therefore, we do not go into details of analyzing the dynamics. Instead we focus on the major differences appearing between the system with and without constraint release.

Recall that for semiflexible systems, the internal fluctuations dominate the behavior of almost all other observables at times $t < \tau_{i,l}$, see Chap. 4. Due to this high significance, we again start by analyzing the mean square displacement of the end-to-end distance δR^2. As can be seen in Fig. 5.2 the behavior of the internal relaxation changes significantly when eliminating constraint release. While the free relaxation up to the Odijk length at time τ_e is identical for both systems, the intermediate regime exhibits a distinctly different scaling. In a fixed environment, the relaxation is found to occur much more slowly and, correspondingly, the saturation time is much higher. Comparing the curves for the different mesh sizes on the left of Fig. 5.2 shows that the difference in $\tau_{i,l}$ increases with the density. This suggests that $\tau_{i,l}$ follows different scaling laws in the two systems. Finally, for the lower, dense system of Fig. 5.2 with fixed obstacles, δR^2 seems to develop a regime with almost negligible relaxation at high times, $t/\tau \gtrsim 2$ in Fig. 5.2. The equilibrium saturation value is achieved only at

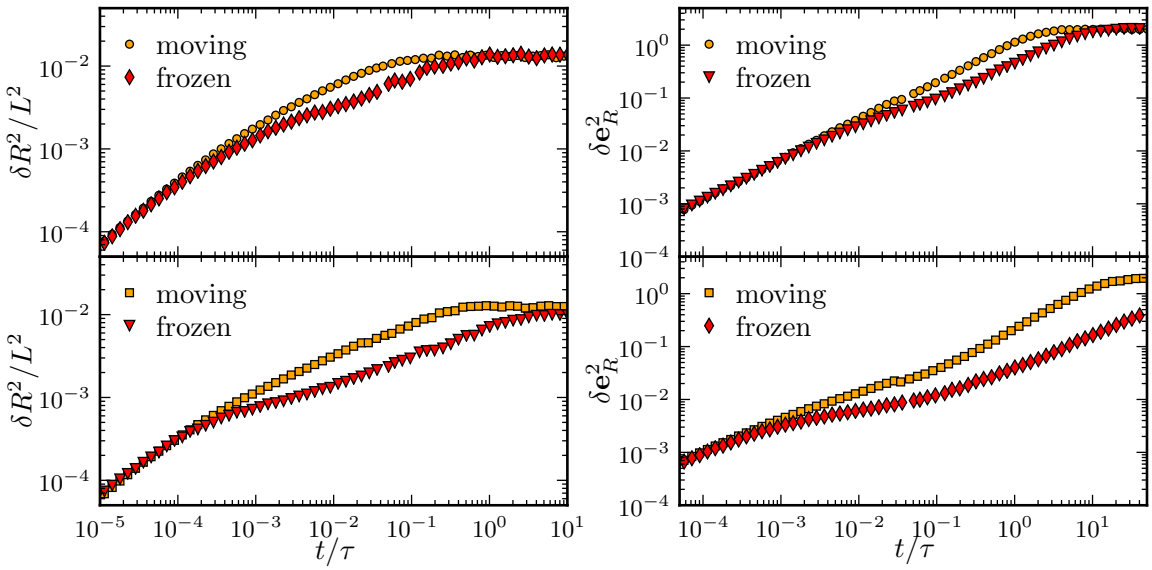

Figure 5.2: Left:Length fluctuations of single polymers in a network with $l_p/L = 1$ for two different mesh sizes. For the upper figure the system parameters are $\xi_m/L = 0.12$, the lower is for $\xi_m/L = 0.086$. Right: Rotational MSD of single polymers in a network with $l_p/L = 25$ for two different mesh sizes. The upper figure is for $\xi_m/L = 0.21$, the lower for $\xi_m/L = 0.12$.
In the systems label "frozen", only one measured polymer moves through a network of frozen chains acting as fixed obstacles. The curves marked as "moving" correspond to our original, purely entangled system, with dynamics of all chains. In the systems with the higher density the deviation between corresponding curves is more pronounced.

extremely large times, in accordance with previous simulations [31].
Thus, we find large differences in the ensuing internal dynamics, relative to our original system, when eliminating constraint release.

Comparing the rotational relaxation for a chain in a moving mesh and a chain in a fixed mesh, we find completely different behavior for times above τ_e, see right of Fig. 5.2. In a dense system with fixed obstacles an almost constant plateau of $\delta \mathbf{e}_R^2$ is found indeed, following the free rotation up to τ_e, see lower right plot of Fig. 5.2. Even in the following regime, the dynamics exhibit different behavior. Most importantly, the rotational relaxation time, which is the longest relaxation time of the whole system, shows no relation between the two systems. In other words, in the two cases τ_r differs by more than just a numerical prefactor as the discrepancy depends on the system parameters ξ_m/L and l_p/L.
More general, compare the two systems of different mesh size in Fig. 5.2 for each of the two observables discussed up to now. The difference in the saturation time of both processes between the system with and without constraint release increase with the density. Thus, it is clear that the effects of constraint release become much more relevant with decreasing mesh size.

Seeing the differences so far, it would be surprising if the diffusion through the network would be identical in the two simulations. Indeed, for the parallel component of the center monomer diffusion, see the left part of Fig. 5.3 severe discrepancies arise. Again they increase with the

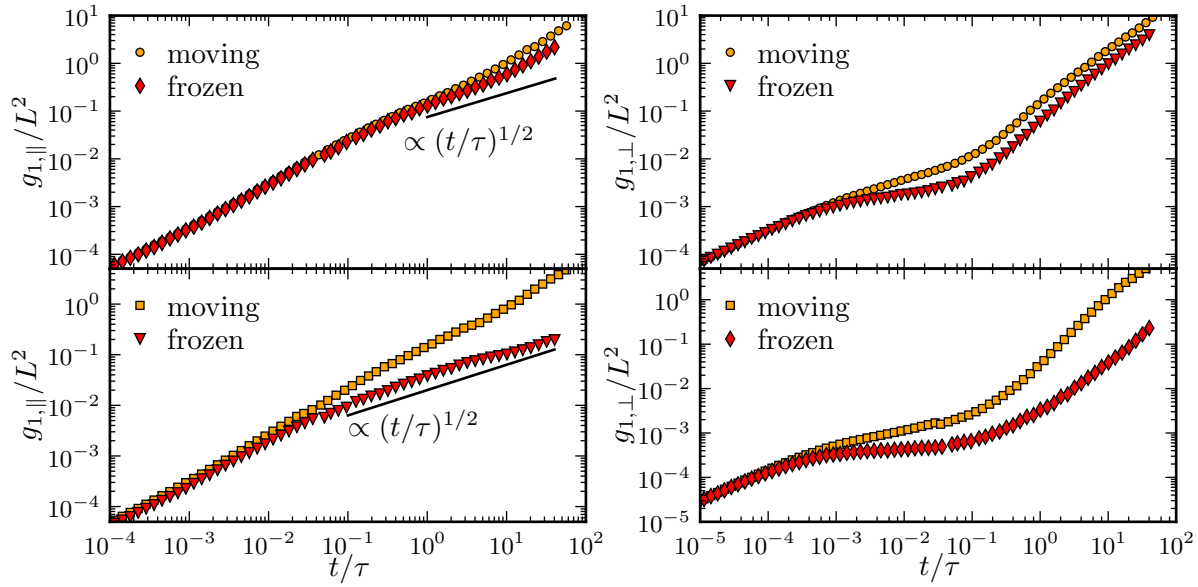

Figure 5.3: Left: Parallel diffusion of the center monomer of single polymers in a network with $l_p/L = 1$ for two different mesh sizes. The upper figure is for a system with $\xi_m/L = 0.12$, the lower is for $\xi_m/L = 0.086$.
Right: For two different values of the stiffness, $l_p/L = 1$ in the upper part, $l_p/L = 25$ in the lower figure, the orthogonal diffusion of single polymers in a network with $\xi_m/L = 0.12$ is given.
In the systems label "frozen", only one measured polymer moves through a network of frozen chains acting as fixed obstacles. For a single polymer moving in a dense network of fixed obstacles a $t^{1/2}$ regime appears. From the right plots it follows that the effect of constraint release becomes more pronounced for stiffer chains.

network density. Similar to previous simulational studies [31], a $t^{1/2}$ regime is found for $g_{1,\parallel}(t)$ in a dense network of fixed obstacles. As stressed before, an analogous regime is completely absent in our results, see Sec. 4.3.1. This is a remarkable finding: It shows that constraint release does not just slightly alter the behavior while keeping the types and number of regimes constant. Instead, lack of constraint release completely changes the dynamics of the system. In the orthogonal diffusion of the center monomer, we find the by now expected deviations between the system with and without constraint release, see Fig. 5.3. With fixed obstacles we especially recover the constant regime in $g_{1,\perp}$ above the entanglement time and before the polymer diffuses out of its original tube. Contrast this with the strict increase observed in the corresponding intermediate regime in our simulations. This observation leads us to believe that constraint release allows the chains to exhibit a significant lateral diffusion at all times. As expected from previously discussed differences, both the functional form and the amplitude of the super-diffusive regime differ severely in the two systems.
As usual, analogous statements hold for the center of mass diffusion $g_3(t)$, see Fig. B.7 in the appendix.

In the right part of Fig. 5.3, we compare two systems of identical mesh size, but with different stiffness. Comparing the differences between each pair of curves shows that the significance of constraint release increases for stiffer chains. For an intuitive visualization of the increased significance of constraint release consider a bowl filled with boiled spaghetti. When pulling

at a single chain, the conformation of the remaining spaghetti hardly changes. In contrast consider playing a game of Mikado, where you have to pull rigid sticks out of a stack without collapsing the stack. In this setting, the change of a single stick may drastically alter the configuration of the whole system.
Our conclusion is consistent with the results on flexible chains, for which constraint release has been shown to result only in a weak correction to standard reptation [30,41,44–46,46,80]. At the same time, there is a surprising aspect: Recall that our result on the terminal relaxation time of stiff chains correspond to Doi's prediction assuming fixed obstacles, see Sec. 2.2.3. However, as discussed in Sec. 2.2.3 for this limiting case there is a separate argument for the validity of the scaling of τ_r for both systems with and without constraint release. Thus for this special case, it is reasonable that only the prefactor changes. However, our results suggest that this effect on the numerical prefactor is rather strong.
In the further discussion, we omit this stiff regime. There already is a correct scaling prediction for this case, such that the system is fairly well described. Instead we focus on the semiflexible regime. In our system with constraint release, we find a smooth transition from the semiflexible to the stiff case, cf. Sec. 4.2.1. Note that for systems with fixed obstacles, it is not clear if a crossover in the behavior and terminal relaxation time of a semiflexible network exists. If it exists, which is quite likely, the lack of constraint release may affect the position of the crossover. In the remainder of this thesis, we only discuss a regime with $x = \frac{l_p \xi_m^2}{L^3} \ll 0.1$. Thus, we should safely stay in the semiflexible regime in all cases.

We conclude that for semiflexible and stiff polymers constraint release through motion of the tube is the dominant process for the diffusion and relaxation of polymers in a dense mesh. In the biologically highly relevant range of actin with $l_p/L \approx 1$ the neglect of constraint release leads to the prediction of erroneous behavior like the existence of a $t^{1/2}$ regime in the parallel diffusion.
We are now faced with the challenging question of clarifying how constraint release actually occurs in the entangled system. If possible we want to determine which mechanisms are dominant and need to be considered for an accurate theoretical description.

5.2 Motions involved in constraint release

In order to clarify the dominant mechanism of constraint release we use the ability to almost arbitrarily modify and control each chain individually, which is a unique advantage of the numerical approach. We modify our existing simulation in order to separate the different types of motion and study the individual effect of each type on the relaxation of our system. Specifically, we split the motion of the polymer chains into two parts and eliminate them in turn. On the one hand, there is the internal relaxation and contour fluctuations around the average position. On the other hand, we consider the global diffusion of the whole polymer through the network, which includes the standard reptation process.

As stated previously, we focus on the semiflexible regime with $x = \frac{l_p \xi_m^2}{L^3} < 0.1$. In this regime we find a completely new scaling behavior of several relevant timescales, most notably the terminal relaxation time, see Sec. 4.2.1. The relaxation dynamics exhibit surprising properties as well, especially in the form of the intermediate regime. Based on all previous findings, we assume that constraint release is the primary source of these new features. Furthermore, this

regime is interesting as it is most relevant for the cytoskeleton. The stiffness of actin is about $l_p/L \approx 1$ [6]. For entanglement to be dominant $\xi_m/L \lesssim 0.25$ seems a reasonable boundary, such that for most entangled actin solution $x < 0.1$.

We focus on the internal relaxation dynamics $\delta R^2(t)$ and especially $\tau_{i,l}$. Ideally we would like to find a scaling argument to predict this time, in this way clarifying the dominant constraint release mechanism. To justify this simplification to one observable, remember that the internal fluctuations influences the behavior of other observables as well. In particular, we find a direct relation between terminal and internal relaxation times. Thus this internal process dominates the relaxation of the whole system.
Also, this process allows for the easiest interpretation. If the polymer is confined in a fixed tube, the orthogonal fluctuations and hence $\delta R^2(t)$ are bounded by the tube radius. For $\delta R^2(t)$ to relax further, the tube itself has to rearrange, thus relaxing the constraint on the polymer. In other words the observation of the internal relaxation corresponds to analyzing the relaxation of the tube. Especially it follows that at $\tau_{i,l}$ all constraints in the range of the observed polymer have relaxed.
Consequently examining $\delta R^2(t)$ should give a good, almost complete description of the dominant tube relaxation process. In the following we use the expressions tube relaxation and constraint release analogously, if not stated otherwise.

Also, we intend to clarify whether the properties of the observed chain or those of the neighboring polymers are more relevant for tube relaxation. Recall that many proposed constraint release mechanisms, like convective constraint release, strongly depend on the characteristics of the surrounding mesh, see Sec. 2.2.5. It is reasonable to assume that there is some relation of this type for the tube relaxation process. As the constraint around one filament relaxes, this polymer contributes less to the constraints around its neighboring chains. Our tests should give us a good impression which motion of the surrounding polymers actually allows for tube relaxation.
In our simulation this is tested by dropping the homogeneity of the system and attributing different properties to individual chains. To avoid averaging out the desired effect, we observe a single chain. Hence we do not average over all chains in the simulation box, which slightly increases the statistical errors, see the increased symbol size in the following plots.

5.2.1 Weak effect of network contour fluctuations

With respect to the influence of the contour fluctuations on constraint release, we gain some knowledge from our already established results. We find that the tube relaxation, corresponding to the intermediate regime of $\delta R^2(t)$, slows down with increasing stiffness, i.e., the kinetic exponent α_i decreases, see Sec. 4.1. If the polymer becomes stiff and $x > 1$, tube relaxation no longer is the dominant relaxation mechanism in the system. Obviously strong enough contour fluctuations are required for tube relaxation, as a stiff polymer may not explore lateral space by fluctuations. In this context it is even more surprising that $\tau_{i,l}$ lacks an l_p dependence, see Sec. 4.1. However, this may be explained by a process where the stiffness influences several aspects which cancel each other for the relaxation time. For an example of an argument of this kind, see Odijk's argument in Sec. 2.2.4 where the tube diameter does not appear in the terminal relaxation time.

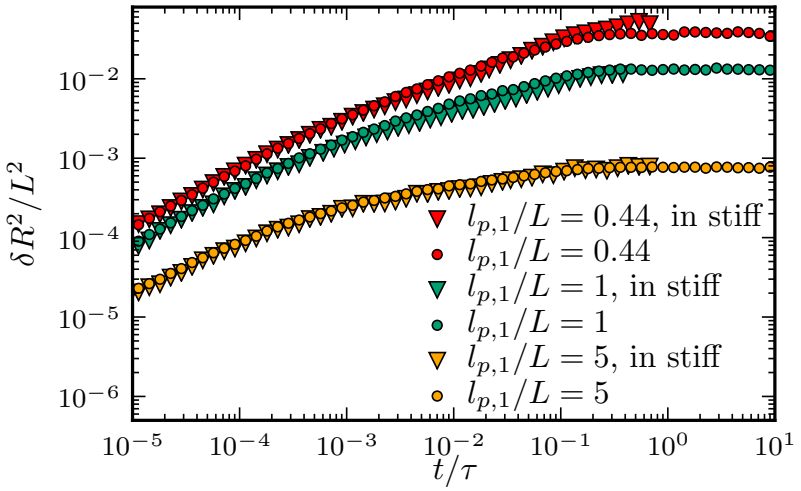

Figure 5.4: $\delta R^2/L^2$ for single polymers of different stiffness in dense solutions with $\xi_m/L = 0.086$. The legend gives the stiffness of the single measured chain. Except for this chain, all surrounding chains have an increased stiffness of $l_{p,k}/L = 25$. For comparison, the triangles give $\delta R^2/L^2$ of the original homogeneous system. The stiffness of the surrounding hardly affects the constraint release.

To determine the effect of the contour fluctuations of the surrounding network, we replace the persistence length by a chain dependent value, i.e., $l_p \to l_{p,k}$ in Eq. (3.1). To gain a clear picture, we use a system where the measured chain $k = 1$ has a variable stiffness $l_{p,1}/L$ and the other chains exhibit small contour fluctuations with a persistence length of $l_{p,k}/L = 25$ for all $1 < k \leq M$.

In Fig. 5.4 we compare the tube relaxation of this single chain in a stiff surrounding to the relaxation of an identical chain in a homogeneous system as determined before. It clearly shows that the stiffness of the surrounding networks hardly affects the relaxation of an individual chain.

Consequently, a low stiffness and strong enough fluctuations of the observed polymers are required for tube relaxation. This suggests that only the global diffusion of the surrounding network polymers contributes to the dominant constraint release mechanism.

5.2.2 Strong contribution of global diffusion to constraint release

Complementary to the internal fluctuations, now we turn to scrutinizing the effect of global diffusion of the chains on the tube renewal process. To eliminate the global diffusion without affecting the internal relaxation of each chain, we restrict the center of mass diffusion. To achieve this, we add another potential to $\mathcal{U}_{\text{total},i,k}$ in the equation of motion (3.4). This potential is a simple spring potential acting on each chain k in the form:

$$\mathcal{U}_{\text{fix},k} = 30000 k_B T [\mathbf{r}_{\text{cm},k}(t) - \mathbf{r}_{\text{cm},k}(0)]^2 \,, \tag{5.1}$$

where $\mathbf{r}_{\text{cm},k}(t) = \frac{1}{N}\sum_{i=1}^{N} \mathbf{r}_{i,k}(t)$ is the center of mass of chain k at time t. With this potential, in the modified simulations the mean square displacement of the center of mass is typically

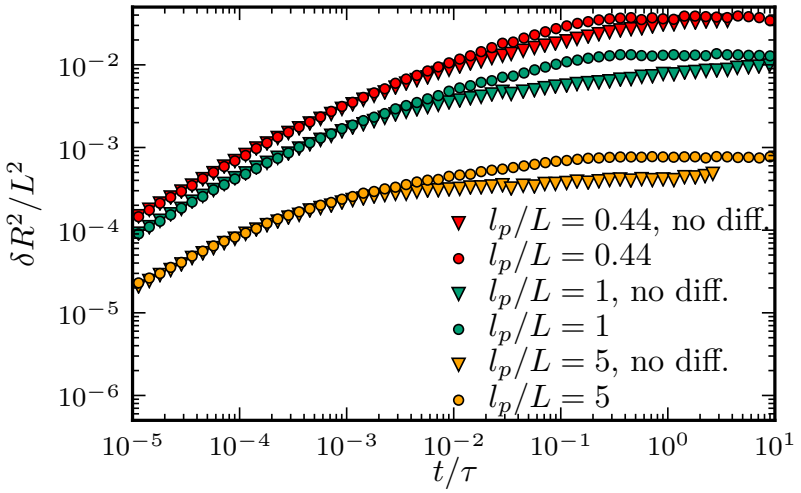

Figure 5.5: Internal relaxation for systems with restricted global diffusion, marked by "no diff.", compared to the original system. The simulation is for $\xi_m/L = 0.086$ and various values of the stiffness. If the global diffusion of the chain is suppressed, the internal relaxation slows down. This effect is found to increase with the stiffness. Our data seems to hint that it nevertheless relaxes completely to the equilibrium value of the fluctuations.

bounded by $g_3(t)/L^2 \lesssim 2\ 10^{-6}$.
The polymers in our simulation box are thus essentially fixed in space and may only relax by rotation and internal fluctuations. In particular, standard reptation is no longer available as a relaxation mechanism. In Fig. 5.5 we compare the internal relaxation $\delta R^2(t)$ in such a system without diffusion to our original results. The first deviation between the two measurements is found to occur systematically at times above τ_e. This is reasonable as the first contact is determined by fluctuations alone. At times shortly after the contact, the polymers may slightly adapt their local conformations to their respective partner. The difference then arises once this adapted region of original contact slides away along the tube in the system without the potential. This in turn happens at a time larger than τ_e, explaining the observed behavior. In the system with restricted diffusion the internal relaxation proceeds much slower than in the original measurement. It is found that the difference in relaxation speed increases with the stiffness of the filaments. This is hardly surprising as the fluctuations of all chains decrease and thus the surrounding of each chain becomes more static. Interestingly, it seems that the polymers still relax to their equilibrium value $\delta R^2 = L^4/45l_p^2$, at least for systems with $l_p/L \lesssim 5$. A possible explanation of this effect is based on the fact that all chains exhibit orthogonal fluctuations on the same order of magnitude, or even of identical amplitude. Also, remember that the chains do not actually fill the tubes completely. If one chain comes into contact with a tube boundary, the opposite side of its tube is empty. Therefore, a polymer entering this vacated region is not hindered at that moment in spite of being locally outside its tube. Thus, this polymer may relax on a scale larger than its actual tube diameter, which in turn affects the chains close to this polymer expanding their accessible region. In principle the fluctuation may relax as a kind of traveling wave throughout the system in this way.
We conclude that the internal fluctuations suffice for the system to achieve full internal relaxation, a fact neglected in the standard tube model. However, this process alone is

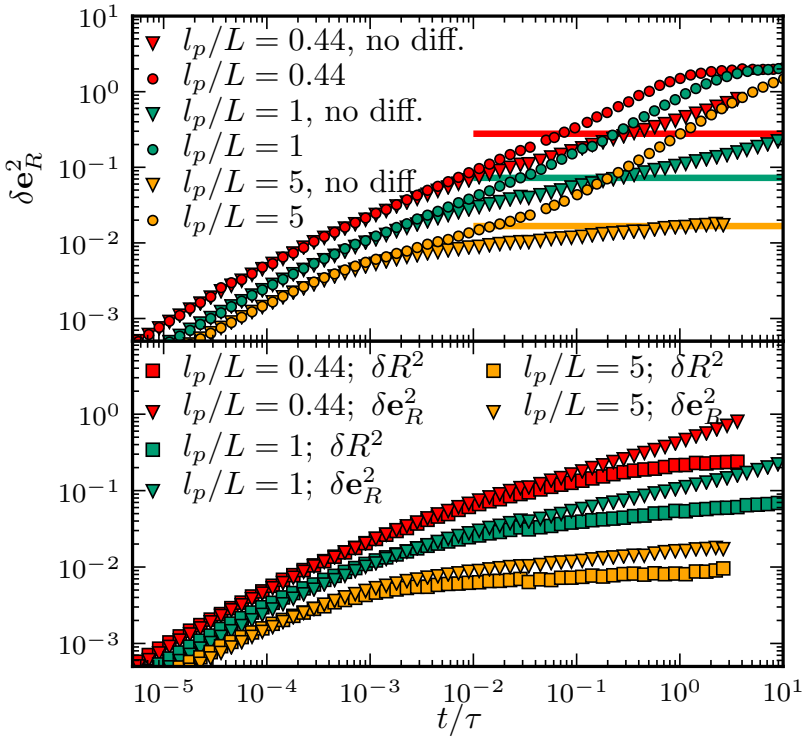

Figure 5.6: Top: Even for semiflexible chains with fixed center of mass (triangles), marked by "no diff." in the legend, the rotational MSD increases after contact with the tube. However, with increasing stiffness this effect quickly decreases. As a comparison the data of the original system is shown. The horizontal lines indicate the maximum possible value of $\delta \mathbf{e}_R^2$ originating only in orthogonal chain fluctuations. The color of each line corresponds to the one of the data set with that mesh size. The rotational MSD does not saturate at those values.
Bottom: In a system with restricted diffusion the rotational relaxation (triangles) increases faster than the internal relaxation (squares). For better comparison of the slopes, the amplitude of the internal relaxation has been scaled such that a fit with $\delta \mathbf{e}_R^2$ is achieved at small times.
Thus, we find that there must be an explicit rotation mechanism. Both figures are for a system with $\xi_m/L = 0.086$.

very slow compared to the typical tube relaxation in systems with global diffusion.

In the system with restricted center of mass diffusion another remarkable finding may be gained when observing the rotational relaxation of the chains, see upper part of Fig. 5.6. As expected, at small times there is no difference between $\delta \mathbf{e}_R^2$ in the system with and without global diffusion. Approximately at the same time as for δR^2, the system with the restrictive potential starts to exhibit a significant decreased rotational relaxation. The behavior is thus quite similar to δR^2, in accordance with the dominance of the orthogonal fluctuations for the rotation at small times, see Sec. 4.2.2. A more detailed analysis exposes important deviations from this simple explanation.
Consider the maximum achievable rotational relaxation due to the contour fluctuations. It may easily be inferred from our results for the original system with diffusion. For times $t < \tau_{i,l}$ we find that $\delta \mathbf{e}_R^2$ is dominated by fluctuations, see Sec. 4.2.2. Hence at time $\tau_{i,l}$,

i.e., at the crossover to the $2 - 2\exp(t/\tau_r)$ regime, the maximal value due to the contour fluctuations is acquired. Obviously, this value serves as an upper boundary for our system with restricted diffusion.[1] For better visibility the corresponding values for each stiffness are shown by horizontal lines in the upper part of Fig. 5.6. We find that the rotational relaxation is not limited by this boundary, i.e., larger values than allowed by the orthogonal contour fluctuations alone are achieved.
Furthermore, if we assume that the rotation only relaxes due to the orthogonal fluctuations, it follows $\delta \mathbf{e}_R^2 \propto \delta R^2(t)$, similar to the discussion in Sec. 4.2.2. In the lower part of Fig. 5.6 we compare the time evolution of $\delta \mathbf{e}_R^2$ and δR^2 in a system with restricted diffusion. For all used values of the stiffness, the rotation increases significantly faster than the orthogonal fluctuations, which are proportional to δR^2.
In conclusion, we find that even without motion of the center of mass, and thus without reptation, a polymer network is able to relax the orientation of the individual filaments.[2] The mechanism for this rotational relaxation has to be related to the contour fluctuations of the semiflexible polymers, as there is no alternative process. The decreasing speed of the rotational relaxation with increasing stiffness agrees with this proposition. While the process is driven by the contour fluctuations, we present clear evidence that it is not just an alternative effect of those fluctuations but a particular relaxation process. Unfortunately, due to the limitation of computational resources we were not able to clarify whether the rotational MSD relaxes completely. We assume that full relaxation is achieved eventually, as to our best knowledge there is no argument limiting the newly observed process.

To identify the contribution of the neighboring chains on the relaxation of a specific chain, we drop the restriction on the center of mass for a single chain. Thus $M - 1$ chains are subjected to the additional fixing potential as before, and only the one diffusing chain is observed. In principle, this system is similar to the setting with fixed obstacles analyzed in Sec. 5.1. However, now all polymers exhibit contour fluctuations and global rotation, such that the surrounding of the observed chain may react to this chain.
In Fig. 5.7 we compare the internal relaxation of the original setting to the relaxation behavior found in this special setting of a single diffusing chain in a network of chains with only contour fluctuations. As an additional reference, δR^2 of the system with restricted diffusion of all chains is given. Compared to the system with restricted diffusion of all chains, a filament relaxes much faster if it may move through the network. This has been anticipated, as it corresponds to the basic assumption of the reptation theory: the individual movement of chains through the network is a major relaxation process. Still, even if the observed chain diffuses and all other chains rotate and exhibit contour fluctuations, the relaxation dynamics are slower than in the original system, see Fig. 5.7. This is in accord with our previous assumption that the global movement of the confining polymers is relevant for the dominant constraint release mechanism.

If we inverse this setting and only restrict the diffusion of the single observed chain, the resulting relaxation is almost identical to the previous case, see Fig. 5.7. This is a remarkable finding. If the observed chain moves through a network exhibiting only rotation and contour fluctuations of each chain, any effect of the reptation of that chain contributes to its relaxation.

[1] Note that the standard tube picture predicts an even smaller maximum rotational MSD, if there is no diffusion out of the tube.

[2] Note that this process may not originate in the global rotation of the whole system, which is forbidden as the potential fixes chains at various points in space.

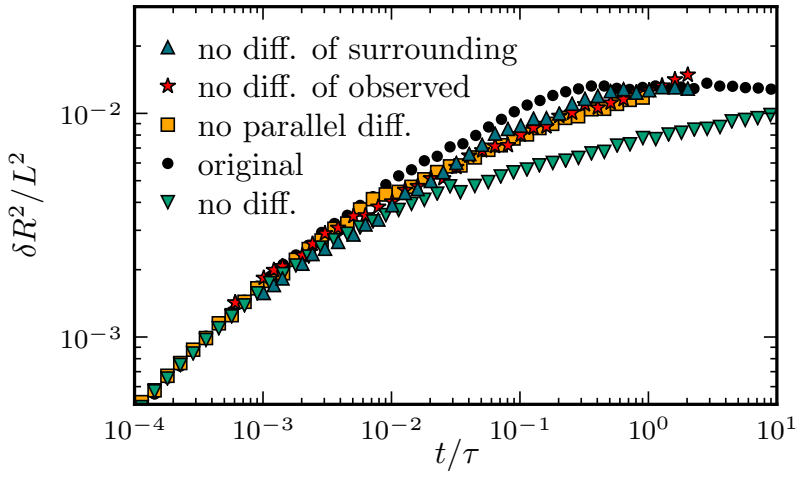

Figure 5.7: Internal relaxation of a chain in a network of $\xi_m/L = 0.086$ and $l_p/L = 1$ with various additional restrictions compared to the original system (circles). In the case marked "no diff." the center of mass diffusion for all chains is suppressed (triangles with tip down). If some diffusion is allowed, the tube relaxes significantly faster, yet always slower than without restrictions. For a single free chain in a network of chains with restricted diffusion (triangles with tip up) and for a single restricted chain in a network of diffusing chains (stars) the resulting relaxation is almost identical. Also in a system where all chains exhibit only orthogonal diffusion (squares), the relaxation matches the one observed in the previous two restricted cases.

In the second case of restricted diffusion of the observed chain, reptation of that chain does not occur. Therefore, any relaxation cannot be related to its reptation movement. Yet, in both cases relaxation occurs almost identically. The reptation of a chain along its tube seems not to be the dominant constraint release mechanism. As this mechanism in turn determines the terminal relaxation time, see Sec. 4.2.1, reptation is not the most important mechanism in the system.

To test this conclusion and determine any special significance of the diffusion along the tube, we restrict only the reptation movement. Analogously to before this is implemented by an additional potential on each chain k of the form:

$$\mathcal{U}_{\mathrm{fix},\parallel,k} = 30000 k_B T \left[(\mathbf{r}_{\mathrm{cm},k}(t) - \mathbf{r}_{\mathrm{cm},k}(0)) \cdot \mathbf{e}_R(0) \right]^2 \ . \tag{5.2}$$

This substantially reduces the diffusion parallel to the end-to-end vector, but allows for orthogonal diffusion. Remember that the latter is supposed to be marginal in the tube picture. However, in our original data, cf. Sec. 4.3.2 we find clear evidence that there is orthogonal diffusion.
In a system with reptation of all chains restricted by the potential $\mathcal{U}_{\mathrm{fix},\parallel,k}$, we find that tube relaxation and constraint release occur significantly faster than in the system where diffusion in all directions is restricted, see Fig. 5.7. In fact, δR^2 of each chain relaxes almost identically to the case of a free chain in a surrounding of chains without global diffusion. In other words, the orthogonal diffusion neglected in the reptation ansatz gives a contribution to tube relaxation approximately identical to reptation itself.

Note that restricting the diffusion parallel to the current end-to-end vector $\mathbf{e}_R(t)$ instead of the initial $\mathbf{e}_R(0)$ in Eq. (5.2) results, within the statistical errors, to almost identical relaxation, see Fig. B.8 in the appendix.

The results of this section give important insights which processes are relevant for constraint release. We find that neither global diffusion nor the contour fluctuations alone suffice to achieve the required constraint release. In all cases the resulting tube relaxation occurs slower than in the system without restriction.

5.3 Multi-particle interaction dominate constraint release

As we have not yet identified the dominant constraint release process, we continue scrutinizing the timescale of tube relaxation $\tau_{i,l}$. Also, this allows for a better comparison with existing constraint release models, see Sec. 2.2.5. Especially the convective constraint release is worth considering, see Sec. 2.2.5. For a monodisperse melt of semiflexible filaments of length L, the reptation time τ_d is proportional to L^3 and the tube relaxation time is predicted to scale with L^5/L_e^2. As L_e is usually close to ξ_m this prediction is close to our findings of $\tau_{i,l}$.

To elucidate the relevance of convective constraint release, we employ a polydisperse system, where this effect is expected to become more pronounced. In the scaling argument of convective constraint release the basic timescale is given by the reptation time of the chains acting as obstacles for the observed filament. If the network filaments have a length L_n, then $\tau_d \propto L_n^3$ has to be used in Eq. (2.72). The tube relaxation time should thus scale as $L^2L_n^3/L_e^2$. This prediction may easily be tested.

We modify our standard simulation to cope with polydisperse solutions of polymers with different lengths. To avoid additional effects like depletion forces [135, 136], we simulate a single test-polymer of length L in a network of polymers, all of which have length L_n. Also, this allows to continue using the mesh size for the density, as the effect of the single chain may be neglected. Since we establish that the stiffness of the surrounding network hardly affects the relaxation, see Sec. 5.2.1, we do not consider this aspect explicitly. Instead, we assume that all filaments in the solution are of the same material and have identical persistence length. For the case of an increased length of the surrounding chains, $L_n = 2L$, we use a simulation box of edge length $\hat{A} = 2.1L$ to avoid self-interaction of the chains.
As before only the test-polymer is observed such that we may clearly separate the effects of the different contour lengths on the relaxation of a single chain. In Fig. 5.8 we show that by rescaling the time with L/L_n we achieve a good data collapse of the longest relaxation time for all ratios of length used. It is easy to see that tube relaxation speeds up if the network consists of shorter segments. Hence, like most constraint release mechanisms already discussed in the literature, see Sec. 2.2.5, the importance of constraint release increases even further for polydisperse systems containing short chains.

Most importantly, our result is in stark contrast to the prediction of convective constraint release, which scales with L_n^3. Instead, we find in Fig. 5.8:

$$\tau_{i,l} = \frac{\zeta_n L^4 L_n}{\xi_m^2 k_B T} \,, \tag{5.3}$$

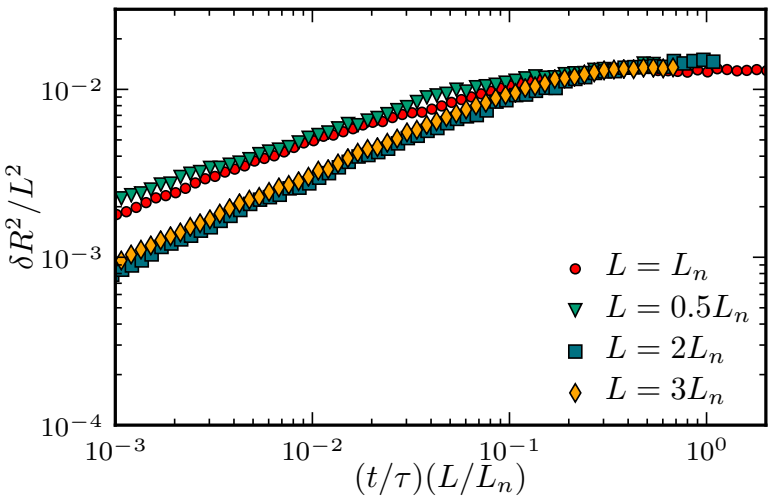

Figure 5.8: δR^2 for a single polymer of length L in a network of polymers with contour length L_n. The mesh size is $\xi_m/L = 0.086$, and all polymers have a persistence length $l_p = L$. The legend gives the ratio of chain lengths for each curve, and the time is rescaled by that ratio. With this scaling, we find good agreement of the longest internal relaxation time.

where the exponents of L and L_n should be taken with a grain of salt. Thus convective constraint release does not explain the behavior observed in our system. It is worth to note that this problem arises from the choice of the basic timescale τ_d. One might consider a variation of the convective constraint release model, which incorporates a correlation between the different segments of the effective chain. However, as the problem arises from τ_d this approach does not solve the discrepancy. If the general picture holds, either the network has to have an additional effect not yet considered or a different basic process must be the basis of the correct scaling argument.

On what other process should a scaling argument to derive $\tau_{i,l}$ be based, if there is any single process? This question is connected to our results in the previous section, where we considered the inverse question: How does eliminating a certain process affect constraint release? From this analysis we know that the internal relaxation of the surrounding chains is not the basic process. However, every other type of motion seems to be involved in some way.
Now, our major aim is to determine the basic timescale, which should be used in the scaling argument for $\tau_{i,l}$. With that knowledge it should be much easier to develop the correct scaling argument.

The primary question is whether the basic timescale results from the measured chain or from the surrounding network. Intuitively, the diffusion of the surrounding polymers should contribute, as they form the tube. This is also the reasoning of the convective constraint release approach. However, in Sec. 5.2.2 we show that the diffusion of the observed polymer gives a significant contribution as well.

In our choice of units, $k_BT = 1$ and friction per unit length $\zeta = 1$, any time is of order length to the third power. To change a characteristic time, we would have to change a length-scale, like in the polydisperse case discussed just now. However, this changes the properties of the

system itself. Consequently, the previous approaches always affect not only the timescale, but also the amplitude of any occurring process. Hence, it is difficult to determine whether the resulting change in $\tau_{i,l}$ is actually due to the different timescale.
In order to clarify this problem, a more cunning approach is required: We divide our system into species of polymers with different friction coefficients. There are several advantages to this approach. The friction is a property of each individual chain, which does not affect its statistics, e.g., the saturation value of the orthogonal fluctuations is not affected by the friction. Thus, we may separate the timescales of different chains without altering any other aspect of the system. If there is a single dominant timescale, $\tau_{i,l}$ should scale linearly with the friction coefficient of that species.

This modification of our basic simulation is quite simple. The friction coefficient ζ in Eqs. (3.4) and (3.5) is replaced by the value ζ_k for all beads of a chain k. As before, we only differentiate between a single observed polymer with a friction $\zeta_1 = \zeta$ and the chains forming the network with friction $\zeta_k = \zeta_n$ for all $1 < k \leq M$. The remaining procedure is as discussed before when observing a single chain in a network with restrictions, see Sec. 5.2.
In our simulations we keep one of the two friction coefficients at 1 and vary the other. In the two upper plots of Fig. 5.9 we show that the internal relaxation of a chain slows down significantly if increasing its friction ζ. For this measurements the rearrangement speed of the surrounding network is not altered and $\zeta_n = 1$. By rescaling the data, we find that a data collapse of the tube relaxation time is achieved by rescaling the time with $(\zeta_n/\zeta)^{2/3}$. This is a surprising result, as this would require an additional dependence on the friction coefficient of the network to actually achieve the desired unit. Indeed, by varying ζ_n for fixed $\zeta = 1$ we find that $\tau_{i,l} \propto \zeta_n^{1/3}$, as required for consistency. In summary, we find:

$$\tau_{i,l} \propto \zeta^{2/3} \zeta_n^{1/3} \,. \tag{5.4}$$

Our results prove that both a timescale of the network and of the observed filament contribute to constraint release. We combine the scaling of $\tau_{i,l}$ with the friction coefficients with our results for the dependence on the length of the surrounding networks, Eq. (5.3). Then we separate the two contributions of the test-polymer and the network polymers and rewrite $\tau_{i,l}$ as a mixture of two timescales:

$$\tau_{i,l} \propto \left(\frac{\zeta L^6}{\xi_m^3 k_B T} \right)^{2/3} \left(\frac{\zeta_n L_n^3}{k_B T} \right)^{1/3} \,. \tag{5.5}$$

This formulation is just a proposition to interpret our result at least partially. Note that the latter contribution is just the diffusion time of a network filament. This is in accord with our previous findings, that the diffusion and not the internal relaxation of the network are more important. Also, the larger exponent of 2/3 in the dependence on the properties of the observed chain agrees with our previous results that the diffusion of the measured filament itself contributes a large part to constraint release, see Sec. 5.2.2. Furthermore, a behavior like in Eq. (5.5) explains the difference to a system with fixed obstacles, see Sec. 5.1. If one of the participating processes is missing, constraint release is not only slowed down, but ceases to occur.
Unfortunately we do not have a proposition to explain the expression representing the contribution of the observed polymer.

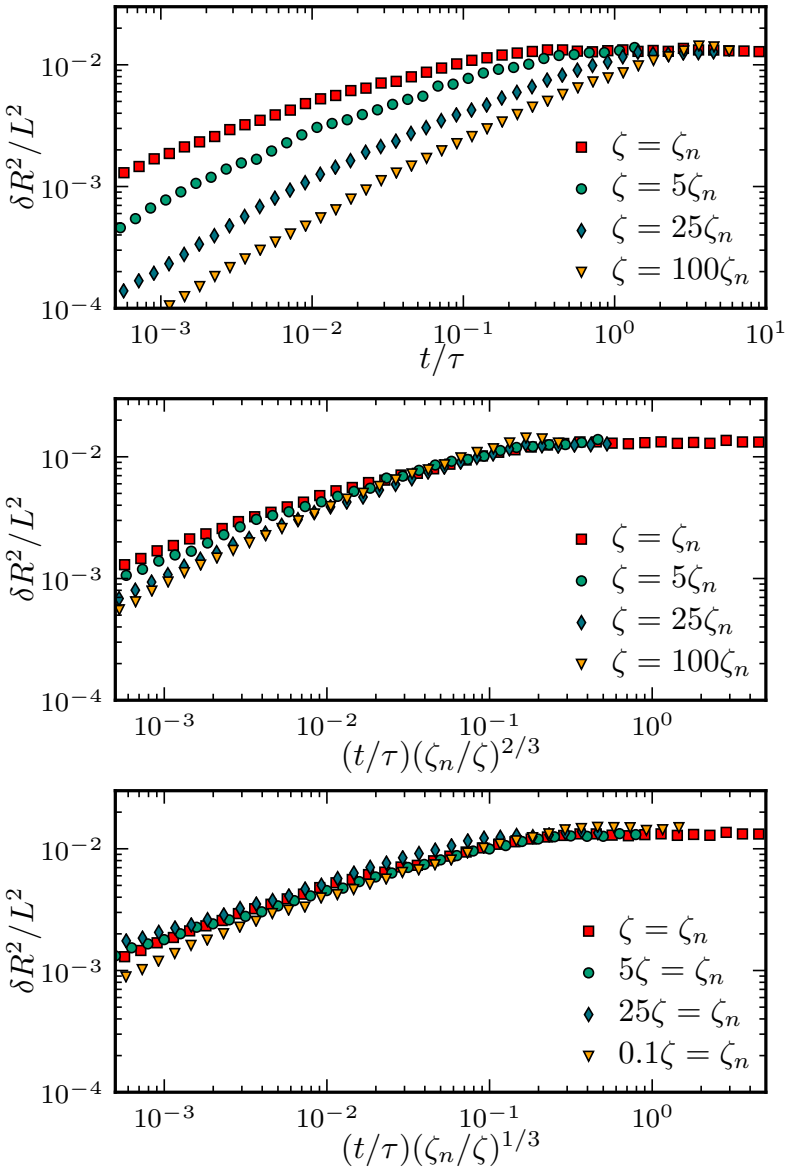

Figure 5.9: δR^2 for a single polymer with a friction coefficient ζ in a network of polymers with friction coefficient ζ_n. The mesh size is $\xi_m/L = 0.086$ and the stiffness is $l_p/L = 1$. The legend gives the ratio of the friction coefficient for each curve. In the two upper figures the friction coefficient of the network is fixed, $\zeta_n = 1$, in the bottom figure the network is changed and $\zeta = 1$.
If changing the friction of the single chain, rescaling the time with $(\zeta_n/\zeta)^{2/3}$ results in a good collapse of the internal relaxation time. Consistently using $(\zeta_n/\zeta)^{1/3}$ achieves a data collapse, if the friction coefficient of the neighboring chains is altered. For easier comparison τ is always calculated for the chains with the fixed friction.

However, our result definitely refutes the assumption of a single characteristic timescale governing the constraint release process. Recall that this also holds for the highly relevant longest relaxation time, which we show to be related to $\tau_{i,l}$ in Sec. 4.2.1. Therefore it is almost impossible to give a simple scaling argument to describe the dominant relaxation mechanism in a semiflexible, densely entangled network. Instead, the observation that timescales of disjunct filaments mix for the behavior of each filament, indicates that a genuine multi-particle interaction is involved.

6 Concluding discussion

In this thesis we study the motion of single filaments in a purely entangled, homogeneous network of worm-like chains. The system is dense, such that the typical distance between polymers, ξ_m, is much smaller than the contour length L of the chains: $\xi_m \ll L$. We employ a highly optimized Brownian dynamics simulation and analyze the resulting data. Where possible, we provide scaling arguments to explain the behavior found in the simulations. We focus on the semiflexible to stiff regime where the persistence length is much larger than the typical distance between polymers, $l_p \gg \xi_m$.

Among our most important findings is the existence of two distinct parameter regimes of semiflexible and stiff behavior. We introduce the critical stiffness $\hat{l}_p/L = (\xi_m/L)^2$, where the orientational changes due to global rotation and due to contour fluctuations are identical. We show that this quantity allows to distinguish between the dominant relaxation mechanisms:

- For systems of polymers above the critical stiffness $l_p > \hat{l}_p$, we find that global rotation, a persistence length-independent process, dominates the terminal relaxation of the system. It is similar to a system of rigid rods.

- In the regime $l_p < \hat{l}_p$ the orthogonal contour fluctuations allow for a faster rotation, and a stiffness dependent relaxation process is dominant. We call these systems semiflexible.

The boundaries of these regimes may be treated as critical densities using the definition of the mesh size. The critical number density $\hat{\nu}$ is related to the critical stiffness by $\hat{\nu} = 3\hat{l}_p/L^4$. As previously predicted, there is an additional transition to the weakly entangled regime at $l_{p,c}/L = (L/\xi_m)^4$ [87]. However, we find that this transition only affects the short-time dynamics. In the considered densities this critical persistence length and the associated transition are irrelevant for the terminal relaxation of the whole system. Also, note that most biological polymer networks, e.g., those based on actin, are in the semiflexible regime with $l_p/L \lesssim (L/\xi_m)^2$.

We show that the terminal relaxation time τ_r follows a scaling law throughout both parameter regimes. Using the dimensionless scaling parameter $x = l_p/\hat{l}_p$ we write $\tau_r = \tau(L/\xi_m)^4\hat{\tau}_r(x)$. The scaling function $\hat{\tau}_r(x)$ is linear in x for $x \lesssim 0.1$. For $x \gtrsim 1$ the scaling function is constant, $\hat{\tau}_r(x) \propto 1$. Each of these two parameter regimes has distinct relaxation dynamics.

The dynamics of the system are summarized by the motion of a single chain segment, e.g., $g_1(t)$. In accordance with previous studies, we find that the motion along the tube is essentially free diffusion, independent of the stiffness regime. On the other hand, the orthogonal diffusion depends on both the density and on the stiffness.
In the rigid regime $l_p/L > (L/\xi_m)^4$ one may neglect contour fluctuations. Then we describe

relaxation by:

$$g_{1,\perp} \propto \begin{cases} t & \text{for } t \lesssim 10\tau(\xi_m/L)^4 \\ t^\beta & \text{for } 10\tau(\xi_m/L)^4 \lesssim t \lesssim 9\zeta L\xi_m^2/2k_BT \\ t(1-\exp(t/\tau_r)) & \text{for } 9\zeta L\xi_m^2/2k_BT \lesssim t \end{cases}, \tag{6.1}$$

where β depends on the density of the system. In the dense regime, we find that approximately $\beta \propto \xi_m/L$. We establish that in this regime the rigid rod-like rotation of the filament dominates the relaxation. In particular, our findings agree with the scaling predicted by Doi for the terminal relaxation time of rigid rods [38]. Thus, the terminal relaxation time is $\tau_r \propto L^7/\xi_m^4$.
In the semiflexible regime $l_p \lesssim \hat{l}_p$, the orthogonal contour fluctuations of each chain dominate the relaxation. We find:

$$g_{1,\perp} \propto \begin{cases} t^{3/4} & \text{for } t \lesssim \tau_e \\ t^{\alpha_i} & \text{for } \tau_e \lesssim t \lesssim \tau_{i,l} \\ t(1-\exp(t/\tau_r)) & \text{for } \tau_{i,l} \lesssim t \end{cases}, \tag{6.2}$$

where the entanglement time $\tau_e \propto \xi_m^{16/5}/l_p^{1/5}$ is in accordance with the Semenov scaling for the tube diameter. The contour fluctuations saturate at the internal relaxation time $\tau_{i,l} \approx 10^{-3}\frac{\zeta L^5}{k_BT\xi_m^2}$. Note that the saturation value is identical to the dilute case, even if the polymer does not completely leave its initial tube. The exponent of internal relaxation α_i depends logarithmically on the system parameters, to good approximation as given in Eq. (4.8). For flexible chains α_i converges to 1/2 in accordance with classical reptation theory [36,37]. With increasing stiffness, α_i smoothly declines to smaller values and quickly converges to zero when approaching $l_{p,c}$. In the semiflexible regime, the contour fluctuations allow for a faster rotation. We introduce an argument establishing a direct relation between the longest internal relaxation time $\tau_{i,l}$ and the terminal relaxation time of the form $\tau_r \propto \tau_{i,l} l_p/L$.
For $(L/\xi_m)^2 < l_p/L < (L/\xi_m)^4$ contour fluctuations dominate the small time relaxation dynamics. In contrast, the behavior at later times and the terminal relaxation corresponds to the rigid rod behavior. For numerical reasons we do not establish a scaling of the crossover time between those two regimes. The slopes of both processes in the intermediate regime, where the crossover occurs, are quite small. Therefore we assume that this transition is of marginal importance.

In the semiflexible case, another regime is possible in the limit $\tau_d < \tau_{i,l}$. Due to numerical restrictions we were not able to simulate systems of this kind to analyze this possible transition. Since the reptation time τ_d scales with L^3 and $\tau_{i,l}$ with L^5/ξ_m^2, this limit is reached for very dense systems. However, due to the small prefactor of approximately 10^{-3}, the internal relaxation time is smaller than τ_d for most systems of interest. To see this, note that the transition occurs at a mesh size $\xi_m/L \approx 10^{-3/2}$. Then, consider a typical biological system of, e.g., actin filaments. The diameter is of order 10nm and the length of order 10μm, resulting in an aspect ratio of about 10^3. The critical density to avoid a nematic transition is then equivalent to a mesh size $\xi_m/L \gtrsim 10^{-3/2}$, see Eq. (3.15). Consequently, in most biologically relevant systems, the limit $\tau_d < \tau_{i,l}$ does not occur in the isotropic state. Therefore, even if this transition were to change the dynamics, we assume that it is irrelevant for most applications.

Although the behavior at times above τ_r, and times below the first contact with the tube are as expected, there are two regimes which require additional interpretation. To begin with, there is a super-diffusive regime occurring in the orthogonal motion of the polymer segments. We argue, and show evidence, that this regime is related to the rotation of the polymer and a consequence of the projection procedure. Our tube rotation argument implies $g_{1,\perp} \propto t\delta\mathbf{e}_R^2$ in good agreement with our data. Consistently, we find a corresponding regime in the parallel component of the motion.

Another interesting feature is the intermediate regime with system-dependent behavior. We find that all observables strictly increase with time up to their respective saturation time. In particular, there is no constant plateau. This is in stark contrast to the tube model and previous simulations based on fixed obstacles [31, 42]. We attribute this effect to additional constraint release mechanisms which occur due to the movement of the network surrounding each filament.
This constraint release is most relevant in the semiflexible regime $l_p < \hat{l}_p$, which should cover the biologically interesting range of actin filaments with $l_p/L \sim 1$. In this regime the orthogonal fluctuations are not bounded by the tube diameter, even at times before the polymer leaves its initial tube. The orthogonal fluctuations usually saturate to the identical value as in a dilute solution before leaving the tube. This requires that the tube deforms, thus releasing the constraint around the polymer. We find that this mechanism determines the terminal relaxation of the network. Therefore, constraint release is the most relevant process in this parameter regime.

To characterize the effects of constraint release on the relaxation of a solution of entangled polymers, we eliminate constraint release by fixing the network around a single chain. These fixed obstacles lead to a completely different behavior. Apart from different scaling laws for the crossover and saturation times of the processes, entirely different regimes appear, in accordance with previous simulations using fixed obstacles [31]. Thus neglecting constraint release leads to predicting erroneous behavior.

Our further simulations show that the stiffness of the network around a polymer does not affect the dominant constraint release mechanism of this chain. Thus, only the diffusion, but not the contour fluctuations of the network filaments need to be considered for this mechanism. This insight also eliminates tube length fluctuations of the network polymers as a candidate of constraint release. For semiflexible filaments, the fluctuations of the end-to-end distance strongly depend on the stiffness. As the tube length should behave similarly to the polymer length, tube length fluctuations would result in a stiffness dependence of the constraint release time.

Additionally, the results of our simulations show that the orthogonal diffusion gives a significant contribution to the dominant relaxation mechanism. This contribution is comparable to the one originating in the sliding of the observed polymer along the tube. Another mechanism of similar relevance is the sliding of the surrounding chains along their respective tubes. Yet, we find that this process alone does not suffice to explain constraint release. All these findings contradict basic assumptions of the reptation theory without constraint release. Furthermore, even the existing constraint release models based on the tube picture do not explain our findings.

Finally, the typical constraint release time, which directly relates to the terminal relaxation

time, depends on timescales of several different chains:

$$\tau_{i,l} \propto \left(\frac{\zeta L^6}{k_B T \xi_m^3}\right)^{2/3} \left(\frac{\zeta_n L_n^3}{k_B T}\right)^{1/3} , \tag{6.3}$$

where ζ_n and L_n are the friction coefficient and contour length of the surrounding chains, i.e., the network chains. The first factor in this expression depends only on the density and properties of the observed chain and gives the larger contribution. The second term describes the diffusion of the network chains around the observed polymers. This mixture of timescales of different time-scales suggests that a multi-particle interaction governs the constraint release. In other words constraint release seems to be a cooperative effect between each chain and its surrounding. This would also explain the structure of $\tau_{i,l}$ as a geometric mean over the involved processes. Also, this finding explains the differences to the case with fixed obstacles, which is a singular limit of this expression.
To capture such a multi-particle effect a mean-field theory like the tube model is unsuitable. In order to include this effect and describe constraint release, a different, completely new approach is required. This is the only way to correctly describe the relaxation of an entangled polymer network with $l_p/\hat{l}_p < 1$.

Up to now, neither intermediate regimes of this kind nor the corresponding scaling of the longest relaxation time have been directly observed in experiments. However, there is indirect evidence that relaxation should occur in the intermediate regimes. In several microrheology experiments on actin solutions, an increase instead of a plateau is observed in the viscoelasticity [43, 56, 137–139]. This regime is related to the intermediate regime in the motion of the filaments, and thus hints at a behavior similar to the behavior in our simulations. For a more direct comparison and a critical discussion, see Appendix A.
In addition, our results have an important experimental implication. When measuring a single fluorescent chain over an elongated time, the width of the resulting fluorescent path does in general not give the tube diameter. As the orthogonal fluctuations do not exhibit a constant plateau, the apparent tube diameter determined by this procedure depends on the duration of the measurement. This process is visualized in Fig. 5.1 and may result in incorrect interpretation of the data. To correctly determine the tube diameter, only fluctuations up to the Odijk time τ_e should be measured. As discussed in Sec. 3.1, τ is typically of order 10^4s. Then τ_e is approximately of order 1s, see Fig. 4.3. To observe the full relaxation process, it would be necessary to observe times up to $\tau_{i,l}$, which is of order 10^3s, see Fig. 4.3.

Future numerical simulations could be helpful to gain further insights into constraint release mechanisms. Also, the exact transition between the semiflexible and the rigid rod regime $(\xi_m/L)^2 < l_p/L < (\xi_m/L)^4$ is left for further research. Although it is of minor relevance for biological systems as detailed above, a closer examination of the regime with $\tau_d < \tau_{i,l}$ may help in understanding the other regimes. Thus, entangled polymer solutions are a worthwhile topic for following numerical studies. However, this is likely to require an increase in the available computational resources or faster simulational techniques. Another interesting extension of this study would be to use heterogeneous systems, e.g., polydisperse systems. As constraint release and the diffusion properties depend differently on the contour length, these systems may exhibit new effects.

From a theoretical point of view, a better understanding of constraint release is required. For example, it is interesting to understand how releasing a single constraint affects surrounding

constraints. A comparison to a similar, slightly simpler problem might be helpful for the development of new theories.
Consider the cage effect in colloids [140, 141]: For dense suspensions of hard spheres at small times, the fluctuations of each object are limited by the surrounding spheres. Thus each particle is confined to an effective cage, similar to the tube in reptation theory. The rearrangement of the neighboring spheres releases the initial constraint and allows to move over larger distances. The ensuing dynamics exhibit a striking resemblance to the orthogonal diffusion of a chain segment in a polymer solution [140]: At small times free relaxation is observed, followed by an intermediate regime with sub-diffusive relaxation. Like in our polymer system, in this intermediate regime, constraint release determines the dynamics. At some terminal relaxation time determined by constraint release, diffusion becomes linear. Of course, no super-diffusive regime appears in the colloidal system, as there is no projection procedure involved. For all other regimes it seems possible to relate the behavior of the colloids and our observed behavior for polymer segments.
Hence, understanding the constraint release process in the cage effect might help in describing entangled polymer solutions, too. Unfortunately, in spite of intensive research, the cage effect and its dynamics are not yet completely clarified and the dominant mechanism is still unknown [141]. Note that the collisions of hard, spherical objects is much simpler to analyze than that of polymer chains. Therefore, it will be challenging to transfer the insights from the colloidal system to the polymer system. Especially the elongated shape and finite bending stiffness of the polymers probably cause additional coupling in the motion of several chains. In conclusion, constraint release and its effects are a challenging open question well worth of further attention.

A Viscoelasticity of an entangled polymer network

The global response of a polymer solution to external forces is described by the viscoelasticity of the network. This is a macroscopic description of the whole solution, such that the viscoelastic properties are among the most important for technical applications on all scales above the single molecule level [57]. While viscoelasticity is a macroscopic quantity, it is closely connected to the microscopic properties and the corresponding relaxation behavior [21, 39].

The viscoelasticity of a polymer network is usually quantified by the shear relaxation modulus G, which describes the linear response to a shear strain. More explicitly, the shear stress $\boldsymbol{\sigma}(t)$ at time t after an infinitesimal step strain $\boldsymbol{\gamma}$ is given by $\boldsymbol{\sigma}(t) = G(t)\left(\boldsymbol{\gamma} + \boldsymbol{\gamma}^T\right)$, where $\boldsymbol{\gamma}^T$ denotes the transpose of $\boldsymbol{\gamma}$ [21, 39]. Depending on the system, external forces, or the focus of the study, there are several equivalent ways to express the viscoelasticity [57]. A common alternative to $G(t)$ is the complex shear modulus $G^*(\omega)$, which is defined as [21, 142]

$$G^*(\omega) = i\omega \int_0^\infty G(t) \exp(-i\omega t) \mathrm{d}t \,. \tag{A.1}$$

This form is especially suitable for systems exposed to an oscillatory shear, as it is commonly used in experiments. To allow for an easier interpretation, $G^*(\omega)$ is frequently separated into its real and complex component:

$$G'(\omega) = \mathrm{Re}\left(G^*(\omega)\right) \; ; \quad G''(\omega) = \mathrm{Im}\left(G^*(\omega)\right) \; ; \tag{A.2}$$

$G'(\omega)$ is called the storage modulus and $G''(\omega)$ is referred to as the loss modulus [21, 57, 142].

There are two distinctly different approaches to determine the viscoelasticity of a solution. Using classical rheology probes the solution as a whole by, e.g., applying a global periodic shear to the sample. In experiments, this method is limited by the mechanical properties of the measurement apparatus. Therefore only frequencies below approximately 10^3Hz are accessible [138, 143].
In the alternative approach, which is termed microrheology, the local properties of the sample are probed. This is usually achieved by embedding colloidal probe particles into the solution and tracking their diffusion [138, 144, 145]. These particles may either be actively driven by an external field or are subject to thermal motion only. The latter technique is called passive microrheology. These methods allow a much better time resolution than classical rheology, determining the response to frequencies up to 10^5Hz [57]. However, these methods are limited in the low frequency range.
Up to now a rigorous proof is still lacking that these two methods measure the same physical quantity. Nevertheless, there is some experimental data that suggests that they are in agreement for at least a limited range of intermediate frequencies [57, 138, 143].

The implementation of a global shear into a numerical simulation with a small sample size could suffer from finite size effects and requires specification of additional free parameters. Therefore, we intend to mimic a passive microrheology experiment with our simulations. The major advantage of this approach is that it is practically free of additional assumptions.

We employ our basic simulation as detailed in Sec. 3.1 and extend it by adding a single observation bead, also called test-bead, of diameter $r_b = 1.5\xi_m$. With exception of the range of the steric interaction, this bead interacts with the polymers by the same repulsive potential as introduced for the polymers, see Eq. (3.3). To compensate for the volume occupied by the bead we adjust the simulation box by increasing its volume to $V + \frac{\pi}{6} r_b^3$. Hence, the mesh size does not change. In order to avoid interactions of different observation beads by, e.g., the depletion interaction, we embed only a single bead into the polymer network. The bead is subject to Brownian motion with the same temperature as the polymer solution and a friction proportional to its size, $\zeta_{\text{bead}} = r_b/2\zeta$. The motion of the bead governed by its friction, noise and the repulsive potential is then implemented completely analogously to the motion of a bead belonging to a polymer chain, cf. Sec. 3.1.

For such a test-bead, we record its movement over time and calculate the mean square displacement $\langle \delta x^2 \rangle = \langle [\mathbf{x}(t) - \mathbf{x}(0)]^2 \rangle$, where $\mathbf{x}(t)$ denotes the position of the bead at time t. The observable is determined in simulations performed for four different, independent initial conditions. For each simulation 250 time-series of the bead motion, each initiated a time of 0.05τ after the previous, were recorded. No significant deviation larger than statistical fluctuation between the different initial conditions could be observed, such that we use the average over all recorded data for the following analysis.

As expected, the mean square displacement of the observation bead exhibits four different regimes. According to standard theory of viscoelasticity, these regimes are closely related to the dynamics of the polymers [21, 39].
At very small times the test-bead exhibits free diffusion, until it is in constant contact with the surrounding chains. Then, the bead follows the dynamics of the polymer segment, with which it is in contact. Since the bead diameter is larger than the mesh size, which measures the typical distance between the chains, it is almost always in contact with several chains. At small times the polymers predominantly perform free fluctuations dominated by the orthogonal contour fluctuations, as discussed in Sec. 4.1. Hence, also the bead exhibits a $t^{3/4}$ power law, as familiar for the free relaxation of semiflexible polymers. Note that these times are very small relative to the longest relaxation time of the network. Thus, there is virtually no rearrangement of the network at these times. At the Odijk time τ_e the interaction between the different polymer chains becomes relevant and the dynamics change to a more complex behavior. Indeed, we find that the time, at which δx^2 departs from the $t^{3/4}$ power law, is in good agreement with the scaling of the Odijk time, see Fig. A.1.
In the following time regime, the network rearrangement and constraint release become relevant. Accordingly, the constraints on the bead imposed by the initially surrounding polymer start to relax, leading to some sub-diffusive increase of δx^2, see Fig. A.1, comparable but not necessarily identical to the constraint release dynamics of a single filament. As this observable is just an auxiliary quantity in determining G, we do not analyze this region further.
Finally, at times larger than the time required to release the topological constraints around the bead, once again it is supposed to exhibit linear diffusion. The release of the constraints is related to rearrangements of the polymer network, and should thus be proportional to τ_r.

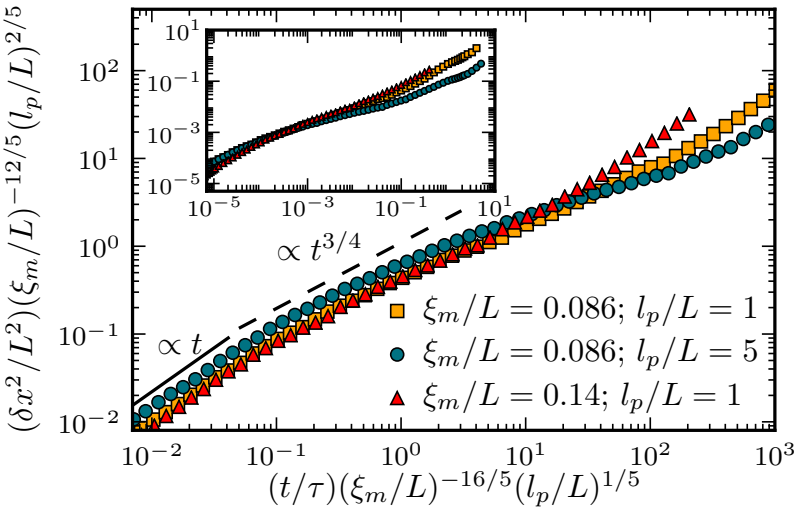

Figure A.1: Examples for the mean square displacement of a test-bead $\delta x^2/L^2$ with a diameter $r_b = 1.5\xi_m$ in networks of different characteristics. The inset shows the unscaled data $\delta x^2/L^2$ in dependence on t/τ. By rescaling the time with the Odijk time τ_e and $\delta x^2/L^2$ with the amplitude of the orthogonal fluctuations of the polymer at that time, we find that the dynamics of the test-bead at small times is dominated by the motion of the surrounding polymer chains. Especially the familiar $t^{3/4}$ scaling law of internal polymer relaxation also occurs for the test-bead, as indicated in the figure. At even smaller times, the bead diffuses freely.

In Fig. A.2 we find that the crossover to the final regime of δx^2 is proportional to the longest relaxation time of the network τ_r, indeed. Note that there is an additional factor of L/r_b to account for the different friction coefficients of the test-bead and the polymer. Thus, the dynamics of a test-bead is closely related to the characteristics of the polymer network.

There are several, in principle equivalent possibilities to extract the elastic modulus form the measured mean square displacement of the test-bead, see the excellent review of Waigh [57] for an overview. There are two quite common approaches, which we shortly discuss here.

A possible method is to calculate the power spectral density $\langle x^2(\omega)\rangle$ of the test-bead, which due to the fluctuation-dissipation theorem is directly related to the complex part of the response function $\alpha(\omega)$ by $\mathrm{Im}(\alpha(\omega)) = \alpha''(\omega) = \frac{\omega}{2k_BT}\langle x^2(\omega)\rangle$ [144, 145]. Given the complex part of an analytic, complex function confined to the upper half of the complex plane, i.e., a causal system, it is possible to calculate the full function using the Kramers-Kronig relations [146, 147]. Thus, ideally we may calculate the real part of the response function from its imaginary part by

$$\mathrm{Re}(\alpha(\omega)) = \alpha'(\omega) = \frac{2}{\pi} P \int_0^\infty \frac{\zeta \alpha''(\zeta)}{\zeta^2 - \omega^2} \mathrm{d}\zeta \ .$$

This requires the calculation of a principal-value integral $P\int_0^\infty \mathrm{d}\zeta$. As solving this integral with a finite set of (noisy) data points is not feasible, an approximative method in this step is employed, which is usually based on successively applying a discrete sine and cosine

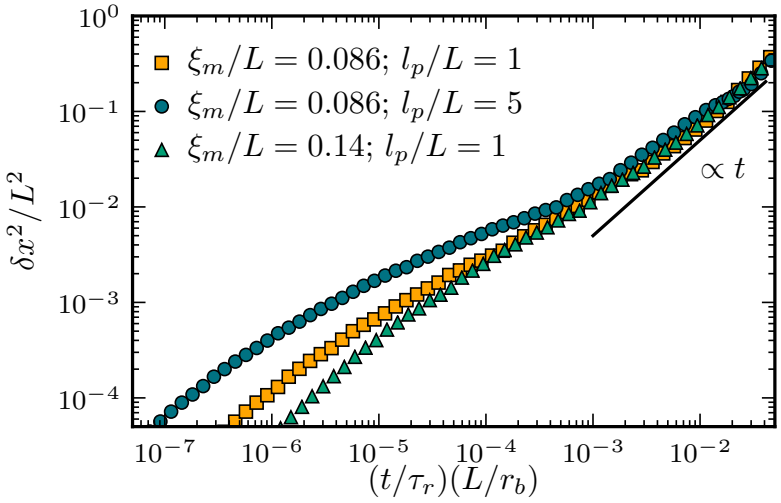

Figure A.2: Examples for the mean square displacement of a test-bead with a radius $r_b = 1.5\xi_m$ in networks of different characteristics, where the time is rescaled by the longest relaxation time of the polymer network τ_r and the friction of the test-bead. We find an acceptable data collapse for the onset of the final linear diffusive regime, thus showing that the longest relaxation time of the polymer network τ_r is proportional to the longest relaxation time of the test-bead. For comparison a linear scaling law is shown close to the final regime [black line].

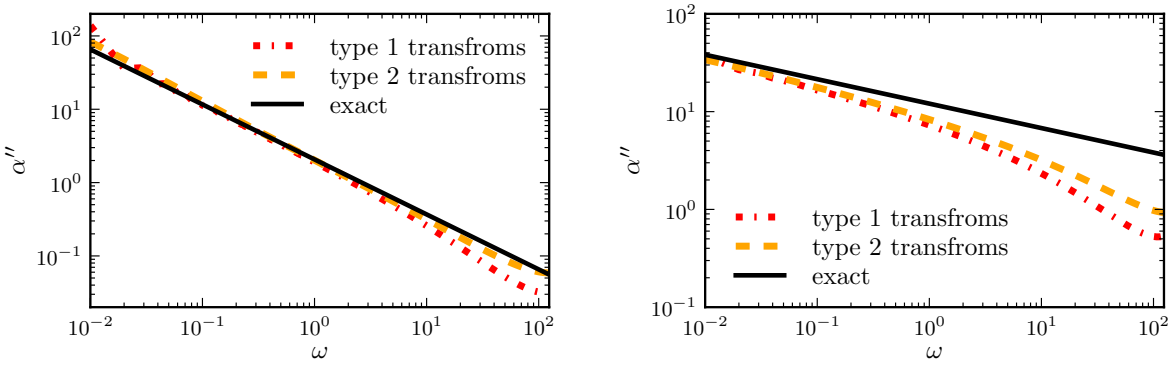

Figure A.3: Two examples for the accuracy in reconstructing α'' from a given power law for α'. In the left figure we assume $\alpha'(\omega) = 5\omega^{-3/4}$, the right is for $\alpha'(\omega) = 5\omega^{-1/4}$. The continuous black line gives the exact solution of the Kramers-Kronig relation over the finite region considered here, whereas the other lines give two possible realizations of the approximative solution based on 20480 evenly spaced data points. The dashed-dotted lines gives the results gained by using discrete type 1 transformations, the dashed lined is for type 2 transformations. Both transformations are calculated in Mathematica. In the left figure only a small deviation between the procedures is observed. However, in the right figure the approximative method implies a completely erroneous behavior.

transformation. The common form is [145]:

$$\alpha'(\omega) = \frac{2}{\pi} \int_0^\infty \cos(\omega t) \int_0^\infty \alpha''(\zeta) \sin(\zeta t) \mathrm{d}\zeta \mathrm{d}t \,, \tag{A.3}$$

where for applications the integrals are replaced by a discrete transform to cope with the discrete data. The numerical analysis is simplified by noting that the transforms may be realized by a discrete fast Fourier transformation [145]. Note that there are several types of discrete sine and cosine transformations, and it is not clear which type to use. As we do not use this method, we do not go into details on these transformations here. Given the complete complex response function and assuming that the network may be described as a single-component medium it is possible to calculate $G^*(\omega)$ from $\alpha(\omega)$ [145]. While this method is widely used, there are several major drawbacks, which should be kept in mind when interpreting results gained by this procedure.
First of all, in calculating the power spectral density of a limited set of data, strong fluctuations in the high frequency limit of the data occur even for an almost perfect data set with small fluctuations. Secondly, the approximative solution of the Kramers-Kronig relations changes the scaling behavior. This may easily be shown by assuming a simple power law for $\mathrm{Im}(\alpha(\omega)) = C\omega^\gamma$ with a constant C, for which the exact solution to the principal value integral can be calculated, see Fig. A.3. For the approximative solution, the discrete transformations are performed with a large number of 20480 data points. Therefore, any deviations primarily result from the approximations, not from the discrete nature of the data. We find that the approximative solution gives best results for power laws with an exponent γ close to -1, and increasing deviations from the exact solutions occur with increasing γ. As one of the points of major interest is the plateau behavior of the storage modulus, a regime with a weak power law dependence with γ close to zero is expected. In particular, for this regime major deviations may arise from this method of analysis. To explain this deviation, consider a strict mathematical argument. Then the Kramers-Kronig relations are not valid for this problem. The relations require that the functions involved vanish faster than $1/|\omega|$ for $\omega \to \infty$. As the high frequency behavior is dominated by the contour fluctuations, $\alpha(\omega)$ only decreases with $\omega^{3/4}$, failing this requirement. Due to all these drawbacks we apply a different method, although it is still less common.

In this thesis, we use the method of Mason [142]. The idea is to give an analytic expression for $G^*(\omega)$ in dependence on $\langle \delta x^2(t) \rangle$. To achieve this, the approximation of local power law behavior is needed, which is well justified by our data on the diffusion of the test-bead. The full formula corresponds to calculating the Laplace transform of $\langle \delta x^2(t) \rangle$ and then using a generalized Stokes-Einstein equation to determine $\tilde{G}(s)$, the Laplace transform of $G(t)$. Finally, employing analytic continuity directly derives G' and G'' from $\tilde{G}(s)$. Taking all these steps together, the viscoelasticity may be calculated by [142]:

$$G'(\omega) = |G^*(\omega)| \cos(\pi\beta(\omega)/2) \quad \text{and} \tag{A.4}$$

$$G''(\omega) = |G^*(\omega)| \sin(\pi\beta(\omega)/2) \,, \tag{A.5}$$

with $\beta(\omega) = \left. \frac{\partial \ln \langle \delta x^2(t) \rangle}{\partial \ln t} \right|_{t=1/\omega}$. The absolute value of the complex shear modulus is approximated by:

$$|G^*(\omega)| \approx \frac{k_B T}{\pi r_b \langle \delta x^2(t) \rangle \Gamma[1 + \beta(\omega)]} \,, \tag{A.6}$$

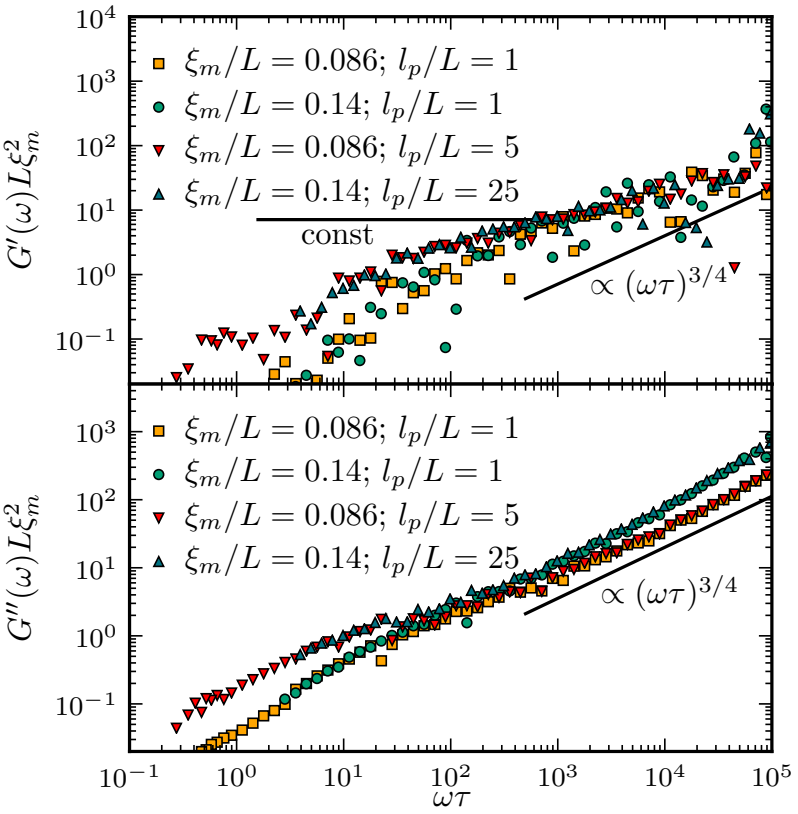

Figure A.4: Typical examples for the storage and loss modulus, G' and G'', respectively, of polymer networks of different characteristics calculated from the mean square displacement of a test-bead. No clear plateau may be observed in the storage modulus G'. For comparison, the black line shows the expected value of the plateau. For both storage and loss modulus we find an increase with $\omega^{3/4}$ in the high frequency regime in accordance with experimental results. The horizontal line gives the theoretical value of the plateau modulus for the system with $\xi_m/L = 0.086$ and $l_p/L = 1$ according to Eq. (A.7).

where we have to evaluate $\langle \delta x^2(t) \rangle$ at time $t = 1/\omega$. Apart from avoiding the problems of discrete transformations in the other approach, this formula has the advantage that we may directly use exponentially spaced data points, which is more efficient in a numerical simulation.

Our results for the storage and loss modulus calculated by this method are shown in Fig. A.4. For G'', in accordance with experiments and theoretical predictions [21,57,145], we find a 3/4 power law behavior for high frequencies, cf. Fig. A.4. At smaller frequencies the dependence of the loss modulus on ω decreases, also in accord with existing data [21,57,145]. The decrease seems to be more pronounced for networks with a high stiffness and small mesh size, see Fig. A.4.

The calculated storage modulus G' exhibits significantly stronger fluctuations than G'', such that we are limited in the analysis. From experiments, we expect to find a plateau in the

storage modulus at low to intermediate frequencies in the range of $10^{-1} \lesssim \omega\tau \lesssim 10^3$ and an increase with $(\omega\tau)^{3/4}$ at high frequencies [57]. Like for the loss modulus, the power law behavior at high frequencies also occurs in out data. However, it is impossible to discern a clear plateau at lower frequencies. There seems to exist a deviation from the high frequency behavior in the form of a flattening, which seems to be stronger for higher densities, i.e., smaller mesh size and higher values of l_p/L, see Fig. A.4. The value of G' at the plateau has received considerable attention before and there are several theoretical predictions based on the tube model. For a purely entangled network the plateau modulus is expected to be [43, 148]:

$$G'_0 = \frac{9k_BT}{5\xi_m^2 L_e}\,. \tag{A.7}$$

There are alternative approaches which exhibit the same dependence on all parameters, but with slightly different numerical prefactors [21]. As the difference between these factors are of the order of unity, we only use the formula as given in Eq. (A.7) for comparison. For rather stiff polymers, this theoretical prediction has been shown to be in good agreement with experiments [43, 148]. The major problem is that all predictions employ the entanglement length L_e to quantify the network behavior. Note that only the scaling behavior of L_e is known and a numerical prefactor has not yet been established unambiguously. For the comparison in Fig. A.4 we extract the value of L_e from our simulations by assuming that the orthogonal fluctuations of the center monomer $g_{1,\perp}$ are free fluctuations of a semiflexible polymer up to the Odijk time. Thus $g_{1,\perp}$ should be equal to $L_e^3/45l_p$ at the Odijk time. Using this procedure the predicted plateau value is of the same order of magnitude as the results from our simulations and even seems to agree with the flattening region. However, no clear plateau at the expected value is seen.

There are some possible explanations: Our simulation could suffer from finite size effects or the interaction of the bead with the polymers could be different than in experiments. Also, the size of the test particle may be relevant. Unfortunately, our attempts at simulations with larger particles were not yet successful.

Alternatively, the experimental data might be flawed, for example by impurities with cross-linkers. This might also explains the large deviations in the experimentally measured plateau values. Also, the standard evaluation method used in experiments is based on the Kramers-Kronig relations, and the problems discussed there also apply for the resulting data. Note that the reported plateau behavior with a broad region with slope zero, but finite value is impossible in a system for which equations (A.4) and (A.5) hold.

Finally, the predictions for the plateau value are based on the tube model and do not incorporate constraint release and many chain interactions, which we have found to be of major importance in Chapter 5. This agrees with some experiments, where a significant deviation in the whole behavior of G^* of unclear origin has been found for longer, i.e., more flexible chains [137]. As we consider these kinds of polymers in most of our simulations, it probably corresponds to this behavior, which is not yet fully understood. We propose that this complex behavior is related to the constraint release mechanism reported here.

Due to the strong fluctuations in spite of seemingly good data on δx^2 we do not attempt a more complete analysis of the storage and loss modulus with our simulations and leave this topic for further work.

B Additional Figures

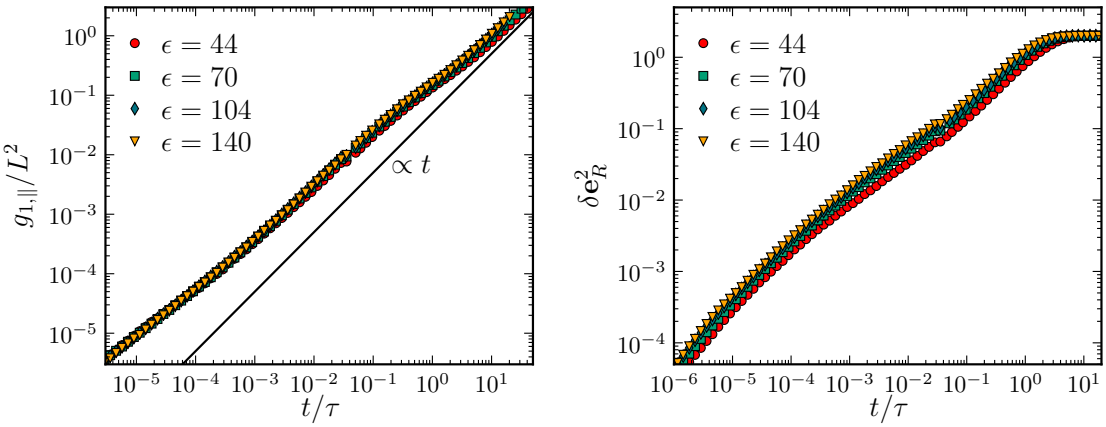

Figure B.1: Parallel diffusion of the center monomer (left) and rotational MSD (right) of single chains in a polymer network with $\xi_m/L = 0.12$ and $l_p/L = 1$ determined from simulations using different values for the aspect ratio. For $\epsilon \gtrsim 70$ the aspect ratio has almost no effect on the results of the simulations.

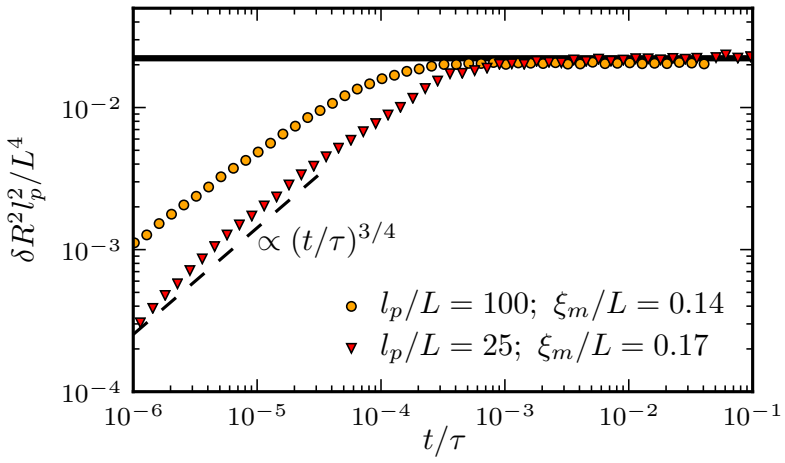

Figure B.2: Internal relaxation of very stiff polymers with $l_p \gtrsim l_{p,c}$ in two different systems. The orthogonal fluctuations saturate to their equilibrium value, shown by the solid line, before contact with the tube is achieved. Consequently the intermediate regime in δR^2 vanishes, as δR^2 is already saturated.

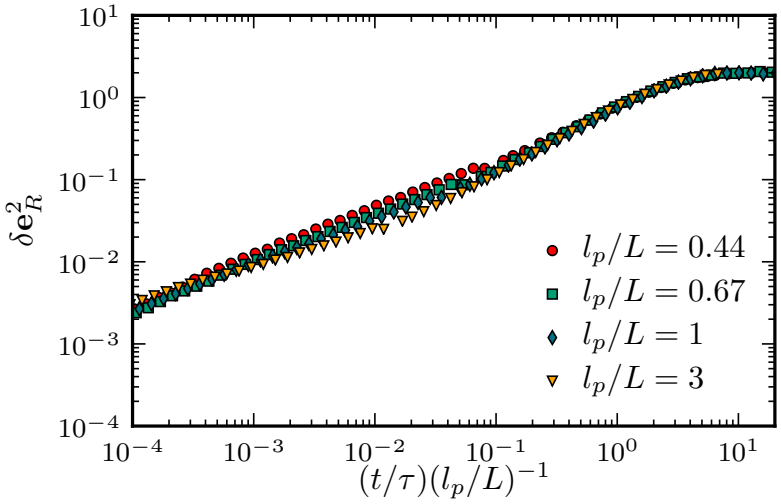

Figure B.3: For several polymer networks with $\xi_m/L = 0.075$ the rotational MSD is given for various values of the stiffness. For this system, by rescaling the time with l_p/L we find a good data collapse of the longest relaxation time, even for chains with $l_p/L < 1$.

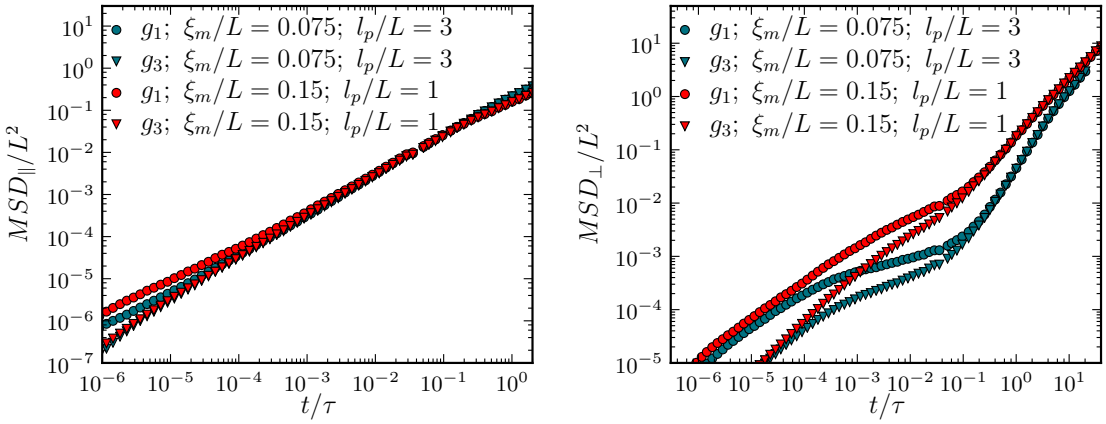

Figure B.4: Comparison of the MSD of the center of mass and the center monomer. Left: MSD parallel to the end-to-end vector. Right: Orthogonal contribution to the MSD. At times above $\tau_{i,l}$, i.e., directly after the crossover from the sub-diffusive to the super-diffusive regime, the two observables $g_1(t)$ and $g_3(t)$ are identical.

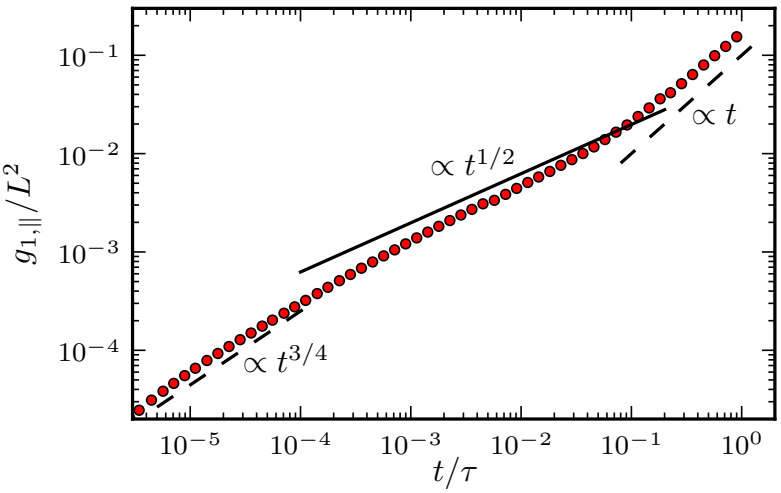

Figure B.5: The parallel MSD of the center monomer for a flexible chain with $l_p < \xi_m$. In this system $\xi_m/L = 0.10$ and $l_p/L = 0.04$. A regime with a behavior of approximately $t^{1/2}$ occurs at intermediate times.

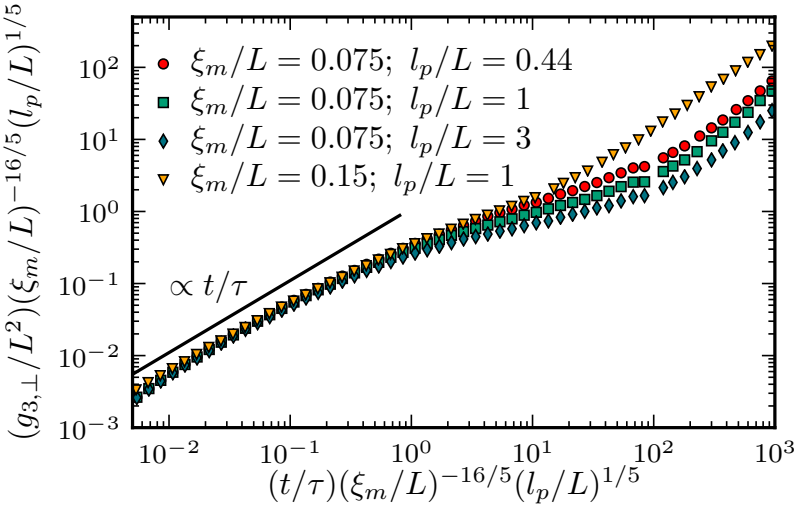

Figure B.6: $g_{3,\perp}$ for different systems in the semiflexible regime. By rescaling the time and $g_{3,\perp}(t)$ with $(\xi_m/L)^{16/5}(l_p/L)^{-1/5}$ we see that free diffusion occurs up to time τ_e, which is proportional to the latter expression.

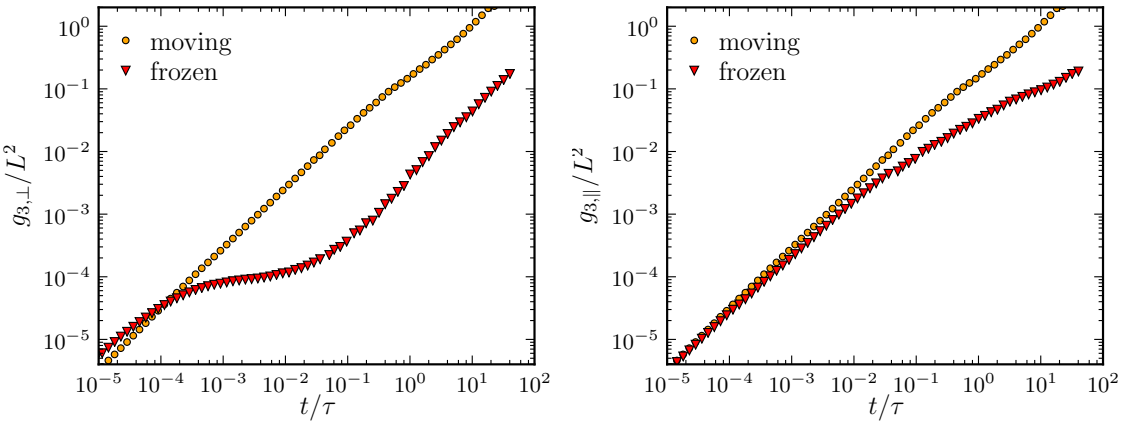

Figure B.7: Comparison of the components of g_3 in a system with fixed obstacles to a purely entangled network. The Figure is for a system with $\xi_m/L = 0.086$ and $l_p/L = 1$. The same deviations as observed for g_1 in Fig. 5.3 occur.

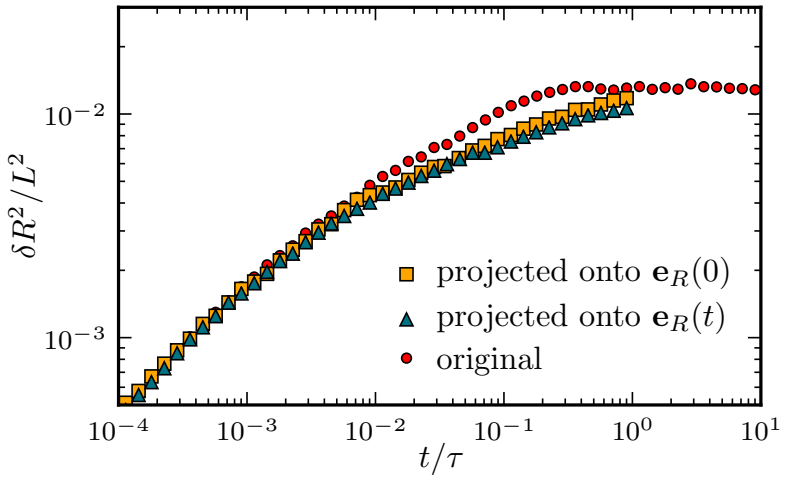

Figure B.8: Internal relaxation of a chain in a network of $\xi_m/L = 0.086$ and $l_p/L = 1$ with restricted parallel diffusion due to an additional potential. In the data marked by yellow squares, the restriction is as given in Eq. (5.2). The results shown as blue triangles are generated using an analogous potential projecting onto the current end-to-end vector $\mathbf{e}_R(t)$ instead of the initial $\mathbf{e}_R(0)$ in Eq. (5.2). For a better comparison with Fig. 5.7, the original data is shown, too. Due to the small rotation at these times, there is only a small difference between the two fixing potentials acting with respect to the different definitions of parallel.

Bibliography

[1] A. R. Bausch and K. Kroy. A bottom-up approach to cell mechanics. *Nature Physics*, 2(4):231–238, 2006.

[2] C. Bustamante, Z. Bryant, and S. B. Smith. Ten years of tension: single-molecule DNA mechanics. *Nature*, 421(6921):423–427, 2003.

[3] B. Alberts, D. Bray, J. Lewis, M. Raff, K. Roberts, and J. Watson. *Molecular Biology of the cell*. Garland Publishing, 3rd edition, 1994.

[4] Wikipedia. Cytoskeleton — wikipedia, the free encyclopedia, 2015. [Online; accessed 9-February-2015].

[5] T. T. Perkins, S. R. Quake, D. E. Smith, and S. Chu. Relaxation of a single DNA molecule observed by optical microscopy. *Science*, 264(5160):822–826, 1994.

[6] L. Le Goff, O. Hallatschek, E. Frey, and F. Amblard. Tracer studies on f-actin fluctuations. *Phys. Rev. Lett.*, 89(25):258101, 2002.

[7] A. Ott, M. Magnasco, A. Simon, and A. Libchaber. Measurement of the persistence length of polymerized actin using fluorescence microscopy. *Phys. Rev. E*, 48(3):R1642–R1645, 1993.

[8] N. B. Becker, A. Rosa, and R. Everaers. The radial distribution function of worm-like chains. *Europ. Phys. J. E*, 32(1):53–69, 2010.

[9] O. Hallatschek, E. Frey, and K. Kroy. Propagation and relaxation of tension in stiff polymers. *Phys. Rev. Lett.*, 94(7):77804, 2005.

[10] F. Pampaloni, G. Lattanzi, A. Jonáš, T. Surrey, E. Frey, and E.-L. Florin. Thermal fluctuations of grafted microtubules provide evidence of a length-dependent persistence length. *PNAS*, 103(27):10248–10253, 2006.

[11] K. M. Taute, F. Pampaloni, E. Frey, and E.-L. Florin. Microtubule dynamics depart from the wormlike chain model. *Phys. Rev. Lett.*, 100(2):028102, 2008.

[12] A. Caspi, M. Elbaum, R. Granek, A. Lachish, and D. Zbaida. Semiflexible polymer network: a view from inside. *Phys. Rev. Lett.*, 80(5):1106, 1998.

[13] M. E. Janson and M. Dogterom. A bending mode analysis for growing microtubules: evidence for a velocity-dependent rigidity. *Biophys. J.*, 87(4):2723–2736, 2004.

[14] C. P. Brangwynne, G. H. Koenderink, E. Barry, Z. Dogic, F. C. MacKintosh, and D. A. Weitz. Bending dynamics of fluctuating biopolymers probed by automated high-resolution filament tracking. *Biophys. J.*, 93(1):346–359, 2007.

[15] J. Shimada and H. Yamakawa. Ring-closure probabilities for twisted wormlike chains. application to DNA. *Macromolecules*, 17(4):689–698, 1984.

[16] J. Wilhelm and E. Frey. Radial distribution function of semiflexible polymers. *Phys. Rev. Lett.*, 77(12):2581, 1996.

[17] F. Gittes, B. Mickey, J. Nettleton, and J. Howard. Flexural rigidity of microtubules and actin-filaments measured from thermal fluctuations in shape. *J. Cell Biol.*, 120(4):923–934, 1993.

[18] Y. Bohbot-Raviv, W. Z. Zhao, M. Feingold, C. H. Wiggins, and R. Granek. Relaxation dynamics of semiflexible polymers. *Phys. Rev. Lett.*, 92(9), 2004.

[19] K. Kroy and E. Frey. Dynamic scattering from solutions of semiflexible polymers. *Phys. Rev. E*, 55(3):3092, 1997.

[20] D. C. Morse. Viscoelasticity of concentrated isotropic solutions of semiflexible polymers. 2. linear response. *Macromolecules*, 31(20):7044–7067, 1998.

[21] D. C. Morse. Viscoelasticity of tightly entangled solutions of semiflexible polymers. *Phys. Rev. E*, 58(2):R1237, 1998.

[22] F. Gittes and F. C. MacKintosh. Dynamic shear modulus of a semiflexible polymer network. *Phys. Rev. E*, 58(2):1241–1244, 1998.

[23] O. Hallatschek, E. Frey, and K. Kroy. Tension dynamics in semiflexible polymers. i. coarse-grained equations of motion. *Phys. Rev. E*, 75(3):031905, 2007.

[24] O. Hallatschek, E. Frey, and K. Kroy. Tension dynamics in semiflexible polymers. ii. scaling solutions and applications. *Phys. Rev. E*, 75(3):031906, 2007.

[25] B. Obermayer, O. Hallatschek, E. Frey, and K. Kroy. Stretching dynamics of semiflexible polymers. *Eur. Phys. J. E*, 23(4):375–388, 2007.

[26] B. Obermayer, W. Möbius, O. Hallatschek, E. Frey, and K. Kroy. Freely relaxing polymers remember how they were straightened. *Phys. Rev. E*, 79(2):021804, 2009.

[27] F. Thüroff, B. Obermayer, and E. Frey. Longitudinal response of confined semiflexible polymers. *Phys. Rev. E*, 83(2):021802, 2011.

[28] A. E. Likhtman and T. C. McLeish. Quantitative theory for linear dynamics of linear entangled polymers. *Macromolecules*, 35(16):6332–6343, 2002.

[29] S. Ramanathan and D. C. Morse. Simulations of dynamics and viscoelasticity in highly entangled solutions of semiflexible rods. *Phys. Rev. E*, 76(1):010501, 2007.

[30] J.-X. Hou, C. Svaneborg, R. Everaers, and G. S. Grest. Stress relaxation in entangled polymer melts. *Phys. Rev. Lett.*, 105(6):068301, 2010.

[31] G. Nam, A. Johner, and N.-K. Lee. Reptation of a semiflexible polymer through porous media. *J. Chem. Phys.*, 133(4):044908, 2010.

[32] G. Nam, A. Johner, and N.-K. Lee. Drift and diffusion of a confined semiflexible chain. *Eur. Phys. J. E*, 32(2):119–126, 2010.

[33] J. Glaser, D. Chakraborty, K. Kroy, I. Lauter, M. Degawa, N. Kirchgeßner, B. Hoffmann, R. Merkel, and M. Giesen. Tube width fluctuations in f-actin solutions. *Phys. Rev. Lett.*, 105(3):037801, 2010.

[34] J. P. Wittmer, H. Meyer, J. Baschnagel, A. Johner, S. Obukhov, L. Mattioni, M. Müller, and A. N. Semenov. Long range bond-bond correlations in dense polymer solutions. *Phys. Rev. Lett.*, 93(14):147801, 2004.

[35] F. Höfling, E. Frey, and T. Franosch. Enhanced diffusion of a needle in a planar array of point obstacles. *Phys. Rev. Lett.*, 101(12):120605, 2008.

[36] P.-G. de Gennes. Reptation of a polymer chain in the presence of fixed obstacles. *J. Chem. Phys.*, 55:572, 1971.

[37] M. Doi and S. F. Edwards. Dynamics of concentrated polymer systems. part 1.—brownian motion in the equilibrium state. *J. Chem Soc. Faraday Trans.*, 74:1789–1801, 1978.

[38] M. Doi and S. F. Edwards. Dynamics of rod-like macromolecules in concentrated solution. part 1. *J. Chem Soc. Faraday Trans.*, 74:560–570, 1978.

[39] S. F. Edwards and M. Doi. *The theory of polymer dynamics*. 1986.

[40] R. Granek. From semi-flexible polymers to membranes: anomalous diffusion and reptation. *J. Phys. II*, 7(12):1761–1788, 1997.

[41] M. Doi, W. W. Graessley, E. Helfand, and D. S. Pearson. Dynamics of polymers in polydisperse melts. *Macromolecules*, 20(8):1900–1906, 1987.

[42] F. Höfling, T. Munk, E. Frey, and T. Franosch. Entangled dynamics of a stiff polymer. *Phys. Rev. E*, 77(6):060904, 2008.

[43] B. Hinner, M. Tempel, E. Sackmann, K. Kroy, and E. Frey. Entanglement, elasticity, and viscous relaxation of actin solutions. *Phys. Rev. Lett.*, 81(12):2614, 1998.

[44] R. S. Graham, A. E. Likhtman, T. C. B. McLeish, and S. T. Milner. Microscopic theory of linear, entangled polymer chains under rapid deformation including chain stretch and convective constraint release. *J. Rheol.*, 47(5):1171–1200, 2003.

[45] G. Marrucci. Relaxation by reptation and tube enlargement: a model for polydisperse polymers. *J. Polym. Sci.: Polym. Phys. Ed.*, 23(1):159–177, 1985.

[46] J. L. Viovy, M. Rubinstein, and R. H. Colby. Constraint release in polymer melts: tube reorganization versus tube dilation. *Macromolecules*, 24(12):3587–3596, 1991.

[47] S. T. Milner and T. C. B. McLeish. Reptation and contour-length fluctuations in melts of linear polymers. *Phys. Rev. Lett.*, 81(3):725, 1998.

[48] S. M. Aharoni. On entanglements of flexible and rodlike polymers. *Macromolecules*, 16(11):1722–1728, 1983.

[49] C. F. Schmidt, M. Baermann, G. Isenberg, and E. Sackmann. Chain dynamics, mesh size, and diffusive transport in networks of polymerized actin: a quasielastic light scattering and microfluorescence study. *Macromolecules*, 22(9):3638–3649, 1989.

[50] T. T. Perkins, D. E. Smith, and S. Chu. Direct observation of tube-like motion of a single polymer chain. *Science*, 264(5160):819–822, 1994.

[51] J. Käs, H. Strey, and E. Sackmann. Direct imaging of reptation for semiflexible actin filaments. *Nature*, 368:226–229, 1994.

[52] E. Sackmann, J. Käs, and H. Strey. The observation of polymer reptation. *Adv. Mat.*, 6(6):507–509, 1994.

[53] J. Käs, H. Strey, J. Tang, D. Finger, R. Ezzell, E. Sackmann, and P. Janmey. F-actin, a model polymer for semiflexible chains in dilute, semidilute, and liquid crystalline solutions. *Biophys. J.*, 70(2):609, 1996.

[54] M. Romanowska, H. Hinsch, N. Kirchgeßner, M. Giesen, M. Degawa, B. Hoffmann, E. Frey, and R. Merkel. Direct observation of the tube model in f-actin solutions: Tube dimensions and curvatures. *Europhys. Lett.*, 86(2):26003, 2009.

[55] N. Fakhri, F. C. MacKintosh, B. Lounis, L. Cognet, and M. Pasquali. Brownian motion of stiff filaments in a crowded environment. *Science*, 330(6012):1804–1807, 2010.

[56] J. Liu, M. L. Gardel, K. Kroy, E. Frey, B. D. Hoffman, J. C. Crocker, A. R. Bausch, and D. A. Weitz. Microrheology probes length scale dependent rheology. *Phys. Rev. Lett.*, 96(11):118104, 2006.

[57] T. A. Waigh. Microrheology of complex fluids. *Rep. Prog. Phys.*, 68(3):685, 2005.

[58] K. Kremer and G. S. Grest. Dynamics of entangled linear polymer melts: A molecular-dynamics simulation. *J. Chem. Phys.*, 92:5057, 1990.

[59] K. Kremer and G. S. Grest. Simulations for structural and dynamic properties of dense polymer systems. *J. Chem. Soc., Faraday Trans.*, 88(13):1707–1717, 1992.

[60] M. Doi and H. See. *Introduction to polymer physics*. Clarendon Press Oxford, 1996.

[61] E. Frey and D. R. Nelson. Dynamics of flat membranes and flickering in red blood cells. *J. Phys. I (France)*, 1(12):1715–1757, 1991.

[62] G. K. Batchelor. Slender-body theory for particles of arbitrary cross-section in stokes flow. *J. Fluid Mech.*, 44:419–440, 1970.

[63] J. Howard et al. *Mechanics of motor proteins and the cytoskeleton*. Sinauer Associates Sunderland, MA, 2001.

[64] P. E. Rouse Jr. A theory of the linear viscoelastic properties of dilute solutions of coiling polymers. *J. Chem. Phys.*, 21(7):1272–1280, 1953.

[65] M. Rubinstein and R. H. Colby. *Polymers Physics*. Oxford, 2003.

[66] O. Kratky and G. Porod. Röntgenuntersuchung gelöster Fadenmoleküle. *Recl. Trav. Chim.*, 68(12):1106–1122, 1949.

[67] N. Saitô, K. Takahash, and Y. Yunoki. Statistical mechanical theory of stiff chains. *J. Phys. Soc. Jpn.*, 22(1):219–226, 1967.

[68] J. F. Marko. DNA under high tension: overstretching, undertwisting, and relaxation dynamics. *Phys. Rev. E*, 57(2):2134, 1998.

[69] J. Kierfeld, O. Niamploy, V. Sa-Yakanit, and R. Lipowsky. Stretching of semiflexible polymers with elastic bonds. *Eur. Phys. J. E*, 14(1):17–34, 2004.

[70] B. Obermayer and E. Frey. Tension dynamics and viscoelasticity of extensible wormlike chains. *Phys. Rev. E*, 80(4):040801, 2009.

[71] R. R. Netz. Strongly stretched semiflexible extensible polyelectrolytes and DNA. *Macromolecules*, 34(21):7522–7529, 2001.

[72] C. Rivetti, C. Walker, and C. Bustamante. Polymer chain statistics and conformational analysis of DNA molecules with bends or sections of different flexibility. *J. mol. biol.*, 280(1):41–59, 1998.

[73] O. Hallatschek, E. Frey, and K. Kroy. Overdamped stress relaxation in buckled rods. *Phys. Rev. E*, 70(3):031802, 2004.

[74] G.-C. Wick. The evaluation of the collision matrix. *Phys. Rev.*, 80(2):268, 1950.

[75] S. F. Edwards. The statistical mechanics of polymerized material. *Proc. Phys. Soc.*, 92(1):9, 1967.

[76] M. Doi and S. F. Edwards. Dynamics of concentrated polymer systems. part 2.—molecular motion under flow. *J. Chem. Soc., Faraday Trans. 2*, 74:1802–1817, 1978.

[77] M. Doi and S. F. Edwards. Dynamics of concentrated polymer systems. part 3.—the constitutive equation. *J. Chem Soc. Faraday Trans.*, 74:1818–1832, 1978.

[78] E. Frey, K. Kroy, and J. Wilhelm. Viscoelasticity of biopolymer networks and statistical mechanics of semiflexible polymers. *Adv. Struct. Biol.*, 5:135–168, 1999.

[79] W. W. Graessley. Entangled linear, branched and network polymer systems—molecular theories. *Adv. Polym. Sci.*, 47:67–117, 1982.

[80] D. J. Read. Convective constraint release with chain stretch: Solution of the rouse-tube model in the limit of infinite tubes. *J. Rheol.*, 48(2):349–377, 2004.

[81] M. Rubinstein and R. H. Colby. Self-consistent theory of polydisperse entangled polymers: Linear viscoelasticity of binary blends. *J. Chem. Phys.*, 89(8):5291–5306, 1988.

[82] T. A. Kavassalis and J. Noolandi. A new theory of entanglements and dynamics in dense polymer systems. *Macromolecules*, 21(9):2869–2879, 1988.

[83] W. Hess. Self-diffusion and reptation in semidilute polymer solutions. *Macromolecules*, 19(5):1395–1404, 1986.

[84] T. P. Lodge, N. A. Rotstein, and S. Prager. Dynamics of entangled polymer liquids: Do linear chains reptate? *Adv. Chem. Phys.*, 79:1–132, 1990.

[85] H. Wendel and J. Noolandi. Generalized reptation model. *Macromolecules*, 15(5):1318–1320, 1982.

[86] M. Doi and S. F. Edwards. Dynamics of rod-like macromolecules in concentrated solution. part 2. *J. Chem Soc. Faraday Trans.*, 74:918–932, 1978.

[87] D. C. Morse. Viscoelasticity of concentrated isotropic solutions of semiflexible polymers. 1. model and stress tensor. *Macromolecules*, 31(20):7030–7043, 1998.

[88] L. Onsager. The effects of shape on the interaction of colloidal particles. *Ann. N.Y. Acad. Sci.*, 51(4):627–659, 1949.

[89] M. Dijkstra and D. Frenkel. Simulation study of the isotropic-to-nematic transitions of semiflexible polymers. *Phys. Rev. E*, 51(6):5891, 1995.

[90] A. R. Khokhlov and A. N. Semenov. Liquid-crystalline ordering in the solution of long persistent chains. *Physica A*, 108(2):546–556, 1981.

[91] A. R. Khokhlov and A. N. Semenov. Liquid-crystalline ordering in the solution of partially flexible macromolecules. *Physica A*, 112(3):605–614, 1982.

[92] F. C. Bawden and N. W. Pirie. The isolation and some properties of liquid crystalline substances from solanaceous plants infected with three strains of tobacco mosaic virus. *Proc. Royal Soc. (London) Series B*, pages 274–320, 1937.

[93] H. Löwen. Anisotropic self-diffusion in colloidal nematic phases. *Phys. Rev. E*, 59(2):1989, 1999.

[94] C. M. Coppin and P. C. Leavis. Quantitation of liquid-crystalline ordering in f-actin solutions. *Biophys. J.*, 63(3):794–807, 1992.

[95] J. F. Maguire, J.-P. McTague, and F. Rondelez. Rotational diffusion of sterically interacting rodlike macromolecules. *Phys. Rev. Lett.*, 45(23):1891, 1980.

[96] H. Isambert and A. C. Maggs. Dynamics and rheology of actin solutions. *Macromolecules*, 29(3):1036–1040, 1996.

[97] T. Odijk. The statistics and dynamics of confined or entangled stiff polymers. *Macromolecules*, 16(8):1340–1344, 1983.

[98] A. N. Semenov. Dynamics of concentrated solutions of rigid-chain polymers. part 1.—brownian motion of persistent macromolecules in isotropic solution. *J. Chem. Soc., Faraday Trans. 2*, 82(3):317–329, 1986.

[99] K. Kroy and E. Frey. Force-extension relation and plateau modulus for wormlike chains. *Phys. Rev. Lett.*, 77:306–309, 1996.

[100] M. Doi. Effect of chain flexibility on the dynamics of rodlike polymers in the entangled state. In *J. Polym. Sci.: Polym. Symp*, volume 73, pages 93–103. Wiley Online Library, 1985.

[101] M. Doi. Explanation for the 3.4 power law of viscosity of polymeric liquids on the basis of the tube model. *J. Poly. Sci., Polym. Lett. Ed.*, 19(5):265–273, 1981.

[102] M. Doi. Explanation for the 3.4-power law for viscosity of polymeric liquids on the basis of the tube model. *J. Polym. Sci. Polym. Phys. Ed.*, 21(5):667–684, 1983.

[103] J. Klein. The onset of entangled behavior in semidilute and concentrated polymer solutions. *Macromolecules*, 11(5):852–858, 1978.

[104] M. Daoud and P. G. De Gennes. Some remarks on the dynamics of polymer melts. *J. Polym. Sci.: Polym. Phys. Ed.*, 17(11):1971–1981, 1979.

[105] D. J. Read, K. Jagannathan, and A. E. Likhtman. Entangled polymers: Constraint release, mean paths, and tube bending energy. *Macromolecules*, 41(18):6843–6853, 2008.

[106] A. Ramirez-Hernandez, F. A. Detcheverry, B. L. Peters, V. C. Chappa, K. S. Schweizer, M. Müller, and J. J. de Pablo. Dynamical simulations of coarse grain polymeric systems: Rouse and entangled dynamics. *Macromolecules*, 46(15):6287–6299, 2013.

[107] K. Binder and W. Paul. Monte carlo simulations of polymer dynamics: Recent advances. *J. Polym. Sci. Part B: Polym. Phys.*, 35(1):1–31, 1997.

[108] T. Kreer, J. Baschnagel, M. Müller, and K. Binder. Monte carlo simulation of long chain polymer melts: Crossover from rouse to reptation dynamics. *Macromolecules*, 34(4):1105–1117, 2001.

[109] C. P. Broedersz, M. Sheinman, and F. C. MacKintosh. Filament-length-controlled elasticity in 3d fiber networks. *Phys. Rev. Lett.*, 108(7):078102, 2012.

[110] A. E. Likhtman, S. K. Sukumaran, and J. Ramirez. Linear viscoelasticity from molecular dynamics simulation of entangled polymers. *Macromolecules*, 40(18):6748–6757, 2007.

[111] F. Sakha and H. Fazli. Three-dimensional brownian diffusion of rod-like macromolecules in the presence of randomly distributed spherical obstacles: Molecular dynamics simulation. *J. Chem. Phys.*, 133(23):234904, 2010.

[112] H. Hinsch and E. Frey. Non-affine shear modulus in entangled networks of semiflexible polymers. *arXiv preprint arXiv:0907.1875*, 2009.

[113] P. S. Grassia, E. J. Hinch, and L. C. Nitsche. Computer-simulations of brownian-motion of complex systems. *J. Fluid Mech.*, 282:373–403, 1995.

[114] D. C. Morse. Theory of constrained browninan motion. *Advances in Chemical Physics*, 128:65–189, 2004.

[115] M. Pasquali and D. C. Morse. An efficient algorithm for metric correction forces in simulations of linear polymers with constrained bond lengths. *J. Chem. Phys.*, 116(5):1834–1838, 2002.

[116] N. G. V. Kampen and J. J. Lodder. Constraints. *Am. J. Phys.*, 52(5):419–424, 1984.

[117] M. Hütter and H. C. Öttinger. Fluctuation-dissipation theorem, kinetic stochastic integral and efficient simulations. *J. Chem. Soc. Farady Trans.*, 94(10):1403–1405, 1998.

[118] M. Fixman. Simulation of polymer dynamics .1. general theory. *J. Chem. Phys.*, 69(4):1527–1537, 1978.

[119] A. Montesi, D. C. Morse, and M. Pasquali. Brownian dynamics algorithm for bead-rod semiflexible chain with anisotropic friction. *J. Chem. Phys.*, 122(8):84903, 2005.

[120] H. R. Warner Jr. Kinetic theory and rheology of dilute suspensions of finitely extendible dumbbells. *Ind. Eng. Chem. Fundam.*, 11(3):379–387, 1972.

[121] J. S. Hur, E. S. G. Shaqfeh, and R. G. Larson. Brownian dynamics simulations of single DNA molecules in shear flow. *J. Rheol.*, 44(4):713–742, 2000.

[122] J. D. Weeks, D. Chandler, and H. C. Andersen. Role of repulsive forces in determining the equilibrium structure of simple liquids. *J. Chem. Phys.*, 54:5237, 1971.

[123] G. Cinacchi, Y. Martínez-Ratón, L. Mederos, G. Navascués, A. Tani, and E. Velasco. Large attractive depletion interactions in soft repulsive–sphere binary mixtures. *J. Chem. Phys.*, 127(21):214501, 2007.

[124] M. Galassi, J. Davies, J. Theiler, B. Gough, G. Jungman, M. Booth, and F. Rossi. Gsl–gnu scientific library: Reference manual, 2011.

[125] D. J. Tildesley and M. P. Allen. *Computer simulation of liquids*. Clarendon, Oxford, 1987.

[126] A. Suzuki, T. Maeda, and T. Ito. Formation of liquid crystalline phase of actin filament solutions and its dependence on filament length as studied by optical birefringence. *Biophys. J.*, 59(1):25–30, 1991.

[127] K. M. Jaffer, S. B. Opps, D. Sullivan, B. G. Nickel, and L. Mederos. The nematic-isotropic phase transition in semiflexible fused hard-sphere chain fluids. *J. Chem. Phys.*, 114(7):3314–3324, 2001.

[128] A. Yethiraj and H. Fynewever. Isotropic to nematic transition in semiflexible polymer melts. *Mol. Phys.*, 93(5):693–701, 1998.

[129] Y.-G. Tao, W. K. Den Otter, J. K. G. Dhont, and W. J. Briels. Isotropic-nematic spinodals of rigid long thin rodlike colloids by event-driven brownian dynamics simulations. *J. Chem. Phys.*, 124(13):134906, 2006.

[130] X. Lü and J. T. Kindt. Monte carlo simulation of the self-assembly and phase behavior of semiflexible equilibrium polymers. *J. Chem. Phys.*, 120(21):10328–10338, 2004.

[131] C. McBride, C. Vega, and L. G. MacDowell. Isotropic-nematic phase transition: Influence of intramolecular flexibility using a fused hard sphere model. *Phys. Rev. E*, 64(1):011703, 2001.

[132] H. N. W. Lekkerkerker, P. Coulon, R. Van Der Haegen, and R. Deblieck. On the isotropic-liquid crystal phase separation in a solution of rodlike particles of different lengths. *J. Chem. Phys.*, 80(7):3427–3433, 1984.

[133] P. E. Rouse. A theory of the linear viscoelastic properties of dilute solutions of coiling polymers. *J. Chem. Phys.*, 21(7):1272–1280, 1953.

[134] R. Everaers, F. Jülicher, A. Ajdari, and A. C. Maggs. Dynamic fluctuations of semiflexible filaments. *Phys. Rev. Lett.*, 82(18):3717, 1999.

[135] S. Asakura and F. Oosawa. On interaction between two bodies immersed in a solution of macromolecules. *J. Chem. Phys.*, (22):1255–1256, 1954.

[136] R. Dickman, P. Attard, and V. Simonian. Entropic forces in binary hard sphere mixtures: Theory and simulation. *J. Chem. Phys.*, 107(1):205–213, 1997.

[137] M. Tassieri, R. M. L. Evans, L. Barbu-Tudoran, G. N. Khaname, J. Trinick, and T. A. Waigh. Dynamics of semiflexible polymer solutions in the highly entangled regime. *Phys. Rev. Lett.*, 101(19):198301, 2008.

[138] M. Buchanan, M. Atakhorrami, J. F. Palierne, and C. F. Schmidt. Comparing macrorheology and one-and two-point microrheology in wormlike micelle solutions. *Macromolecules*, 38(21):8840–8844, 2005.

[139] M. L. Gardel, M. T. Valentine, J. C. Crocker, A. R. Bausch, and D. A. Weitz. Microrheology of entangled f-actin solutions. *Phys. Rev. Lett.*, 91(15):158302, 2003.

[140] B. Doliwa and A. Heuer. Cage effect, local anisotropies, and dynamic heterogeneities at the glass transition: A computer study of hard spheres. *Phys. Rev. Lett.*, 80(22):4915, 1998.

[141] L. Berthier and G. Biroli. Theoretical perspective on the glass transition and amorphous materials. *Rev. Mod. Phys.*, 83(2):587, 2011.

[142] T. G. Mason. Estimating the viscoelastic moduli of complex fluids using the generalized stokes–einstein equation. *Rheol. Acta*, 39(4):371–378, 2000.

[143] J. Xu, A. Palmer, and D. Wirtz. Rheology and microrheology of semiflexible polymer solutions: actin filament networks. *Macromolecules*, 31(19):6486–6492, 1998.

[144] F. Gittes, B. Schnurr, P. D. Olmsted, F. C. MacKintosh, and C. F. Schmidt. Microscopic viscoelasticity: shear moduli of soft materials determined from thermal fluctuations. *Phys. Rev. Lett.*, 79(17):3286, 1997.

[145] B. Schnurr, F. Gittes, F. C. MacKintosh, and C. F. Schmidt. Determining microscopic viscoelasticity in flexible and semiflexible polymer networks from thermal fluctuations. *Macromolecules*, 30(25):7781–7792, 1997.

[146] R. d. Kronig. On the theory of dispersion of x-rays. *JOSA*, 12(6):547–556, 1926.

[147] J. S. Toll. Causality and the dispersion relation: logical foundations. *Phys. Rev.*, 104(6):1760, 1956.

[148] M. Keller, R. Tharmann, M. A. Dichtl, A. R. Bausch, and E. Sackmann. Slow filament dynamics and viscoelasticity in entangled and active actin networks. *Phil. Trans. R. Soc. Lond. A*, 361(1805):699–712, 2003.

Danksagung

Ich danke meinem Betreuer, Prof. Dr. Erwin Frey, mir die Dissertation an seinem Lehrstuhl ermöglicht zu haben. Ich habe in dieser Zeit viel gelernt und mich weiter entwickelt. Ich danke ihm für seine Geduld, sein Vertrauen und seine Unterstützung, die es mir erlaubt haben mich in einer großartigen Gruppe frei zu entfalten. Durch die vielen Gespräche mit Ihm konnten erst die tiefen Erkenntnisse entstehen, die zu dieser Arbeit geführt haben.

Ich möchte auch den übrigen Mitgliedern des Lehrstuhls Frey danken. Jeder meiner Kollegen trägt auf seine Art zur herzlichen Atmosphäre in dieser Gruppe bei. Mit Freude erinnere ich mich an die offenen Türen und Ohren bei kleinen und großen Problemen. Ich danke Lorenz Huber, Timo Krüger und Louis Reese für wertvolle Diskussionen.
Insbesondere gilt mein Dank meinem Bürokollegen Cornelius Weig für die angenehme gemeinsame Zeit, tiefe Gespräche, fachliche Diskussionen und unzählige Programmiertipps. Ohne seine Ratschläge wäre diese Arbeit in ihrer aktuellen Form nicht möglich gewesen.

Ich danke dem Doktorandenkolleg NanoBioTechnologie, dessen Förderung mir vieles ermöglicht hat und durch das ich viele spannende Menschen kennen lernen durfte.

Mein Leben wäre ohne Freunde nur halb so schön, deswegen gilt auch ihnen mein Dank. Stellvertretend möchte ich Puls für unsere philosophischen Diskussionen und Wiltrud für ihr Verständnis danken.

Schließlich danke ich meiner Familie, die mich stets unterstützt hat. Meine Eltern, die mir in stressigen Phasen den Kopf frei halten, und meinem Bruder für seine Unterstützung und die Bereitschaft, auch über physikalisch-mathematische Probleme zu diskutieren.